TECHNISCHE UNIVERSITÄT MÜNCHEN

Fakultät für Medizin

Investigating epigenetic alterations in Ewing sarcoma – A prospective and promising approach to future therapeutic treatment of ES patients

Tim Hensel

Vollständiger Abdruck der von der Fakultät für Medizin der Technischen Universität München zur Erlangung des akademischen Grades eines

Doktors der Naturwissenschaften

genehmigten Dissertation.

Vorsitzender:	Prof. Dr. R. R. Rad
Prüfer der Dissertation:	1. Priv.-Doz. Dr. Günther Richter
	2. Prof. Dr. M. Habrě de Angelis

Diese Dissertation wurde am 02.01.2018 bei der Technischen Universität München eingereicht und durch die Fakultät am 11.10.2018 angenommen.

“From a few peaks rising above the fog we try to imagine what the hidden landscape underneath might look like”

Pieter W. Postma, during a hiking trip October 1997

Acknowledgement

Even though my name is printed on the cover of this work I want to emphasize that this work could not have been done without the intensive myriad contributions of my advisors and collaborators and the support of my family. Therefore, ’we‘ will be used throughout this text.

To my parents: Thank you for giving me the freedom and the opportunity to realize this thesis and pursue my own interests. Toni, thank you for believing in me and for your patience during this long time.

Günther, thank you for letting me conduct this PhD thesis in your laboratory and your dedication, support and encouragement that created a research environment for me without match. David, Andi, Kristina, Oxana and Chiara thank you for this source of comfort and the time you took away from your own work to provide feedback on this thesis.

Table of contents

1 Introduction

1.1 Ewing Sarcoma

Ewing sarcoma (ES) is a highly malignant bone and soft tissue neoplasia. In 1921 James Stephen Ewing was the first who described it as an "endothelioma of the bone" with "unknown origin and nature" [1], while 45 years later it is still of enigmatic histogenesis [2]. Categorical, ES belong to a group of cancers that are recognized as the Ewing`s sarcoma family of tumors (ESFT) that includes peripheral primitive neurectodermal tumor (PNET), peripheral neuroepithelioma and Askin tumor, which share the same EWS/ETS oncogenic fusion genes, displaying similar biological behavior [3, 4].

Epidemiologically, ES represent the second most common bone and soft tissue tumors in children and adolescents next to osteosarcoma [5]. Tumors usually occur during the second decade of life with a peak incidence of 3.3 in $1x10^6$ under the age of 15 [6, 7]. Its prevalence is slightly increased in males and Caucasians and rarely arises in individuals of African ancestry [3], indicating a genetic predisposition. The most common affected bone sites are the long bones of the extremities, pelvis, chest wall and spine. Lesions of the long bone typically involve the diaphysis [3]. Even though most ES occur in bone, 15% may arise in extra osseous sites including deep soft paravertebral, thoracic and proximal limb tissue, kidney, bladder, lung, prostate and the meninges [8, 9]. ES feature an aggressive behavior and a propensity towards early recurrence after resection, predominantly in the lungs, bone and bone marrow [10].

Histologically, ES belong to a group of small round blue cell tumors that include neuroblastoma, alveolar rhabdomyosarcoma and lymphoblastic leukemia that appear blue under the microscope on hematoxylin and eosin (H&E) staining. They are composed of small cells with a high nuclear to cytoplasmic ratio and typically represent undifferentiated cells. While the cell of origin is still unknown several studies showed that ES cells display features of mesenchymal, neurectodermal and endothelial cells, suggesting

either a mesenchymal or neuroectodermal origin [11, 12]. Despite information and recognition on the morphological, immunocytochemical and sometimes ultrastructural features, the most valuable markers of differential diagnosis from other small round cell tumors of childhood, was the identification of a non-random translocation [13, 14]. While different translocations exist the most prominent is a fusion of the *Ewing sarcoma breakpoint region 1* (EWSR1) and an *ETS* (E-twenty-six) family gene [15-17] which in 85% of cases is a fusion of the EWS transcription factor on 11q24 and the FLI1 gene on 22q12. The consequence is an aberrant chimeric fusion transcript (EWS-FLI1) with increased transcriptional activity compared to normal FLI1 and an altered binding characteristic to many downstream targets and interaction partners, which can be activated or suppressed [18-20]. Type 1 (exon 7 of EWS to exon 6 of FLI1) and type 2 (exon 7 of EWS to exon 5 of FLI1) are the two types of this typical translocation sites. The second most translocation t(21;12)(22;12) results in an EWS-ERG (Ets-related-gene) related fusion [21].

Children and teens with Ewing sarcoma often experience localized pain and / or a mass, frequently mistaken for signs of growth or injury [22]. While the survival and the relapse-free survival improved over time, the most critical prognostic factors today are metastases at diagnosis, primary site and age. Thereby, 22% of all newly diagnosed patients are diagnosed with metastases, which correlates with a bad outcome. Furthermore, once patients relapse the outcome is poor, especially for those relapsing within 2 years of diagnosis who almost invariably die of their disease [23]. The overall 5-year disease-free survival for localized tumors, treated with surgery, radiation and multi-agent chemotherapy is 65-76% [24, 25]. Even though improved local control therapy and the development of improved chemotherapy combinations have reduced the frequency of relapse and improved the overall outcome, patients with metastatic disease have a <30% survival, especially when the bone or the bone marrow is involved [26, 27]. Current treatment modalities include tumor resection whenever possible, radiotherapy for inoperable lesions, chemotherapy and allogenic stem cell transplantation [27-29]. VIDE (vincristine, ifosfamide, doxorubicin and

etoposide) is now the standard chemotherapy for ES patients in Europe. However, no standard therapy exists for treatment of relapsed or refractory Ewing sarcoma.

Since Ewing`s sarcoma comprise one of the lowest mutation rate of all cancers [30, 31] with no actionable recurrent mutation [32], clinical evaluation of EWS-FLI1-targeted therapies are now only beginning. Although, direct targeting of EWS-FLI1 has been largely unsuccessful owing to poor pharmacokinetic properties and a lack of intrinsic enzymatic activity, several trials currently focus on interaction partners and downstream targets. In 2004, Staege et al. [11] identified a ES-specific expression signature of 37 genes that were overexpressed or even specifically expressed in comparison to normal tissue. Some of them are the *enhancer of zeste homolog 2* (EZH2), the *Six transmembrane epithelial antigen of prostate 1* (STEAP1), the *G protein-coupled receptor 64* (GPR64) gene or the *dickkopf 2* (DKK2) gene which promote the oncogenic phenotype, proliferation, invasiveness or the metastatic spread of ES [18, 33-35]. Nonetheless, advanced therapeutical treatment options are still lacking and are therefore one aim of this thesis.

1.2 Beyond conventional genetics

For nearly a century after the term “epigenetics” first appeared, researches tried to untangle the fact that gene expression and function could be altered by more than just changes in DNA sequences. Epigenetics, which are defined as genomic modifications that do not involve a change in the underlying DNA nucleotide sequence, have been expected to play specific roles in normal and transformed cells [36]. While the term is often used very broadly, it has originally been associated with changes that lead to alterations in chromatin conformation, histone appearance, non-histone chromatin proteins and non-coding RNAs [37, 38]. Aberrations in these components are common contributors to diseases. For example, syndromes like Prader-Willi, Silver-Russell or Angelman are often associated with

alterations in DNA methylation [39]. However, also cancer has been associated with aberrations in DNA methylation. Perhaps most commonly aberrations found in cancer are either DNA hypo- or hypermethylation of cytosines that precede guanines. These so called CpG islands are not randomly distributed throughout the genome but are regions with a high frequency of CpG sites. The usual definition of a CpG island is a region with at least 200 bp and a G+C percentage greater than 50% [40]. In humans, about 70% of promoters located near the transcriptional start site (TSS) contain a CpG island and are supposed to control the proximal gene expression [41]. However, recent studies demonstrated that they can also regulate gene expression at distal regions as well as the expression of functional noncoding RNAs including microRNAs [42, 43].

Since the methylation of CpG islands is generally considered as a transcriptionally repressive mark, factors like DNA methyltransferases (DNMTs) that catalyze DNA methylation are interesting anti-cancer targets [44]. In comparison with normal tissue, human tumors exhibit only low level of DNA methylation due to hypomethylation of repetitive DNA sequences and demethylation of coding regions and introns [45, 46]. However, DNA-hypermethylation of the CpG islands in promoter regions of tumor suppressor genes are major events in the origin of many cancers. While global hypomethylation characterizes cancer cells, hypermethylation of CpG islands is another feature affecting specific genes, e.g. genes involved in the cell cycle, DNA repair, the metabolism of carcinogens, cell-to-cell interaction, apoptosis, angiogenesis or tumor suppressor genes [47, 48]. The profiles of these methylation events are specific, defining a DNA methylome for each type of cancer. Mechanistically, DNA methylation is linked at many levels with histone modifications and nuclear organization [49, 50]. To pack huge portions of DNA into tiny compartments, histones facilitate the necessary scaffold for compaction. A histone octamer consists of two copies of each of the four core histone proteins (H2A, H2B, H3 and H4) and can wrap around 147 bp of DNA. It can be modified post-translationally which in turn enables regulatory mechanisms [49, 51]. Histone 1 which completes the histone family does not belong to the core complex but has a more structural

significance, stabilizing the DNA wrapped around the core histones. Over the past few years researchers have investigated mechanisms underlying post-translational modifications of core histones, in part due to dysfunction observed in many cancers. Evolutionarily, histones are highly conserved proteins with globular domains that mediate histone-histone interactions and a C or N terminal residue rich in basic amino acids that extends from the surface of the nucleosome [52]. While these `tails` do not contribute significantly to the structure or stability of nucleosomes, they do play an essential role in controlling the folding of nucleosomes into higher-ordered structures. At least 16 different classes at defined positions of the histone tail are subject to post-translational modifications including methylation, acetylation, ubiquitination, sumoylation, phosphorylation, ribosylation, deamination or isomerization [53]. All of these modifications are dynamic and the interplay and combination of histone modifications, DNA methylation and ATP chromatin remodeling proteins, dynamically regulate chromatin structure and thereby cellular processes [54-56]. Adding to the complexity is the fact that one amino acid residue can accept up to three groups, e.g. lysine can be mono-, di- or tri-methylated while arginine can be mono- or di-methylated. However, given the number of new modification sites identified each year it seems not unlikely that nearly every histone may be accessible for post-translational modifications.

Although histone modifications have been studied for over 40 years, histone modifying enzymes remained elusive until the first discovery of histone acetyltranferases (HATs) [57-60]. Histone acetylation represents a mark generally linked to transcriptional activation, leading to a cascade of additional modifications and the recognition by specific proteins such as bromo domain-containing proteins [37, 52, 53, 55, 61, 62]. However, the level of histone lysine acetylation is regulated via the opposing roles of HATs and histone deacetylases (HDACs) which were also observed to be deregulated in different cancers [63-65].

Histone methylation, in contrast to histone acetylation, correlates with either an activation or a repression of transcription depending on the degree of

methylation and the site [66, 67]. For instance, methylation of histone H3 lysine 9 (H3K9), H3K27 and H4K20 are associated with gene silencing while methylation of histones H3K4, H3K36 and H3K79 have been linked with active gene transcription [68, 69]. Interestingly, an equilibrium between methylation of H3K4 which activates transcription and H3K27 which represses, was reported to be important in the activity of "stemness" transcription patterns to maintain pluripotency [70]. Histone methylation on lysine is mediated by histone methyltransferases (HMTs) transferring a methyl group from the cofactor S-adenosyl-L-methionine (SAM) to the ε-amino group of the lysine [71]. There are two different classes of HMTs: the lysine-specific SET domain containing histone methyltransferases and the non-SET-containing lysine methyltransferases [72]. In contrast to HATs and HDACs, HMTs do show a high degree of specificity towards their histone targets and are able to recognize and modulate different degrees of methylation on the same lysine [66, 67, 73]. Furthermore, due to the stable nature of the C-N bond, research in the early days regarded methylation of histones as an irreversible process [74, 75]. However, the later discovery of histone demethylases disproved this hypothesis, showing that methylation is a very dynamic process that changes throughout different stages of development [76]. Alterations in this process have been implicated in a plethora of different diseases. In fact, epigenetic alterations have been known to occur in cancer cells for decades. However, their recognized role is not causal and many processes leading to this transformation are still unknown. While no single histone modification is predictive per se, several alterations were identified characterizing the clinical outcome of the analyzed patients. Similar to HATs and HDACs, altered activity or expression of HMTs and HDMs has been reported in several cancers [77, 78]. For example EZH2, which is a H3K27 HMT and member of the polycomb repressive complex 2 (PRC2), was found as frequently up-regulated in several cancer entities including breast or prostate cancer as well as in ES [18, 79, 80]. However, understanding the complex mechanisms involved in EZH2 overexpression and how it targets defined genomic alterations are only beginning to be understood.

1.3 Polycomb and EZH2 as a landmark in life

Polycomb and trithorax groups of proteins (PcG) epigenetically remodel chromatin states and thus influence transcriptional programs. Whilst both groups act antagonistically, PcG proteins mediate gene silencing through the regulation of chromatin structure and in part through post-translational modifications of histones, involving at least two kinds of multiprotein complexes. In mammals, the Polycomb Repressive Complex 1 (PRC1) is responsible for monoubiquitylation at lysine 119 of histone H2A [81]. Furthermore, it binds trimethylation marks at lysine 27 of histone 3 and hence act downstream of the Polycomb Repressive Complex 2 (PRC2) [82]. The PRC2 complex is responsible for di- and trimethylation of lysine 27 of histone 3, whether catalyzed by its subunits enhancer of zeste homologue 2 (Ezh2) or Ezh1. Recent research highlights that even though they share a high degree of similarity they might not be interchangeable. Because of the low methyltransferase activity of EZH1 in comparison to EZH2 a frequent theory is that PRC2-EZH2 establishes cellular H3K27me2/3 levels while PRC2-EZH1 restores H3K27me2/3 possibly lost after demethylase activity or histone exchange [83]. However, other core components of this complex are needed likewise. Embryonic ectoderm development (EED), as one of four PRC2 core components, boosts the catalytic activity by linking EZH2 and H3, whereas the remaining two, Suppressor of zeste homologue (SUZ12) and Retinoblastoma binding protein (RbAp46/48), are required for nucleoside association [84]. Mechanistic studies demonstrated that several other polypeptides such as AEBP2, PCLs or JARID2 can be part of the PRC2 too, enhancing its enzymatic activity and the recruitment to genomic loci [85-87]. However, their inactivation resulted in milder consequences than inactivation of a core PRC2 component, so that it remains to be determined whether the composition of PRC2 is modified as a consequence of, or a process during, development, maintenance or tumorigenesis. Thus far, it is known that all PRC2 complexes catalyze a processive H3K27 methylation (H3K27me3 results from monomethylation of H3K27me2). Although it is still unclear how PRC2 is exactly recruited to chromatin it could be shown that notable areas

of enriched G+C sequences seem to be a main target [88]. Studies in *Drosophila* revealed that DNA sequences known as PcG-response elements (PREs) are targets of PcGs recruitment [89]. In mammals reports suggested YY1 to be required for PRC1 and PRC2 recruitment. However, genome wide studies did not show a clear overlap [90, 91] leaving the question unsolved how far potential transcription factors are involved. Another implication was made for long non-coding RNAs (ncRNAs) such as HOTAIR or XIST that regulate chromatin conformation and gene expression *in cis* and *in trans* [92, 93]. A postulated model resulting from these observations is therefore the combination of all known components, that act together and interlaced to attain the necessary energy to recruit PRC2 [82].

EZH2 is the enzymatically subunit of the PRC2 complex. An overexpression of EZH2 was found in several cancers and is accompanied with a worse prognosis. While the reasons for its up-regulation can be different from one cancer to another the main mechanism it facilitates is to confer a proliferative advantage over non-cancerous cells [94]. Additional findings refined this oncogenic role by demonstrating that gain-of-function mutations affecting the catalytic SET domain in certain lymphomas lead to increased levels of H3K27me3 [95]. Other support came from the identification of loss-of-function mutation affecting other chromatin modifiers such as the demethylase UTX (ubiquitously transcribed tetratricopeptide repeat gene on X chromosome) usually antagonizing EZH2 activity and consequently showing analogous effects to those caused by EZH2 gain-of-function mutations [96-98]. Given its substantial role as a transcriptional regulator, collective efforts have been undertaken to identify possible pathways or downstream targets. The Ink4a/Arf tumor suppressor locus as well as E-cadherin or the differentiation factor FOXC1 are examples of direct targets that are silenced through EZH2 by H3K27me3 in tumor cells [99-101]. However, studies in castration-resistant prostate cancer as well as in breast cancer cells showed that EZH2 can also act independently from PRC2, activating the expression of the androgen receptor (AR) or NF-kB, respectively [102, 103]. Further was it indicated that EZH2 can methylate non-histone substrates as STAT3, which in turn promotes tumorigenicity in

glioblastoma [104]. In summary, these results suggest that despite the role of EZH2 as an H3K27 methyltransferase and transcriptional suppressor, it can have also non-canonical functions describing the overall cellular role and the link to an oncogenic transformation.

Previous studies in ES also showed an increased expression of EZH2 which is regulated under the control of EWS-FLI1 [18]. RNA interference (RNAi) of EZH2 suppressed tumor development and metastasis *in vivo* and microarray analysis of EZH2 knock-down revealed an EZH2-maintained, undifferentiated, reversible phenotype [18]. EZH2 suppression resulted in a generalized loss of H3K27me3 as well as increase in H3 acetylation. ChIP-Chip assays for H3K27me3 verified such genes that had specifically lost H3K27me3 upon EZH2 silencing [105], suggesting that malignant *stemness* features are preserved via epigenetic mechanisms.

1.4 BET bromodomain proteins

A fundamental change in the understanding of chromatin regulation was the realization that many regulators possess specialized domains that allows them to survey the chromatin landscape and dock at specific regions. These chromatin readers are able to recognize different modifications on the tails of histones and assemble functional complexes onto specific loci to facilitate DNA-template processes [106, 107]. Several motifs have been identified encompassing proteins with either chromodomains, bromodomains, Tudor domains or DNA methyl-binding domains. While either one is specialized on a certain histone mark bromodomain containing proteins recognize specifically acetyl-lysine modifications. More than 40 different proteins exist containing a bromodomain, with some having multiple of them. They can be clustered into nine major families according to their sequence identity. Although the acetyl-lysine binding pocket is hydrophobic for all of them, certain variations in the electrostatic interactions at the opening of the pocket determines the specificity of individual bromodomains [108]. However, this

also provides the opportunity to develop small molecules that target certain families.

The BET family of proteins belongs to one of the nine bromodomain families. It has three members, bromodomain-containing proteins 2, 3 and 4 (BRD2, BRD3 and BRD4) whose expression is ubiquitous. BRDT is the fourth member while its expression is confined to the testes/oocyte. All of them feature a common structural design of a tandem bromodomain at the N-terminus (BD1 and BD2) and an extraterminal (ET) domain located either at its central region or close to the carboxyl terminus. In addition to these three conserved domains they contain also other conserved regions, for example the SEED (Ser/Glu/Asp-rich region) or carboxyl-terminal motif, that are found not in all of them and are mostly uncharacterized [109, 110]. A unique feature is their association not only with interphase chromatin but also mitotic chromosomes, a feature also seen in viral systems and suggesting a role in transmission of memory across cell division [111]. For example, the E2 transcription/replication factor encoded by BPV-1 (bone papillomavirus type 1) and human papillomaviruses (HPVs) binds directly to BRD4 in order to facilitate selective types of viral genome segregation during mitosis [112, 113]. Further studies on BRD4 demonstrated that it physically interacts with the mediator complex, a multiprotein complex that interacts with transcription factors (TFs) and participates in the recruitment and activation of RNA polymerase II (Pol II) [114]. Consistent with its role in cell growth, interactions of BRD4 and the active form of the positive transcription elongation factor b (p-TEFb) have been observed likewise [115]. Interestingly, even though BRD4 and BRD2 share a high similarity in their mode of action, they comprehend specific histone interactions. In addition, BRD2 as well as BRD3 were also found to associate with specific histone marks on histone H3 or H4 to enable transcriptional elongation [116].

Despite the ongoing effort to elucidate the versatile role of BET proteins, recent research has established a compelling rationale for targeting BRD4 in cancer. Gene rearrangements involving BRD4 were found in aggressive carcinoma such as the NUD-midline carcinoma [117]. This recurrent

translocation expresses the N-terminal bromodomains of BRD4 as an in-frame chimera with the nuclear protein in testis (NUT), conferring a proliferative advantage and differentiation block of this uniformly fatal malignancy [118]. Notably, RNAi of BRD4-NUT arrests proliferation and prompts terminal squamous differentiation. These observations set the motivation for the development of a small molecule named JQ1 [119] that specifically binds to and thereby inhibits the function of BET bromodomains from binding to acetylated histone marks. Particularly interesting was that beyond the successful application of JQ1 in NUD-mudline carcinoma cells *in vitro* and *in vivo*, subsequent observations showed that c-MYC, a master regulator of cell proliferation [120], was downregulated after treatment as well. Although research has referred to MYC (myelocytomatosis) since the late 70`s [121-124] as one of the most frequently deregulated oncogenes in cancer, it has been dubbed “undruggable” due to its lack of a clear ligand-binding domain [125]. MYCN and MYCL are both members of a family of transcription factors to which also MYC belongs to. All three of them are intimately linked to an oncogenic phenotype due to their translocation, amplification or overexpression in human tumors. MYCN and MYCL are frequently amplified and are believed to be a driver in human neuroblastoma and small cell lung cancer (SCLC), respectively [126, 127]. However expression of MYCN and MYCL are more restricted with respect to tissue and developmental stage in contrast to MYC [128, 129]. Nevertheless, a therapeutic approach to target MYC has remained elusive for a long time. The availability of a new and specific small molecule blocking BET bromodomains and subsequently downregulating MYC will therefore prompt informative research broadly on development and disease of MYC or BET deregulated cancers.

1.5 Aim of this thesis and applied experimental approach

The goal of this doctoral thesis was to further illuminate the role of epigenetics in the pathology of ES. For that reason, previously established gene expression data were queried for epigenetic regulators and the MYC gene was found as upregulated [11]. To investigate its potential implication in ES pathogenesis, potent small molecules were selected targeting potential pathways upstream of MYC such as BET bromodomain proteins or the PI3K/AKT/mTOR pathway. The influence of this inhibition was measured in different mesenchymal stem cells and ES cell lines by qRT-PCR. Subsequently, the effect of the inhibition was examined by different *in vitro* assays. Microarray analysis was performed to analyze possible changes on the whole transcriptome. Gene set enrichment analysis (GSEA) was used to study the changes in certain pathways. As the analysis showed pathways involved in apoptosis and an ES specific expression profile change, western-blot was used to confirm these findings. Furthermore, a xenotransplantation model was used to verify findings *in vivo* and to evaluate possible therapeutical availability. Subsequently, immunohistochemical analyses were performed on tumor samples to further examine the *in vivo* results and better quantify the effect of the treatment. Furthermore, the observed effects were tried to mimic by transient and constitutive downregulation of BET bromodomain proteins. The effect of this knock-down was analyzed by different *in vitro* assays and compared to small molecule inhibition. BRD4-interaction studies by means of co-immunoprecipitation (Co-IP) and chromatin immunoprecipitation (ChIP) were carried out to analyze for possible binding sites and interaction partners. One frequent binder was further investigated by inhibition of a small molecule. Changes in the pathogenesis of ES cells were analyzed after treatment by different *in vitro* assays. Due to a potential development of resistance of ES cell lines to BET bromodomain inhibition, combinatorial treatment was tested *in vivo* to further elucidate its therapeutical benefit.

In addition, another epigenetic player by means of EZH2 was further analyzed. As published previously, knock-down of EZH2 inhibited tumor

growth *in vitro* and *in vivo*. Here we applied an inhibitor blocking the enzymatic site of EZH2 and analyzed the resulting changes by different assays.

In summary, this work analyzes the epigenetic circuitry by means of BET bromodomains and EZH2 in ES. Additionally, this study may shed further light on the intricate network in ES triggered by EWS/FLI1 and may contribute to the development of better and refined treatment options.

2 Materials and Methods

2.1 Materials

2.1.1 List of manufacturers

Table 1: List of manufacturers

Manufacturer	Location
Abcam	Cambridge, UK
Abbott	Wiesbaden, Germany
ACEA	San Diego, USA
Active Motif	La Hulpe, Belgium
AEG	Nürnberg, Germany
Affymetrix	High Wycombe, UK
Agilent	Waldbronn, Germany
Ambion	Austin, USA
Amersham Biosciences	Piscataway, USA
Applied Biosystems	Darmstadt, Germany
ATCC	Rockville, USA
B. Braun Biotech Int.	Melsungen, Germany
BD Bioscience Europe	Heidelberg, Germany
Beckman Coulter	Palo Alto, USA
Beckton Dickinson (BD)	Heidelberg, Germany
Berthold detection systems	Pforzheim, Germany
Biochrom	Berlin, Germany
Biometra	Göttingen, Germany
BioRad	Richmond, USA
Biovision	San Francisco, USA
Biozym	Hess. Olendorf, Germany
Brand	Wertheim, Germany
Calbiochem	Darmstadt, Germany
Caliper Life Sciences Inc.	Waltham, USA

Euriso-Top GmbH	Saarbrücken, Germany
Carestream Health, Inc.	Stuttgart, Germany
Cell Signaling Technology	Frankfurt am Main, Germany
Charles River Laboratories	Wilmington, USA
Clonetech – Takara Bio Europe	Saint-Germain-en-Laye, France
DSMZ	Braunschweig, Germany
Dharmacon	Lafayette, USA
Diagenode	Seraing, Belgium
Eppendorf	Hamburg, Germany
Eurofins MWG GmbH	Ebersberg, Germany
Falcon	Oxnard, USA
Feather	Osaka, Japan
Fermentas	St. Leon-Rot, Germany
GE Healthcare	Uppsala, Sweden
Genomed	St. Louis, USA
Genzyme	Neu-Isenburg, Germany
Greiner Bio-One GmbH	Frickenhausen, Germany
Heraeus	Hanau, Germany
Implen GmbH	München, Germany
Instech Laboratories Inc.	Plymouth Meeting, USA
Leica	Wetzlar, Germany
LMS	Brigachtal, Germany
Lonza	Basel, Schwitzerland
Macherey-Nagel	Düren, Germany
Memmert	Schwabach, Germany
Merck KGgA	Darmstadt, Germany
Metabion	Martinsried, Germany
Nalgene	Rochester, NY, USA
Nexcelom	Lawrence, MA, USA
Nunc	Naperville, USA
Nikon	Düsseldorf, Germany
PAA	Cölbe, Germany

Philips	Hamburg, Germany
Promega	Madison, USA
Qiagen	Chatsworth, CA, USA
R&D Systems	Minneapolis, MN, USA
Roche	Mannheim, Germany
Roth	Karlsruhe, Germany
Santa Cruz Biotechnology	Heidelberg, Germany
Sartorius	Göttingen, Germany
Scientific Industries	Bohemia, NY, USA
Scotsman	Milan, Italy
Sempermed	Wien, Austria
Sequiserve	Vaterstetten, Germany
Sigma-Aldrich	St. Louis, MO, USA
Siemens	München, Germany
Systec	Wettenberg, Germany
Taylor-Wharton	Husum, Germany
Techlab	Braunschweig, Germany
Thermo Fisher Scientific	Braunschweig, Germany
TKA GmbH	Niederelbert, Germany
TPP	Trasadingen, Switzerland
Whatman	Dassel, Germany
Zeiss	Jena, Germany

2.1.2 List of consumables

Table 2: List of consumables

Materials	Manufacturer
6-well tissue culture plate	Falcon
24-well non-tissue culture plate	Falcon
96-well culture plate (round and flat bottom)	TPP

Cell culture flasks (25, 75 and 175 mm^2)	Greiner Bio-One
Cell culture dishes (100 and 150 mm^2)	Sarstedt
Combs (Western blot)	Biometra
Cryovials 1,5ml	Sarstedt
Cuvettes	Roth
E-plates (96-well)	ACEA
Filters for cells, Cell strainer	Falcon
Filter for solution (0,2 µm and 0,45 µm)	Sartorius
Gloves (nitril, latex)	Sempermed
Hypodermic needle (23 G, 30 G)	B. Braun
Parafilm	Pechiney Plastic Packaging
Pasteur pipettes	Greiner Bio-One
Pipettes (2, 5, 10, 25 ml)	VWR
Pipette filter tips (10, 100, 200, 1000 µl)	Thermo Fisher Scientific
Plates for invasion-assay (24-well)	BD Bio Science
Plates for qRT-PCR (96-well)	Applied Biosystems
Syringes (27 G x 318``, 0,45 mm x 10 mm)	BD Bioscience
Syringes (GC, 1710LT)	Laborservice
Syringes (Hamilton 100 µl, 250 µl)	Techlab
Syringes (Omnifix-F, 9161406V)	B. Braun
Tubes for cell culture (15, 50 ml)	Falcon
Tubes for molecular biology, safelock (1.5 ml, 2 ml)	Eppendorf
Tubes for FACS™ (5 ml)	Falcon
Whatman paper	Whatman

2.1.3 Instruments and equipment

Table 3: Instruments and equipment

Type		Manufacturer
Airflow		Köttermann
Autoclave	2540EL	Systec
Autoclave	V95	Systec
Bacteria shaker	Certomat BS-T	Sartorius
Bioanalyzer	2100	Agilent
Bioruptor Pico		Diagenode
Centrifuge	Multifuge 3 S-R	Heraeus
Centrifuge	Biofuge fresco	Heraeus
Celigo		Nexcelom
Controlled-freezing box		Nalgene
Drying cabinet		Memmert
Electrophoresis chamber		Biorad
Flow cytometer	FACSCalibur™	Becton Dickinson
Freezer (-80 °C)	Hera freeze	Heraeus
Freezer (-20 °C)	Cool vario	Siemens
Fridge (+4 °C)	Cool vario	Siemens
Gel documentation	Gene genius	Syngene
Ice machine	AF 100	Scotsman
Incubator	B20	Heraeus
Incubator	Hera cell 150	Heraeus
Liquid Nitrogen Tank	L-240 K series	Taylor-Wharton
Multichannel pipette	10-100µl	Eppendorf
Heating block	Thermomixer Comfort	Eppendorf
Hemocytometer	Neubauer	Brand
Micropipettes	0.5-10µl, 10-100µl, 20-200µl, 100-1000µl)	Eppendorf
Microscope	Axio Vert 100	Zeiss

(fluorescence)		
Microscope	DMIL	Leica
Microwave oven		Siemens, AEG
Mini centrifuge	MCF-2360	LMS
Pipetting assistent	Easypet	Eppendorf
Power supplier	Standard Power Pack P25	Biometra
QRT-PCR cycler	7300 Real-time PCR	Applied Biosystems
Rotator		GLW
Scales	770	Kern
Scales	EW3000-2M	Kern
Semi-dry Transfer Apparatus	Fastblot	Biometra
SDS-PAGE chamber	Minigel-Twin	Biometra
Shaker	Polymax 2040	Heidolph Instruments
Spectrophotometer	GeneQuant II	Amersham Biosciences
Sterile Bench		Heraeus
Water bath		GFL
Western blot documentation	Gel Logic 1500 imaging system	Carestream Health, Inc.
Vortexer	Vortex-Genie 2	Scientific Industries
Water purification system	TKA GenPure	TKA GmbH

2.1.4 Chemical and biological reagents

Table 4: Chemical and biological reagents

Reagents	Manufacturer
30% Acrylamide	Sigma-Aldrich
Agar	Sigma-Aldrich
Agarose	Thermo Fisher Scientific

Ampicillin	Merck
Ammonium persulfate (APS)	Sigma-Aldrich
β-Mercaptoethanol	Sigma-Aldrich
BCP (1-brom-3-chloropropane)	Sigma-Aldrich
BenchMark™ Prestained Protein Ladder	Thermo Fisher Scientific
Blasticidin	Gibco
Bromphenol blue	Sigma-Aldrich
BS3 (bis(sulfosuccinimidyl) suberate)	Thermo Fisher Scientific
Calcein AM	Merck
DEPC (diethyl pyrocarbonate)	Sigma-Aldrich
Deoxycholic acid	Sigma-Aldrich
1 kb DNA Ladder	Thermo Fisher Scientific
dFCS (dialyzed fetal bovine serum)	Sigma-Aldrich
dNTPs	Roche
DMEM medium	Thermo Fisher Scientific
DMSO (dimethyl sulfoxide)	Sigma-Aldrich
DTT (Dithioreitol)	Sigma-Aldrich
EDTA (ethylenediaminetetraacetate)	Merck
EGTA (Ethylenglycol-bis(aminoethyl- ether)-*N*,*N*,*N*′,*N*′-tetraessigsäure	Merck
EtBr (Ethidium bromide)	BioRad
Ethanol	Sigma-Aldrich
FBS (fetal bovine serum)	Biochrom
16% Formaldehyde	Thermo Fisher Scientific
Gentamycin	Biochrom
Glycerol	Sigma-Aldrich
Glycine	Merck
G418	PAA
HBSS (Hank's buffered salt solution)	Thermo Fisher Scientific
HCl (hydrochloric acid)	Merck

HEPES	Sigma-Aldrich
HiPerfect Transfection Reagent	Qiagen
Isoflurane	Abbott
Isopropanol	Sigma-Aldrich
KCl (potassium chloride)	Merck
KOH (kaliumhydroxid)	Sigma-Aldrich
L-Arginine (Arg+0)	Sigma-Aldrich
L-Arginine:HCL ($^{13}C_6$;Arg^{+6})	Euriso-Top
L-Arginine:HCL (U-$^{13}C_6$; $^{15}N_4$; Arg^{+10})	Euriso-Top
L-glutamine	Thermo Fisher Scientific
L-Lysine (Lys+0)	Sigma-Aldrich
L-Lysine:2HCL (4,4,5,5-D4; Lys^{+4})	Euriso-Top
L-Lysine:2HCL ($^{13}C_6$,$^{15}N_2$; Lys+8)	Euriso-Top
LiCL (Lithium chloride)	Sigma-Aldrich
Lipofectamine^{TM} 2000 Reagent	Invitrogen
L-Proline	Sigma-Aldrich
Luciferin	Caliper Lifesciences
Matrigel matrix	BD Biosciences
Maxima^{TM} Probe / ROX QRT-PCR Master Mix (2 x)	Fermentas
Methanol	Roth
Methylcellulose	R & D Systems
$MgCl_2$ (magnesium chloride)	Thermo Fisher Scientific
NaCl (sodium chloride)	Merck
$NAHCO_3$ (Natriumhydrogencarbonat)	Sigma-Aldrich
Na_2HPO_4 (sodium phosphate dibasic)	Merck
NaH_2PO_2 (sodium phosphate monobasic)	Merck
NaN_3 (sodium azide)	Merck
NaOH (sodium hydroxide)	Merck
N-Lauroylsarcosine	Sigma-Aldrich
NP-40	Thermo Fisher Scientific

PBS 10 x (phosphate buffered saline)	Thermo Fisher Scientific
PCR Buffer (10x)	Thermo Fisher Scientific
Peptone	Thermo Fisher Scientific
Penicillin / Streptomycin	Thermo Fisher Scientific
Polyprene (hexadimethrine bromide)	Sigma-Aldrich
Proteinase K	Sigma-Aldrich
Puromycin	PAA
Ready-Load 1kb DNA Ladder	Thermo Fisher Scientific
RNase A (Ribonuclease A)	Sigma-Aldrich
RPMI 1640 medium	Thermo Fisher Scientific
SDS	Sigma-Aldrich
SILAC RPMI	Thermo Fisher Scientific
Skim milk powder	Merck
TEMED (N,N,N',N'-Tetramethylethylendiamin)	Sigma-Aldrich
Tris	Merck
Triton X100	Thermo Fisher Scientific
Trypan blue	Sigma-Aldrich
Trypsin / EDTA	Thermo Fisher Scientific
Tween 20	Sigma-Aldrich

2.1.5 Commercial reagent kits

Table 5: Commercial reagent kits

Name	Manufacturer
Affymetrix GeneChip Whole Transcript Sense Target Labeling Kit	Affymetrix
Angiogenesis System: Endothelial Cell Invasion	BD Biosciences
ECL-Plus Western Blot Detection System	GE Healthcare

High-Capacity cDNA Reverse Transcription Kit	Applied Biosystems
Human Methycellulose Base Medium	R & D Systems
NucleoSpin® Plasmid Kit	Macherey-Nagel
MycoAlert Mycoplasma Detection Kit	Lonza
Pierce™ BCA Protein Assay Kit	Thermo Fisher Scientific
QIAEX II Gel Extraction Kit	Qiagen
TRI Reagent RNA Isolation Kit	Ambion
TaqMan® Gene Expression Assays	Applied Biosystems
Immunoprecipitation Kit Dynabeads Protein G	Thermo Fisher Scientific
Immunoprecipitation (IP) Kit	Biovision
ChIP-IT® qPCR Analysis Kit	Active Motif
Qiaquick PCR purification Kit	Qiagen

2.1.6 Media, buffer and solutions

Table 6: Cell culture medium and universal solutions

Name	Ingredients
Standard tumor medium	500 ml RPMI 1640, 10% FBS, 100 µg/ml Pen/Strep
DMEM medium	500ml DMEM High Glucose, 10% FBS, 1% Pen/Strep
4% formaldehyde	4% Formalin, 55 mM Na_2HPO_4, 12 mM NaH_2PO_4, 2 H_2O
FACS staining buffer	2% FBS, 0.05 %NaN_3 dissolved in 1 x PBS
SILAC tumor medium	500 ml SILAC RPMI, 10% dFCS, 1% Pen/Strep, 12ml L-Arginin (Light, Medium or heavy), 12ml L-Lysine (Light, Medium or heavy), 200mg/L L-Proline

Table 7: Buffer and gel for DNA/RNA gel electrophoresis

Name	Ingredients
TAE running buffer	50 x TAE: 2 M Tris, 10% EDTA (0.5 M), 5.71 %HCL
Electrophoresis gel	200 ml TAE (1 x), 1% agarose, 3 µl EtBr

Table 8: Buffer and solutions for cell cycle analysis

Name	Ingredients
Sample buffer	0.1% Glucose (w/v) in 1 x PBS, 0.22 µm filtration, stored at 4 °C
PI staining solution	50 µg/ml Propidium iodide and 100 U/ml RNase A in sample buffer

Table 9: Buffer and gel for western blot analysis

Name	Ingredients
Laemmli buffer (3 x)	0.5 M Tris/HCL pH 6.8, 10% SDS, 45% Glycerol, 0.1% Bromphenol blue
SDS running buffer (1 x)	25 mM Tris, 200 mM Glycine, 0.1% (w/v) SDS
Separating buffer (4 x)	1.5 M Tris, 0.4% SDS, adjusted to pH 8.8 with HCl
Separating gel (8-12,5 %)	10%: 3.33 ml 30% Acrylamide / Bis, 2.5 ml Separating Buffer (4 x), 4.17 ml water, 50 µl APS (10%), 20 µl TEMED
Stacking buffer (4 x)	0.5 % Tris, 0.4% SDS, adjusted to pH 6.8 with HCl
Stacking gel (4,5 %)	750 µl 30% Acrylamide / Bis, 1.25 ml Stacking Buffer (4 x), 3 ml water, 50 µl APS (10%), 20 µl TEMED
Transfer buffer (5 x)	25 mM Tris pH 8.3, 192 mM Glycine

TBS (10 x)	0.5 M Tris-HCL pH 7.4, 1.5 M NaCl
TBS-T	1 x TBS including 0.05% (v/v) Tween®-20

Table 10: ChIP buffer and solutions

Name	Ingredients
11% Formaldehyd solution	50 mM HEPES-KOH pH 7.5, 100 mM NaCl, 1 mM EDTA, 0.5 mM EGTA, 11% Formaldehyd
Lysis buffer 1	50 mM HEPES-KOH pH 7.5, 140 mM NaCl, 1 mM EDTA, 10% glycerol, 0.5% NP-40, 0.25% Triton X-100
Lysis buffer 2	10 mM Tris-HCL pH 8.0, 200 mM NaCl, 1 mM EDTA, 0.5 mM EGTA
Lysis buffer 3	10 mM Tris-HCL pH 8.0, 100 mM NaCl, 1 mM EDTA, 0.5 mM EGTA, 0.1% Na-Deoxycholate, 0.5% N-Lauroylsarcosine
ChIP dilution buffer	50 mM Tris-HCL pH8.0, 167 mM NaCl, 1.1% Triton X-100, 0.11% Na-Deoxycholate
Wash buffer 1	50 mM Tris-HCL pH 8.0, 0.1% SDS, 0.1% Na-Deoxycholate, 1% Triton X-100, 150 mM NaCl, 1 mM EDTA, 0.5 mM EGTA
Wash buffer 2	50 mM Tris-HCL pH 8.0, 0.1% SDS, 0.1% Na-Deoxycholate, 1% Triton X-100, 500 mM NaCl, 1 mM EDTA, 0.5 mM EGTA
Wash buffer 3	50 mM Tris-HCL pH 8.0, 250 mM LiCl, 0.5% Na-Deoxycholate, 0.5% NP-40, 1 mM EDTA, 0.5 mM EGTA

Wash buffer 4	50 mM Tris-HCL pH 8.0, 10 mM EDTA, 5 mM EGTA
Elution buffer	1% SDS, 0.1 M $NaHCO_3$

Table 11: Co-IP buffer and solutions

Name	Ingredients
Conjugation buffer	20 mM Na_3PO_4, 0.15 M NaCl (pH 7-9)
Quenching buffer	1 M Tris-HCL (pH 7.5)
PBS-T	1 X PBS including 0.001% (v/v) Tween®-20

2.1.7 Antibodies

Table 12: Antibodies for western blot or immunohistochemistry

Antibody	Source	Dilution	Product No.	Application	Manufacturer
Anti-EZH2	rabbit	1:1000	07-689	WB	Millipore
Anti-SUZ12	rabbit	1:1000	ab12073	WB	Abcam
Anti-H3	rabbit	1:5000	ab1791	WB	Abcam
Anti-H3ac	rabbit	1:3000	06-599	WB	Milipore
Anti-H3K4me2	rabbit	1:1000	ab32356	WB	Abcam
Anti-H3K4me3	rabbit	1:1000	ab8580	WB	Abcam
Anti-H3K9me2	mouse	1:1000	ab1220	WB	Abcam
Anti-H3K27me3	rabbit	1:5000	pAb-195-050	WB	Diagenode
Anti-H3K27ac	rabbit	1:1000	ab4729	WB	Abcam
Anti-FLI1	rabbit	1:1000	35980	WB, Co-IP	Cell Signaling
Anti-BRD2	rabbit	1:1000	5848	WB	Cell Signaling
Anti-BRD3	mouse	1:500	sc-81202	WB	Santa-Cruz

Anti-BRD4	rabbit	1:1000	ab128874	WB,ChIP, Co-IP	Abcam
Anti-β-Tubulin	rabbit	1:1000	15115	WB	Cell Singaling
Anti-P-CDK9	rabbit	1:1000	2549	WB	Cell Signaling
Anti-PARP	rabbit	1:1000	9532	WB	Cell Signaling
Anti-Caspase3	rabbit	1:200	9664	WB, IHC	Cell Signaling
Anti-Caspase7	mouse	1:1000	9494	WB	Cell Signaling
Anti-rabbit IgG HRP	bovine	1:1000	sc-2370	WB	Santa-Cruz
Anti-mouse IgG HRP	goat	1:1000	sc-2031	WB	Santa-Cruz
Anti-FLAG	mouse	1:1000	F1804	WB, Co-IP	Sigma-Aldrich

2.1.8 Small interfering RNAs

Small interfering RNAs (siRNAs) were obtained from Qiagen.

Table 13: Small interfering RNAs

siRNA Name	Target sequence (5`->3`)
Control (non-silencing)	AAT TCT CCG AAC GTG TCA CGT
EZH2_2	AAG CAA ATT CTC GGT GTC AAA
EZH2_7 validated	AAC CAT GTT TAC AAC TAT CAA
BRD2_8	AAG TAG CAG TGT CAC GCC TTA
BRD3_8	ACG CCG CCT GTC GTC AAG AAA
BRD4_9	ATG GAC TAG AAA CTT CCC AAA

2.1.9 Oligonucleotides for qRT-PCR

The concentration was 900 and 250 nM, respectively.

Table 14: Primers for qRT-PCR

Name	Sequence (5`->3`)
EWS-FLI1-for	TAG TTA CCC ACC CAA ACT GGA T
EWS-FLI1-rev	GGG CCG TTG CTC TGT ATT CTT AC
pSIREN-for	GGG CAG GAA GAG GGC CTA T
pSIREN-rev	GAG ACG TGC TAC TTC CAT TTG TC

Table 15: Primers for ChIP-qRT-PCR

Name	Sequence (5`->3`)
EWSR1-for	CGA CCG TCC CTA GAG CCA
EWSR1-rev	GAC ACT CGG GCC AAA ATA GC
Negative-for	TAG TGC AAA CAA CCC TGG CT
Negative-rev	GCT TTG ATG ACT TTT TCT GAG ACT

2.1.10 Gene expression assays for qRT-PCR

All TaqMan Gene Expression Assays were obtained from Applied Biosystems.

Table 16: TaqMan gene expression assays

Gene	Assay ID
EZH1	Hs00940463_m1
EZH2	Hs00544830_m1
SUZ12	Hs00248742_m1

EED	Hs00537777_m1
EPHB2	Hs00362096_m1
CDK9	Hs00977896_g1
MYC	Hs00153408_m1
BRD2	Hs01121986_g1
BRD3	Hs00978980_m1
BRD4	Hs04188087_m1
BRDT	H200976114_m1
IFITM1	Hs00705137_s1
G1P2	Hs01921425_s1
CCND1	Hs00765553_m1
CCNT1	Hs01059085_m1
STK32B	Hs01031449_m1
STEAP1	Hs00185180_m1
GPR64	Hs00971379_m1
DKK2	Hs00205294_m1
PAPPA	Hs01032307_m1
HOXD10	Hs00157974_m1
NANOG	Hs02387400_g1
CFLAR	Hs01116280_m1
XIAP	Hs00745222_s1
GAPDH	Hs99999905_m1

2.1.11 Human cell lines, bacterial strains and mouse strains

2.1.11.1 Human cell lines

All Human cell lines were provided by the German Collection of Microorganisms and Cell Cultures (DSMZ), except for A673, which was purchased from ATCC (LGC Standards). Human primary cell line SB-KMS-KS1, previously known as SBSR-AKS, was generated in the laboratory and EW7 ES cell line was kindly provided by Prof. Olivier Delattre (Institut National de la Santè et de la Recherche Medicale U830, Paris, France). Packaging cell line 293FT for lentivirus production was obtained from Invitrogen.

Table 17: Description of human cell lines used

Cell line	Description
293FT	Highly transfectable derivative of cell line 293 transduced with the SV40 T-antigen. Capable of producing high lentivirus titers.
A673	ES cell line (type 1 translocation) with p53 mutation, established from the primary tumor of a 15-year-old girl.
A673-Luc	ES cell line A673 transfected in our lab to express firefly luciferase for bioluminescent measurements.
EW7	ES cell line (type 1 translocation), established from the primary tumor localized on scapula of an Ewing Tumor patient.

L87	Bone marrow derived human stromal cell line immortalized with SV40 large T-antigen
MG-63	Osteosarcoma cell line, established from the bone of a 14-year-old Caucasian boy.
MHH-ES1	ES cell line (type 2 translocation), established from the ascites of a 12-year-old Turkish boy with a tumor of the left pelvis and additional peritoneal metastases.
MHH-NB11	Neuroblastoma cell line, established from an adrenal metastasis of a 4-year-old Caucasian boy.
RDES	ES cell line (type 2 translocation), established from the primary tumor of a 19-year-old Caucasian man localized in the humerus.
SB-KMS-KS1	ES cell line (type 1 translocation), established from an extraosseous inguinal metastasis of a 17-year old girl (new nomenclature, originally designated as SBSR-AKS).
SB-KMS-DA	ES cell line (type 2 translocation, fusion of EWS exon 9 and FLI1 exon 5), established from a sacral bone biopsy of an 18-year old girl
SHSY5Y	Neuroblastoma cell line, established from a bone marrow biopsy of a 4-year-old girl with metastatic neuroblastoma.
SK-N-MC	ES cell line (type 1 translocation), established from the supraorbital

	metastases of a 14-year-old girl (Askin's tumor, related to ES)
TC-71	ES cell line (type 1 translocation), established in 1981 from a biopsy of recurrent tumor of a 22-year-old man with metastatic ES (humerus).
U2OS	Osteosarcoma cell line, established from the bone of a 15-year-old Caucasian girl.
VH54.2	Peripheral blood derived human mesenchymal cell line immortalized with SV40 large T-antigen

2.1.11.2 Bacterial strains

The following strains were used for plasmid enrichment to generate stable knock-downs by lenti- or retroviral gene transfer.

Table 18: Description of bacteria strains used

E. coli strain	Genotype description	Origin
One Shot® TOP10 Chemically Competent	F- *mcrA* Δ(*mrr-hsd*RMS-*mcr*BC) ϕ80*lac*ZΔM15 Δ *lac*X74 *rec*A1 *ara*D139 Δ(*araleu*)7697 *gal*U *gal*K *rps*L (StrR) *end*A1 *nup*G	Invitrogen
One Shot® Stbl 3 Chemically Competent	F^-*mcr*B *mrrhsd*S20(r_B^-, m_B^-) *rec*A13 *sup*E44 *ara*-14 *gal*K2 *lac*Y1 *pro*A2 *rps*L20(Str^R) *xyl*-5 λ^- *leumtl*-1	Invitrogen

2.1.11.3 Mouse strains

Table 19: Description of mouse strains used

Mouse strain	Characteristics	Origin
BALB/c Rag2$^{-/-}$ $\gamma_c^{-/-}$	No T-lymphocyte and B-lymphocyte generation and no NK cell function	Central Institute for Experimental Animals (Kawasaki, Japan)

The Recombination activating gene 2 (Rag2)-*gamma(c)* knock-out (Rag2$^{-/-}$ $\gamma_c^{-/-}$) mouse is an immunodeficient model that can be used in studies to test *in vivo* conditions. This gene manipulated mouse strain was generated by backcrossing of two immunocompromised mouse models, the gamma(c) knock-out and the Rag2 knock-out mice. The homozygous *gamma(c)* knock-out mice has no *gamma(c)* receptor gene, why the development of lymphocytes is severely compromised. Consequently, natural killer (NK) cell population is severely decreased in these mice, but they do have a small number of T- and B-lymphocytes. To eliminate the T and B cell population, the *gamma(c)* knock-out mouse was back-crossed onto the *Rag2* knock-out mouse. Homozygous Rag2 knock-out mice do not have several exons of the *Rag2* gene, resulting in the inability to initiate V(D)J rearrangement which is responsible for the viability of antibodies. Therefore, these *Rag2* knock-out mice are incapable of generating any T- and B-lymphocytes [130].
Thus, the back-crossed Rag2$^{-/-}$ $\gamma_c^{-/-}$ mice had neither T-lymphocytes and B-lymphocytes nor NK cell functions.

2.1.12 Expression vectors

Expression vector for lentivirus mediated and doxycycline induced RNAi were obtained from Dharmacon (part of Thermo Fisher Scientific).

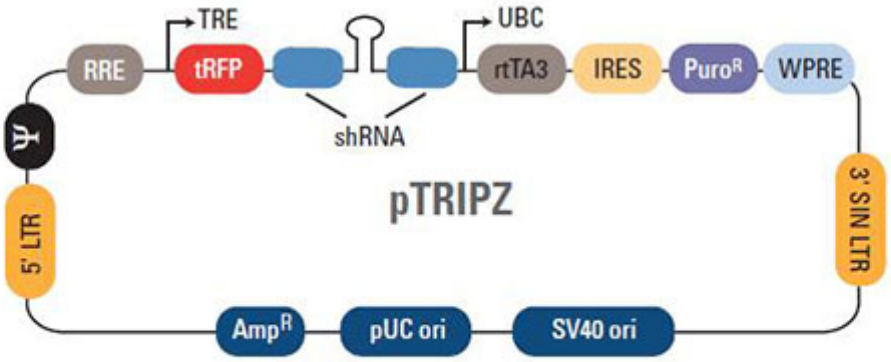

Figure 1: pTRIPZ vector for inducible RNAi. pTRIPZ vector for inducible and stable RNAi was obtained from Dharmacon (part of Thermo Fisher Scientific).

2.2 Methods

2.2.1 Cell culture

ES sarcoma (A673, SK-N-MC, TC-71, RDES, MHH-ES1 and SB-KMS-KS1), neuroblastoma (MHH-NB1, SHS5Y), osteosarcoma (U2OS, MG-63) and mesenchymal stem cell lines (L87, VH54.2) were cultured in either 20 ml standard tumor medium and a medium sized flask (75 cm^2) or 30 ml and a large size flask (175 cm^2) at 37 °C and 5 % CO_2 in a humidified atmosphere. Approximately every three days cells were split 1:4 and cultured in fresh medium.

The lentivirus packaging cell line 293FT was cultured in flasks with 25 ml of D-MEM medium containing 10 % FBS, 2 mM L-glutamine, 0.1 mM MEM Non-Essential Amino Acids, 1 mM MEM Sodium Pyruvate and 1 % Gentamycin. Cells grew as well at 37 °C (8 % CO_2) in a humidified atmosphere.

Depending on the given cell line, concentrations ranging from 1 x 10^6 to 1 x 10^7 cells per ml FBS / 10% DMSO were transferred to pre-cooled cryovials and placed in a freezer box for 12 - 18 h at -80 °C. Subsequently, they were moved to liquid nitrogen (-192 °C) for long-time storage. To re-culture the cryopreserved cells, cryovials were thawed at room temperature. As soon as the content became fluid it was rapidly moved to a tube containing 10 ml standard tumor medium. Cells were pelletized by centrifugation for 5 min. at 1500 rpm, resuspended in pre-warmed standard tumor medium and transferred to a culture flask. Cell amounts were counted with a Neubauer hemocytometer. Cell viability was assessed by Trypan-Blue (Sigma) staining. Contamination by mycoplasma bacteria was routinely checked using MycoAlert™ Mycoplasma Detection Kit (Lonza) per manufacturer's instructions.

2.2.2 RNA isolation

RNA from frozen tissue or cultured cells was isolated using TRI Reagent RNA Isolation Kit per manufacturer`s instruction (Thermo Fisher, Revision August 30, 2010).

Briefly, up to 1 x 10^7 cells were resuspended in TRI Reagent solution and either used immediately or stored at -80 °C for further use. Lysed cells were then mixed with 100 µl BCP (per ml TRI Reagent) by vortexing and incubated on ice for 5 - 15 min. Subsequently phases were separated by centrifugation (12000 x g) for 5 min. at 4 °C. The aqueous phase which contains the RNA was then separated and mixed with 500 µl Isopropanol by vortexing. After an incubation for 10 min. on ice, precipitated RNA was centrifuged again at 4 °C and 12000 x g for 8 min. The RNA was then washed with 1 ml 75 % Ethanol, centrifuged at 7500 x g and 4 °C for 5 min. and briefly air dried. The remaining RNA pellet was resuspended in DEPC-treated H_2O. RNA concentration was measured at 260 nm using a nanophotometer and stored at -80 °C.

2.2.3 Reverse transcription

To analyze gene expression within cells by quantitative real-time polymerase chain reaction (qRT-PCR), previously isolated RNA must be transcribed into complementary DNA (cDNA). Therefore, 5.8 µl reverse transcription master mix containing dNTPs, MultiScribe™ Reverse Transcriptase, random primers and buffer of the High-Capacity cDNA Reverse Transcription Kit (Thermo Fisher) was mixed with 14.2 µl RNA solution (containing 1 µg purified RNA). The cDNA was then synthesized using the following conditions: 10 min. 25 °C; 120 min. 37 °C; 5 min. 85 °C; ∞ 4 °C. The synthesized cDNA was either instantly used or stored at -20 °C.

2.2.4 Quantitative real-time PCR (qRT-PCR)

2.2.4.1 Standard real-time PCR

Quantification of synthesized cDNA was done by qRT-PCR. This allows for a sequence specific quantification using a fluorescent reporter that specifically hybridizes to a corresponding sequence at the gene of interest. Detection of the fluorescence is done after breakdown of the sample by exonuclease activity of the Taq polymerase. This polymerase specifically amplifies the target sequence that was bound by a specific primer. For qRT-PCR, Maxima™ Probe / ROX qPCR Master Mix (2x) was used per manufacturer`s instructions. Briefly, 10 µl of the Maxima™ Probe / ROX qPCR Master Mix (2x) (containing Hot Start Taq DNA Polymerase, PCR buffer and dNTPs) was used together with specific TaqMan® Gene Expression Assays (Thermo Fisher) (consisting of two unlabeled PCR primers and a FAM™ dye-labeled TaqMan® MGB probe). The reaction mix was prepared per manufacturer`s instructions: 10 µl of Maxima™ Probe / ROX qPCR Master Mix (2x) was mixed with 1 µl specific TaqMan® Gene Expression Assay (Table 16), 0.5 µl

cDNA and 8.5 µl RNase-free water. The final concentration of primers and probe were 0.9 and 0.25 µM, respectively. The resulting gene expression profiles were normalized to the expression of the housekeeping gene *glyceraldehyde 3-phosphated dehydrogenase* (GAPDH) and calculated using the 2^{-ddct} method. Microsoft excel was used to calculate the mean value, standard deviations of duplicates and the standard error of the mean of at least two independent experiments. Conventional t-test was carried out to determine the statistical significance. Fluorescence was detected and measured in a StepOnePlus™ Real-Time PCR System (Thermo Fisher) using a three-step cycling protocol: 1 s 50 °C; 10 min. 95 °C; [15 s 95 °C; 1 min. 60 °C] x 40.

2.2.4.2 qRT-PCR using SYBR Green

SYBR Green is a highly specific dsDNA binding fluorescent dye that enables detection of all amplified PCR products without requiring specific dye-labeled probes (SYBR Green-based detection). SYBR Green based qRT-PCR was performed using POWER SYBR™ GREEN PCR Master Mix (Thermo Fisher) containing Green I dye, AmpliTaq Gold® DNA Polymerase, PCR buffer and dNTPs. qRT-PCR was done per manufacturer`s instruction (Active Motif). Briefly, specific primer pairs (2.5 µM each) and 5 µl DNA template were added to 10 µl Master Mix. Gene expression profiles were normalized to a non-regulated genomic loci. The mean value and standard deviation of duplicates are displayed graphically using Microsoft Excel. Statistical significance was determined by conventional t-test. Fluorescence was again detected and measured with StepOnePlus™ Real-Time PCR System (Thermo Fisher) using a two-step cycling protocol: 10 min. 95 °C; [15 s 95 °C, 20 s 58 °C, 20 s 72 °C] x 40.

2.2.4.3 Detection of EWS-FLI1

EWS/FLI1 gene expression levels were detected by specific designed assays and used as followed: 10 µl Maxima™ Probe/ROX qPCR Master Mix (2x) and 7.6 µl of RNase-free water were mixed with 0.6 µl of each primer (0.3 µM) and 0.4 µl of FAM probe (0.2 µM) to a final volume of 19.5 µl per sample in a 96-well plate. Corresponding cDNA was then added (0.5 µl per sample). Expression profiles were normalized to the mRNA levels of the housekeeping gene *glyceraldehyde 3-phosphate dehydrogenase* (*GAPDH*) and calculated using the 2^{-ddCt} method.

Table 20: EWS-FLI1 qRT-PCR primer and probe sequences

Sense primer	5'-TAG TTA CCC ACC CAA ACT GGA T-3'
Antisense primer	5'-GGG CCG TTG CTC TGT ATT CTT AC-3'
FAM probe	5'-FAM-CAG CTA CGG GCA GCA GAA CCC TTC TT-TAMRA -3'

2.2.5 Transient RNA interference

For transient protein knock-down, cells were transfected with small interfering RNA (siRNA). Per manufacturer instructions for large-scale transfections in 100 mm dishes (Qiagen Handbook 05/2008), 1 – 3 x 10^6 cells were plated at a final volume of 12 ml standard medium containing 5 nM siRNA (Table 13) and 36 µl HiPerfect Transfection Reagent. Cells were incubated for 48 - 72 h at 37°C (5 % CO_2) in a humidified atmosphere and RNA was isolated subsequently (see 2.2.2). The reverse transcribed cDNA was then analyzed by qRT-PCR and gene knock-down was examined by qRT-PCR (see 2.2.4). To avoid specificities, different genes were investigated and different siRNAs analyzed. In addition, mRNA levels of the interferon (IFN) response genes (*ubiquitin-like modifier ISG15* (*ISG15)* and

interferon-induced transmembrane protein 1 (*IFITM1)*) were monitored using specific gene expression assays (Table 16).
If mRNA expression of one of these genes was induced more than twofold after siRNA treatment, the respective siRNA was not used for further experiments [18].

2.2.6 Lentivirus mediated and inducible stable RNA interference

For an inducible and reversible knock-down of proteins, 1 - 4 different shRNA constructs were selected (provided by Dharmacon as glycerol stocks). Upon arrival, stocks were expanded and plasmid DNA was purified by NucleoSpin® Plasmid Kit per manufacturer`s instructions (Macherey-Nagel Manual 03/2005/ Rev. 02) and quantitated by a nanophotometer. Lentiviral particles for transduction of target cells were generated per manufacturer`s instructions. Briefly, 1 x 10^6 HEK293T cells were seeded in a 6-well plate and cultured with D-MEM medium under normal conditions for 24 h. For transfection of HEK293T cells a prior prepared mix of 6 µg purified DNA plasmid, 4.3 µl Trans-Lentiviral Packaging Mix containing the pTRIPZ vector (see 2.1.3, Fig. 2) (Thermo Fisher Scientific), 15 µl $CaCl_2$ and 150 µl 2X HBSS was added dropwise for each well of a 6-well plate. Cells were incubated subsequently for 10 - 16 h at normal conditions. After 16 h of incubation medium was removed and reduced serum medium (DMEM, 5% FBS, 2 mM L-Glutamine and 1 % Pen/Strep) added. Viral particle-containing supernatant was harvested 48 h after the medium change and centrifuged at 1600 x g for 10 min. at 4°C. Aliquots were prepared and stored at -80 °C.
For the generation of stable and inducible RNAi cell lines, 1 – 3 x 10^5 target cells were seeded into a 6-well plate and culture with 2 ml serum reduced medium (RPMI 1640, 5 % FCS, 1 % Pen/Strep) for 24 h. The next day 1 ml of serum was removed and substituted with 1 ml of Lentiviral particle-containing supernatant and incubated for 24 – 48 h. Virus containing medium was discarded subsequently and transduced target cells cultured for 48 h

with normal medium und normal culture conditions. 2 µg/ml Puromycin was added subsequently to select for stably transduced cells. Knock-down efficiency was analyzed by qRT-PCR and western blotting and compared to negative controls (pTRIPZ$^{neg.shRNA}$). As described in 2.2.5, mRNA levels of *ISG15* and *IFITM1* were monitored to exclude an induction of IFN response.

2.2.7 xCELLigence proliferation assay

Proliferation of different adherent cell lines was measured in an impedance-based, label-free real-time analysis system (xCELLigence, Roche/ACEA Biosciences) previously described [33]. Briefly, 1 - 3 x 10^4 cells were seeded into 96-well E-plates with 200 µl standard tumor medium and allowed to grow up to 72 - 160 h. Cellular impedance was measured periodically every 4 h across interdigitated gold micro-electrodes on the bottom of tissue culture E-plates. The presence of the cells on top of the electrodes will affect the local ionic environment at the electrode/solution interface, leading to an increase in the electrode impedance, which is displayed as cell index (CI) values. The more cells attach to the electrodes, the larger the increase in electrode impedance.

2.2.8 Cell cycle analysis

Cell cycle analysis was performed using flow cytometry and propidium iodide (PI) staining as an DNA double-stranded intercalating agent that emits a fluorescence signal after excitation at 488 nm. The fluorescence intensity of the stained cells correlates to the amount of DNA they contain. This also allows the differentiation between different cell cycles as cells in the G_2/M phase have, due to DNA duplication in the intermediate S phase, twice the amount of DNA as cells in the G_0/G_1 phase.

To analyze these differences, 2 x 10^6 cells per sample were washed twice with pre-cooled sample buffer (Table 6) and centrifuged for 10 min. (4 °C) at 12000 rpm. Subsequently, cells were fixed for 18 – 24 h and 4 °C by drop-wise addition of 1 ml of 70 % ethanol and continuous vortexing. After incubation cells were centrifuged and resuspended in 1 ml staining buffer containing RNase A and PI to remove any RNA for 30 – 60 min. under room temperature and constant agitation. Cell cycle was analyzed in a FACScalibur™ Flow cytometer.

2.2.9 Western blot (WB)

Procedures were essentially as describe previously [18]. Cells were trypsinized, counted and washed twice with 1 x PBS. 2 – 4 x 10^6 cells were resuspended in 200 µl 3 x Laemmli (containing 50 µl β-Mercaptoethanol per 1 ml 3 x Laemmli) and incubated for 10 min. at 70 °C to denature proteins. Lysates were then homogenized through a 23 gauge needle and centrifuged for 5 min at 14000 rpm. Aliquots of the supernatants were stored at -80 °C or immediately processed for SDS-polyacrylamide gel electrophoresis (SDS-PAGE).

Depending on the molecular weight of the protein of interest, 8 - 12.5 % polyacrylamide gels were used for SDS-PAGE. 10 – 30 µl of protein sample were transferred to the gel and electrophoresis was carried out at 100-120 V for 1.5 - 2.5 h. Molecular weight of the separated proteins was determined by comparison with a prestained molecular weight standard.

For the detection of specific proteins, polyacrylamide gel containing separated proteins was sandwiched between Whatman filter paper (soaked in 1 x transfer buffer, Table 9) and transferred onto a PVDF membrane for 2 h at 0.8 mA / cm^2 using a “Semidry”-Blot device. Unspecific binding sites were blocked by incubating the membrane in 5 % skimmed milk / 0,05 % Tween 20 for 1 h at room temperature or overnight at 4 °C and continuous shaking.

The pre-blocked membrane was then incubated with primary antibody (Table 11) of interest for appropriate time. Dilution of the antibodies was done per manufacturer`s instructions (Table 11) in 5 % skim milk / 0.05 % Tween 20. Subsequently, the membrane was washed three times (5 min. per wash) in 1 x TBS-T, incubated for 1 h with secondary horseradish peroxidase (HRP) coupled antibody and washed again twice with 1 x TBS-T and once with 1 x TBS.

Antibody-antigen complexes were detected using the ECL-Plus Western Blotting Detection System (GE Healthcare Booklet RPN2132PL Rev D 2006) per manufacturer`s instructions. Signals of antibody-antigen complexes were detected with the Gel Logic 1500 imaging system and analyzed with Kodak Molecular Imaging Software (Version 5.0).

Reactivation of the dried PVDF membrane was done by incubating it for 1 min. at room temperature with methanol and immediate washing with 1 x TBS-T. Blocking of the membrane was done as previously for 1 h in 5 % skim milk / 0.05 % Tween 20.

2.2.10 Chromatin immunoprecipitation (ChIP)

Cells were seeded at 6 – 10 x 10^6 cells in a large cell culture flask and cultivated under normal conditions for 24 – 72 h. Crosslinking was performed with 1 x formaldehyde diluted in formaldehyde solution (Table 10) for 10 min. under constant agitation. Remaining formaldehyde was quenched for 5 min. by adding 0.125 M glycine. Cells were then scraped from the culture flask, centrifuged for 5 min. and 2000 g, washed in ice-cold 1X PBS and centrifuged as before. The remaining pellet was either stored at -80 °C or used immediately for cell lysis by resuspension in lysis buffer 1 (Table 10) and incubation for 10 min. at 4 °C. Cells were than centrifuged for 5 min. at 2000 g (4 °C) and resuspended subsequently with lysis buffer 2 for 10 min. (4 °C). The released chromatin was centrifuged for 10 min. and 2000 g (4

°C) and resuspended in lysis buffer 3. Chromatin was cut by sonication in a Bioruptor® Pico (Diagenode) to an average length of 200 – 600 bp. Sample was then centrifuged at 14000 rpm for 10 min. (4 °C) to remove remaining cell debris and Input sample was taken. Preclearing was done by 2 h incubation with IgG pre-blocked protein G magnetic beads at constant rotation (4 °C). The pre-cleared sample was then incubated overnight with desired antibody. Beads for immunoprecipitation were also incubated overnight with 1 mg/ml BSA. The next day BSA blocked beads were washed thrice with washing buffer 1 (Table 10). Chromatin-antibody conjugates were then incubated with pre-blocked beads for 3 h at 4 °C. Conjugates were then washed twice with wash buffer 1, once wash buffer 2, once wash buffer 3, twice wash buffer 4 for 5 min at 4°C each. Chromatin was eluted in 130 µl elution buffer (Table 10) at 65 °C for 15 min. Supernatant was collected and remaining chromatin re-eluted in 100 µl as before. Reverse crosslinking was performed by addition of ribonuclease A (final concentration 200 µg/ml) and incubation for 45 min. at 37 °C. Proteins were removed by addition NaCl (final concentration 200 mM), proteinase K (final concentration 200 µg/ml) and incubation at 65 °C overnight. DNA was purified with QIAquick PCR purification Kit (Qiagen). DNA concentration was measured with the Qubit® DNA HS Kit (Thermo Fisher) on a Celigo® (Nexcelom) and quality was assessed on the 2100 Bioanalyzer (Agilent) with the Agilent High Sensitivity Kit. Specificity was analyzed by qRT-PCR (see 2.2.4.2) and specific primer (Table 15).

2.2.11 Co-immunoprecipitation (Co-IP)

For Co-IP cells were seeded at 6 – 10 x 10^6 cells in a 150 mm^2 cell culture dish and cultivated under normal conditions until cells reached 90 % confluence. Medium was discarded and cells washed twice with ice-cold 1X PBS. Non-denaturating lysis reagent (Biovision) was prepared by adding Protease Inhibitor Cocktail per manufacturer's instructions. Culture plate was put on ice and 1.5 ml Lysis Buffer was added per culture dish and distributed

equally. After 1 min. incubation cells were scraped off and transferred into a pre-chilled 15 ml Falcon tube. Cells were then incubated for 30 min. at 4 °C and constant rotation on a rotary mixer followed by centrifugation at 10.000 x g for 10 min. at 4 °C. The supernatant which contains the proteins were then transferred into a new 15 ml falcon tube. Protein concentration was measured by bichinonic acid assay (BCA) (Thermo Fisher). Protein G magnetic beads where resuspended and 50 µl per Co-IP transferred into a new 1.5 ml tube. After 1 min. incubation on a magnetic stand, the supernatant was removed and protein G magnetic beads resuspended in 200 µl PBS-T (pH 7.4; 0.001 % Tween®-20) containing Antibody of interest (typically 1 – 10 µg) for 30 min. at room temperature and constant rotation. The tube was then placed on a magnetic stand for 1 min. and the supernatant was removed. The Ab-beads conjugate was then washed twice in 200 µl conjugation buffer (Table 11), resuspended in 250 µl 5 mM BS3 (Thermo Fisher) and incubated for 30 min. at room temperature and constant rotation. Cross-linking was quenched by adding 12.5 µl quenching buffer for 15 min. followed by three times washing with 200 µl PBS-T. Sample containing the desired antigen was added (typically 700 - 1000 µg) and incubated for 30 min. at room temperature and constant rotation. The beads-antibody-antigen conjugate was then washed three times using 200 µl washing buffer (Immunoprecipitation Kit, Thermo Fisher Scientific) and the proteins eluted in NuPAGE LDS sample buffer for 10 min. at 95 °C. Samples were then further analyzed by western blotting or mass spectrometry.

2.2.12 Colony forming assay

Procedures were done as previously described [18]. 5 x 10^3 cells were resuspended in 300 µl cell resuspension solution and seeded in duplicates into a 35 mm plate containing 1.5 ml methylcellulose-based medium (R&D Systems) per manufacturer`s instructions and cultured for 10 – 14 days at 37°C (5 % CO_2) in a humidified atmosphere.

2.2.13 Invasion assay

Cell invasion was analyzed as previously described [18] by use of the BioCoat Angiogenesis System: Endothelial Cell Invasion Assay per the manufacturer's instructions (BD Bioscience Manual SPC-354141-G rev 3.0). Briefly, the plate containing the microporous membrane was adjusted to room temperature. Pre-warmed RPMI medium was added to the insert wells and allowed to rehydrate the membranes for 2 h at 37 °C (5 % CO_2) in a humidified atmosphere. Subsequently, the medium was removed and 5 x 10^4 cells resuspended in RPMI without FBS were added to each insert well. As a chemoattractant, 700 µl RPMI containing 10 % FBS was added to the bottom of the wells. RPMI medium without FBS was used as a negative control and added to the bottom of the remaining wells. After 48 h, invasive cells at the bottom side of the membrane were stained with Calcein AM solution. Therefore, inserts were transferred to a new BD Falcon 24-well plate containing 0.5 ml/well Calcein AM (4 µg/ml) in pre-warmed HBSS (Hank`s buffered salt solution) with 0.15 % DMSO and incubated for 90 min. at 37 °C (5 % CO_2) in a humidified atmosphere. Cells were imaged by fluorescence microscopy using a Zeiss AxioVert 100 with AxioVision 4.7.1 software.

2.2.14 Endothelial differentiation assay

Endothelial differentiation was done as previously described [18, 131] using the Matrigel matrix assay per manufacturer's instruction (BD Biosciences Manual SPC-356234 Rev 5.0). Briefly, 4 - 7 x 10^4 cells were seeded per well onto 75 µl Matrigel at a final volume of 100 µl in a 96-well plate and incubated for 24 - 48 h at 37 °C (5 % CO_2) in a humidified atmosphere. Following, cells were washed once with 1 x PBS and stained with 1 µg/ml Calcein AM for 30 min. in the dark. Cellular tube formation was examined by fluorescence microscopy using a Nikon Eclipse TS 100 with an attached Nikon Coolpix 5400 camera.

2.2.15 Mice and *in vivo* experiments

All experiments were performed in 6 – 16 week-old immunodeficient Rag2$^{-/-}$ $\gamma_c^{-/-}$ mice on a BALB/c background. Mice were obtained from the Central Institute for Experimental Animals (Kawasaki) and maintained under pathogen-free conditions in accordance with the institutional guidelines and approval by the Regierung von Oberbayern.

To analyze *in vivo* tumor growth, 2 – 4 x 10^6 ES cells resuspended in 150 - 200 µl PBS and injected subcutaneously either into the inguinal or the lower back region using a 26-gauge needle attached to a 1 ml syringe. The amount of 2 – 4 x 10^6 cells has been previously reported to be optimal for assessment of local growth of ES xenografts [18, 132]. Tumor size was assessed by regular caliper measurement. Mice bearing tumors > 10 mm in diameter were considered positive and sacrificed. Tumors were excised and subjected to immunohistochemistry (see 2.2.14) and RNA was isolated for *ex vivo* gene expression analysis (see 2.2.2, 2.2.3 and 2.2.4).

Metastatic potential of tumor cells was analyzed by intravenous injection. Five weeks later mice were euthanized and metastasis was monitored in individual organs. Visible metastases within the dissected organs were counted. Tumors and affected tissues were excised for histology and gene expression analysis.

2.2.16 Immunohistochemistry (IHC) of murine samples

Histological analysis was done in cooperation with Dr. Julia Calzada-Wack and Dr. Katja Steiger (Institute of Pathology, Helmholtz Center Munich, Neuherberg; and Institute of General Pathology and Pathological Anatomy, Klinikum rechts der Isar, TU Munich, Germany). Tumors and affected organs were fixed in 4 % formaldehyde and embedded in paraffin. Sections of 3 – 5 µm were cut from each sample and stained with hematoxylin and eosin (H&E), as previously described [18, 33]. Apoptosis was analyzed by staining with caspase 3 antibody (Table 11). All sections were reviewed and interpreted by two pathologists.

2.2.17 Microarray analysis

Microarrays were done at our Core Expression facility and used to analyze changes in expression profiles after knock-down or inhibitor treatment. Experiments were essentially done as previously described [18, 33, 133]. RNA from cells of interest was isolated (see 2.2.2), quantified spectrophotometrically and RNA quality was analyzed by 0.7 % agarose gel electrophoresis or the Agilent RNA 6000 Nano Kit on a 2100 Bioanalyzer (Agilent). Total RNA (200 ng) was amplified and labeled using Affymetrix GeneChip Whole Transcript Sense Target Labeling Kit per manufacturer`s instructions. cRNA was hybridized to a Affymetrix Human Gene 1.0 ST array and analyzed by Affymetrix software expression console, version 1.1. For data analysis, robust multichip average (RMA) normalization was performed, including background correlation, quantile normalization, and median polish summary method. For the identification of differentially expressed genes, significance analysis of microarrays (SAM) was used [134]. Transcripts were functionally assigned using GO-annotations (http://www.cgap.nci.nih.gov). Gene set enrichment analysis (GSEA) and pathway analysis was performed with the GSEA tool (http://www.broad.mit.edu/gsea) [135]. Probes of the normal body map (NBA) included tissues of normal PBMC, bone marrow, spleen, thymus, stomach (2), small intestine, colon with mucosa, heart, liver, lung, skeletal muscle, brain (whole), brain cerebellum, spinal cord, trachea, salivary gland, prostate, testis, uterus, fetal brain, and fetal liver. Array data were submitted at GEO (GSE45544) [133].

2.2.18 Statistical analysis

Data are mean ± SEM as indicated. Differences were analyzed by unpaired two-tailed student's t-test using Microsoft Excel or Prism 5 (GraphPad Software); p values < 0.05 were considered statistically significant.

3 Results

3.1 BET bromodomain proteins and downstream targets in Ewing sarcoma

3.1.1 MYC expression is significantly up-regulated in Ewing sarcoma

In a previous analysis, customized high-density DNA microarrays (EOS-Hu01) containing 35356 oligonucleotide probe sets were used to analyze a total of 25194 gene clusters. Thereby, 22 ES samples were analyzed and compared to 10 osteosarcoma and 23 normal tissues of diverse origin [133] One of the genes that showed up as constantly up-regulated in contrast to normal tissue was MYC, an oncogene that facilitates diverse functions and biological effects and is known to be activated in a variety of different of cancers (Figure 2) (reviewed in [120, 136, 137]).

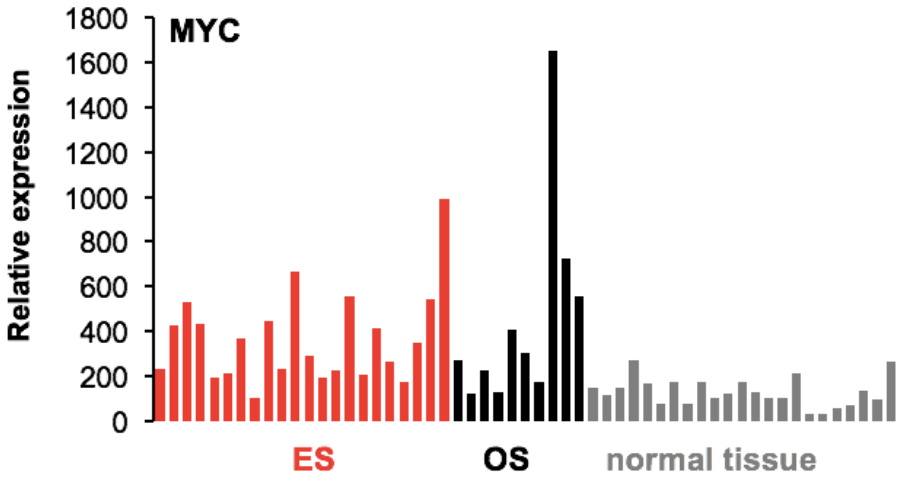

Figure 2: MYC expression in ES compared to osteosarcoma and normal tissue. Microarray data of primary ES samples (red), osteosarcoma (OS) (black) and normal body tissue (gray) shows a significant up-regulation of MYC in comparison to normal tissue.

Even though MYC has long been known as an important player in carcinogenic regulation, it is also considered as undruggable since it has no known “active site” accessible by conventional small drug-like molecules (reviewed in [138]). A common approach to analyze MYC is therefore to target possible upstream regulators. Here we selected two prominent players frequently described to regulate MYC expression.

3.1.2 PI3K/mTOR pathway and BET bromodomain proteins in ES

The Phosphatidylinositol-4,5-bisphosphate 3-kinase (PI3K) and mechanistic target of rapamycin (mTOR) pathway was recently described to modulate EWS-FLI1 gene expression [139]. Moreover, numerous studies not only demonstrated the importance of the PI3K/mTOR pathway for the support of ES growth [140-145] but also revealed to control MYC expression as well as its cooperation’s in deregulated cell proliferation and transformation [146-149] (Figure 3A). Therefore, we analyzed PI3K and mTOR expression in ES tumor samples and compared it to OS and normal tissue (Figure 3B). However, both genes did not indicate a significant up- or downregulation. To further analyze the possible role of this pathway we selected a small molecule inhibiting PI3K and mTOR activity (Figure 3C). This dual inhibition in addition should prevent feedback activation normally observed with mTORC1 inhibitors [150].

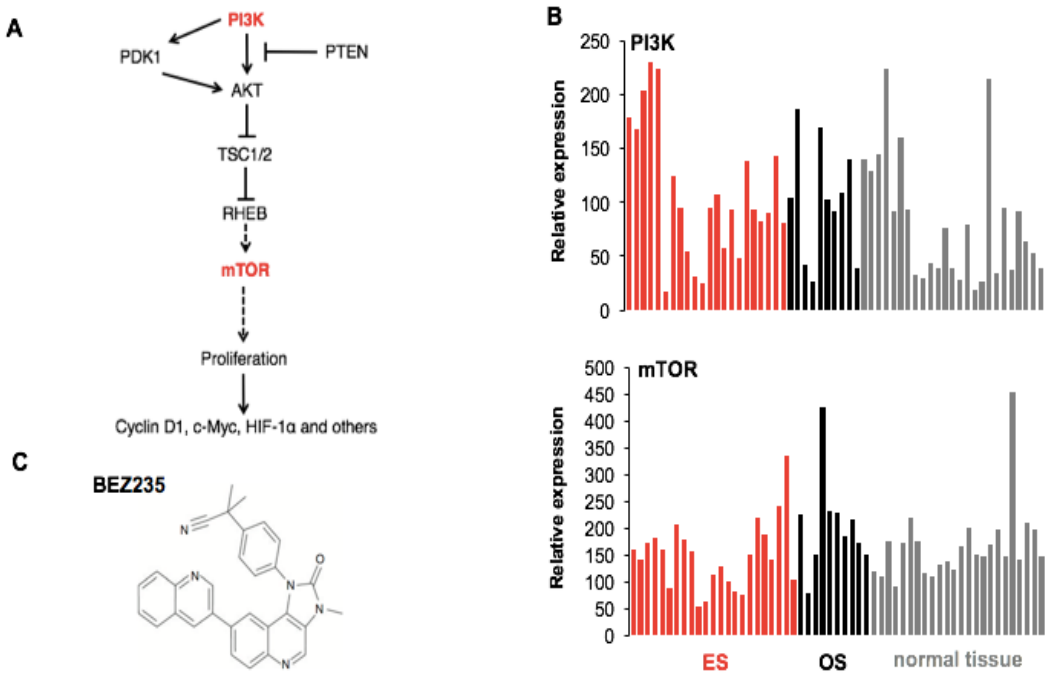

Figure 3: PI3K/mTOR pathway and expression in ES compared to OS and normal tissue. A. The PI3K/mTOR pathway regulates proliferation and transformation via targeting various proteins including cyclin D1, MYC, HIF1alpha or others. **B.** Microarray data showing PI3K and mTOR expression in primary ES samples (red) compared to osteosarcoma (OS) and normal body tissue (gray). No significant deregulation was observed. **C.** The dual PI3K and mTOR inhibitor BEZ235 was subsequently used to analyze influence on MYC expression.

Recent results further indicate that EWS-ETS proteins not only deregulate components of the epigenetic machinery in ES [1], but in addition create specific epigenetic marks [20, 21] that are bound by bromodomain proteins and might be addressed by epigenetic therapy. BRD4, the best studied in a family of 4 different BET bromodomain proteins and a mediator of transcriptional elongation was also linked to MYC dependent transcription [151]. Therefore, we analyzed the expression of 4 of these proteins in ES tumor samples and compared them as before to OS and normal tissue (Figure 4). BRDT, a protein exclusively expressed in testes and oocytes was shown as not expressed in ES samples while BRD2, BRD3 and BRD4 were ubiquitously expressed in all tissues but not displayed as deregulated. To further analyze a possible implication of these proteins in the regulation of MYC and its expression we selected another small molecule inhibitor. JQ1, a thoroughly characterized inhibitor of the BET-family of bromodomain proteins

has previously shown to result in the displacement of BRDs from chromatin and inhibition of transcription of key genes as BCL2, MYC and CDK6 [152] and was therefore selected for further analysis.

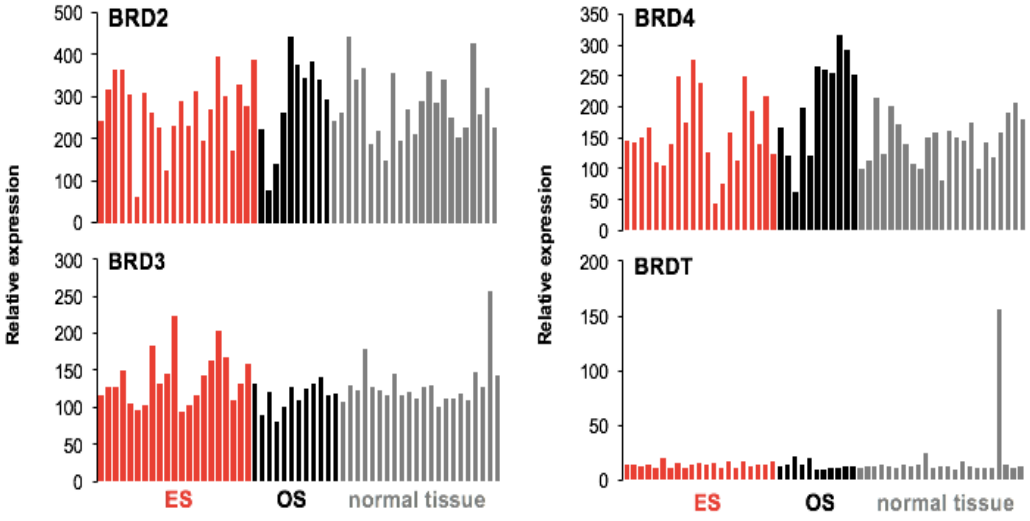

Figure 4: BET bromodomain proteins BRD2, BRD3, BRD4 or BRDT are not significantly deregulated in Ewing sarcoma samples compared to OS and normal tissue.

3.1.3 Blockade of BET bromodomain proteins or the PI3K/mTOR pathway blocks EWS-FLI1 expression but not MYC.

To investigate MYC regulation in ES we treated the cell lines A673, SK-N-MC and TC-71 as well as mesenchymal stem cells (MSCs) VH54.2 and L87 with 1, 2 or 5 µM JQ1 for 48 h and assessed expressional changes on the RNA level via qRT-PCR. By use of a specific gene expression assay for MYC no downregulation was observed in ES cell lines for all concentrations rather than a significant up-regulation in some cells (Figure 5A). In contrast, MSCs revealed a significant inhibition down to 35 % in VH54.2 after 5 µM JQ1 treatment. Therefore, we became curious whether the characteristic

oncofusion protein EWS-FLI1 may be influenced by BRD inhibition and analyzed its expression upon treatment as well (Figure 5B). The regulation of EWS-FLI1 was detected by qRT-PCR with specific EWS-FLI1 primers (see 2.2.4.3). Surprisingly, expression of EWS-FLI1 was reduced upon single treatment for 48 h with either 0.1, 1 or 2 µM JQ1, 500 nM BEZ235 or 500 nM BEZ235 in combination with 2 µM JQ1 (Figure 5B). Furthermore, downregulation of EWS-FLI1 was most significant past single agent JQ1 treatment. This was confirmed on the protein level as determined by western blot analysis (Figure 5C) wherein EWS-FLI1 expression was measured using an anti-FLI1 antibody detecting the 68 kDa EWS-FLI1 fusion protein. Already after 24 h as well as after 48 h of 500 nM BEZ235, 2 µM JQ1 or 500 nM BEZ235 in combination with 2 µM JQ1 treatment protein levels of EWS-FLI1 were significantly decreased in all three ES cell lines (A673, SK-N-MC and TC-71) analyzed. In addition, the analysis of activated apoptotic pathways as measured by antibodies detecting cleaved PARP and Caspase 7 also indicated to be activated especially post treatment with 2 µM JQ1 or 500 nM BEZ235 in combination with 2 µM JQ1 for A673, SK-N-MC and TC-71 (Figure 5C) (western blot analysis was performed by Chiara Giorgi, a collaborating scientist at the Children`s Cancer Research Centre, University Children`s Hospital, Zurich, Switzerland). Due to similar observations made especially after single agent treatment with 2 µM JQ1 as well as combination of 500 nM BEZ235 with 2 µM JQ1 subsequent analysis will focus on the implications of JQ1 in ES treatment.

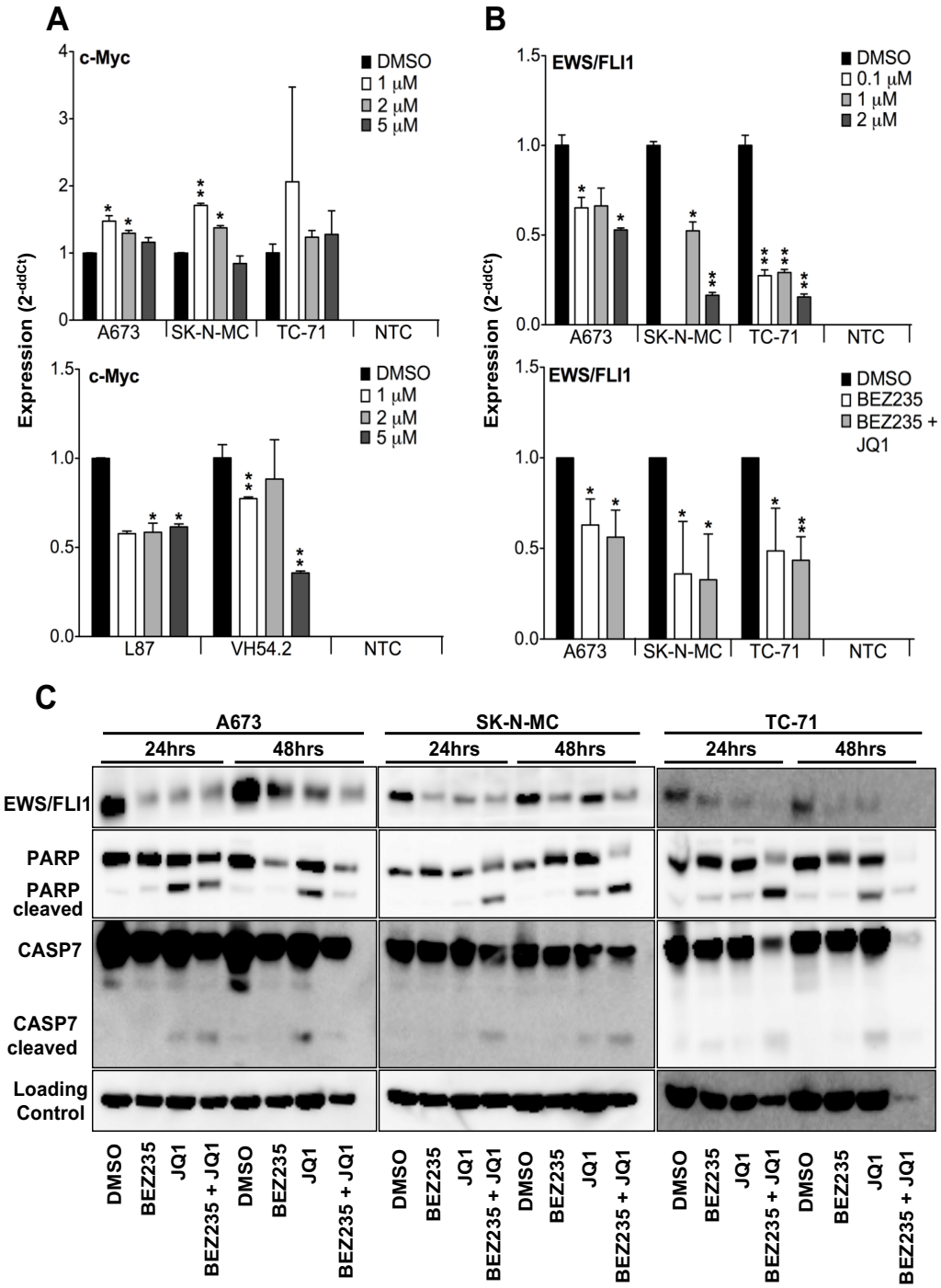

Figure 5: Blockade of BET bromodomain proteins blocks EWS-FLI1 but not MYC expression. A. Top, MYC expression in ES cell lines A673, SK-N-MC and TC-71 and, bottom, in mesenchymal stem cells L87 and VH54.2 after 48 h JQ1 treatment as measured by qRT-PCR. Data are mean ± SEM; t-test. NTC: non-template control. **B**. Top, different dosages of JQ1 inhibit EWS-FLI1 expression in ES cell lines A673, SK-N-MC or TC-71, respectively. Bottom, relative expression of EWS-FLI1 measured by qRT-PCR in A673, SK-N-MC and TC-71 cells after 24 h treatment with 500 nM BEZ235 and 500 nM BEZ235 in combination with 2 μM JQ1 compared to DMSO control. Data are mean ± SEM; t-test. NTC: non-template control. **C**. Protein level measured by western blot of EWS-FLI1, PARP, CASP7 and loading control. Cells were treated for 24 and 48 h with 500 nM BEZ235, 2 μM JQ1, 500 nM BEZ235 in combination with 2 μM JQ1 compared to DMSO control A673, SK-N-MC and TC-71 cells. Shown is a representative experiment (n=3). **P*-value < 0.05; ***P*-value < 0.005.

3.1.4 JQ1 down-regulates a ES specific expression profile

To clarify to which extent JQ1 influences gene expression on the transcriptome level, microarray analysis for A673 and TC-71 cell lines after treatment for 48 h with 2 µM JQ1 or DMSO were carried out. Volcano plots were used as the most amenable way to graphically illustrate significantly up- or down-regulated genes. Further does it provide information if there is a bias between up- or down-regulated genes as well as on differences between cell lines. For A673 we found 405 genes as significantly deregulated (*P*-value < 0.01) wherein genes were similarly up- or down-regulated (Figure 6A, left panel). TC-71 indicated 720 genes as significantly deregulated (*P*-value < 0.01) with slightly more genes down-regulated than up-regulated after treatment (Figure 6A, right panel). To further evaluate whether there is any overlap between the data sets of both cell lines, we compared the expression by Venn diagram analysis of genes ±1.5-fold differentially expressed. Herein, we found that of 1231 and 3290 influenced genes for A673 and TC-71, respectively, 811 were found to be consistently deregulated in both data sets (Figure 6B). Next, we queried if most were down- or up-regulated and drew a heat map from the top 244 differentially expressed genes (fold change > 1.8) of the overlapped data sets (Figure 6C). Concordantly the map showed that 188 genes were similarly down-regulated after treatment in A673 and TC-71, while only 57 were displayed as significantly up-regulated in both data sets. Subsequent gene set enrichment analysis identified gene sets enriched for EWS-FLI1 fusion targets by e.g. Zhang [153] and colleagues as well as those for Ewing sarcoma progenitors as identified by Riggi *et al.* [154] (Figure 6D). The normalized enrichment score (NES) for both data sets demonstrated a negative enrichment comprising genes that were mostly down-regulated. This also indicated that JQ1 inhibits EWS-FLI1 expression and similarly an ES associated expression profile (see supplemental table 21).

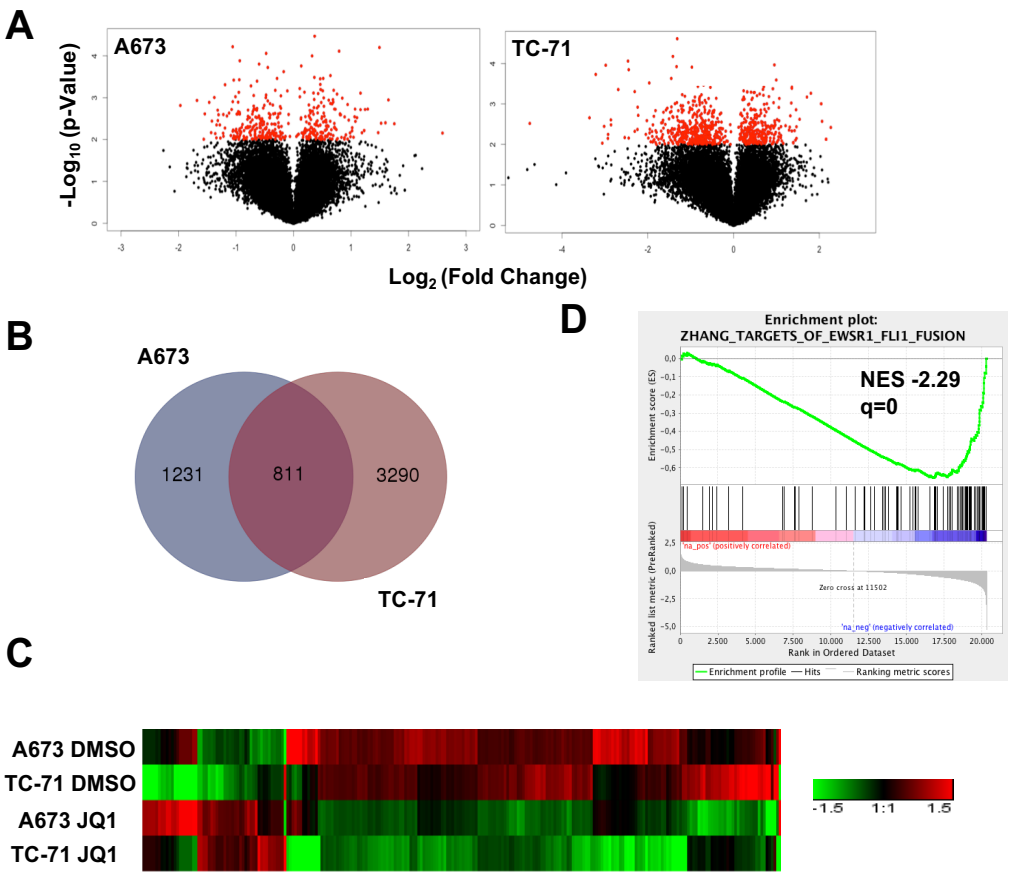

Figure 6: JQ1 treatment blocks a typical ES associated expression profile. A. Volcano plots for DMSO against JQ1 treated ES cell lines A673 and TC-71, showing the adjusted *P*-value (-log$_{10}$) plotted over 2-fold change (log2). Red, genes with significance $P < 0.01$. Microarray data with their normalized fluorescent signal intensities were used (RMA, see 2.2.17, GSE72673). Cells were treated for 48 h with 2 µM JQ1 or DMSO, collected (see 2.2.2) and then analyzed. **B.** Shared genes differentially expressed after JQ1 treatment in A673 and TC-71. Genes ± 1.5-fold differentially expressed were selected for the analysis in a Venn diagram (http://bioinformatics.psb.ugent.be/webtools/Venn/). **C.** Heat map of 244 genes, ± 1.8-fold differentially expressed in A673 and TC-71 are shown. Each column represents 1 individual array. **D.** GSEA enrichment plots of down-regulated genes after JQ1 treatment. GSEA: http://www.broadinstitute.org/gsea/index.jsp

3.1.5 RNA interference of BRD3 and BRD4 by specific siRNAs mimics the JQ1 treatment effect on the RNA level

Genes known as constitutively up-regulated in ES including *DKK2*, *EZH2*, *GPR64*, *PAPPA*, *STEAP1* and *STK32B* were found in this study as significantly down-regulated after JQ1 treatment. To verify this finding, genes

marked as down-regulated were analyzed after JQ1 treatment by qRT- PCR, confirming results of the microarray analysis (Figure 7A). While JQ1 has been reported to be most specific for BRD4 protein, it was also reported to have certain affinities to the remaining BET bromodomain proteins BRD2 and BRD3 [119]. Therefore, we transiently knocked down each BRD on the mRNA level by specific siRNAs using RNA interference (RNAi) (Figure 7B) and validated the expression of genes found as down-regulated after JQ1 treatment (Figure 7A) by qRT-PCR. Interestingly, none of the analyzed genes was down-regulated after BRD2 knock-down (Supplemental Figure 21). However, after knock-down of BRD3 as well as after knock-down of BRD4 genes were similarly down-regulated as observed after JQ1 treatment. While *STK32B* in A673 and *GPR64* in TC-71 were displayed as up- or not de-regulated. Concluding, BRD3 and BRD4 but not BRD2 might be the essential targets of JQ1, facilitating the pathognomonic EWS-FLI1 driven expression profile.

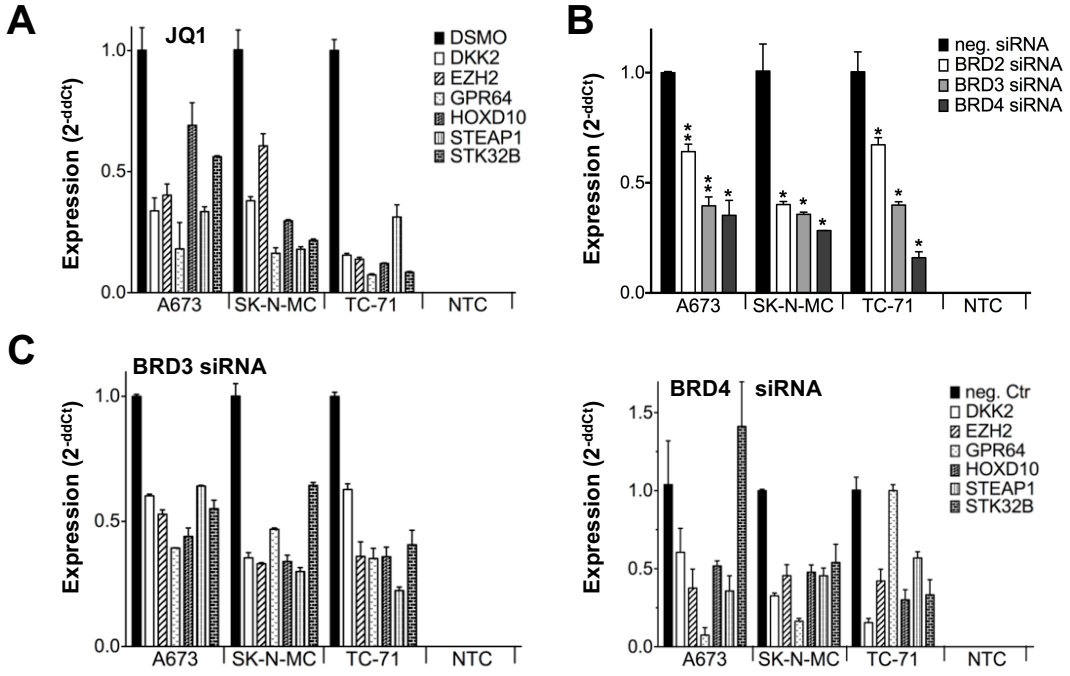

Figure 7: Verification of microarray data after JQ1 treatment by qRT-PCR and knock-down of specific BRDs to evaluate their influence on a ES specific expression profile. **A.** Verification of selected genes from microarray data by qRT-PCR. Consistently, ES specific genes were significantly down-regulated after JQ1 treatment in all three cell lines analyzed. **B.** RNA interference (RNAi) effectively knocks down (see 2.2.5) BRD2, BRD3 and BRD4 in A673, SK-N-MC and TC-71. siRNA efficiency was compared to neg. control (non-silencing RNA). Results of qRT-PCR 48 h after transfection are shown. Data are mean ±

3.1.6 JQ1 inhibits proliferation and promotes apoptosis

Having demonstrated that an ES specific expression profile is down-regulated after JQ1 treatment, we asked whether this inhibition might also influence growth abilities of ES. Therefore, we used the xCELLigence assay to compare the contact dependent growth of ES cell lines A673, SK-N-MC and TC-71, treated with either 2 µM JQ1 or DMSO (Figure 8A). The cellular impedance was measured every 4 h for a maximum time of 150 h and is displayed as cell index. Interestingly, of the analyzed A673, SK-N-MC or TC-71 hexaplicates all showed a significant growth inhibition. While for A673 and TC-71 the cell index showed a little increase in the beginning, this soon receded assuming a delayed effect of JQ1. SK-N-MC in contrast showed a decrease in cell index from the beginning that reached minimum after 60 h and lasted until the end. Similarly, a contact independent growth assay revealed a broad reduction of colony formation (Figure 8B). SK-N-MC showed the broadest impairment with only ~2 % of the colonies compared to the control. A673 and TC-71 also demonstrated a significant reduction with only ~36 % and ~31 % colonies, respectively compared to control. We further asked whether this observed block of proliferation and colony formation might be due to cell cycle changes. To test this hypothesis cell lines treated with either 2 µM JQ1, 500 nM BEZ235 or 500 nM BEZ235 in combination with 2 µM JQ1 were analyzed by flow cytometry using the DNA intercalating agent propidium iodide (PI) (see 2.2.9). Although changes like a general decrease in G2-M phase as well as an increase of G1 phase for SK-N-MC and TC-71 after JQ1 treatment or an extended S phase in A673 and SK-N-MC (Figure 8C) could be observed, none of these results explained the broad proliferation block observed after JQ1 treatment.

SEM; t-test. NTC: non-template control. **C.** RNAi of BRD3 and BRD4 with specific siRNAs affects the same ES specific genes as after JQ1 treatment. Data are mean ± SEM; t-test. NTC: non-template control.

In addition, caspase 3 glow assay (carried out by Chiara Giorgi, collaborating scientist) showed an increased apoptosis after JQ1 treatment for A673 and TC-71, that was further increased for all three cell lines after combination treatment of BEZ235 and JQ1 (Figure 8D). This, together with the observed cleavage of PARP and Caspase 7 (Figure 5C) indicated a strong induction of apoptotic pathways after JQ1 or JQ1 in combination with BEZ235 treatment.

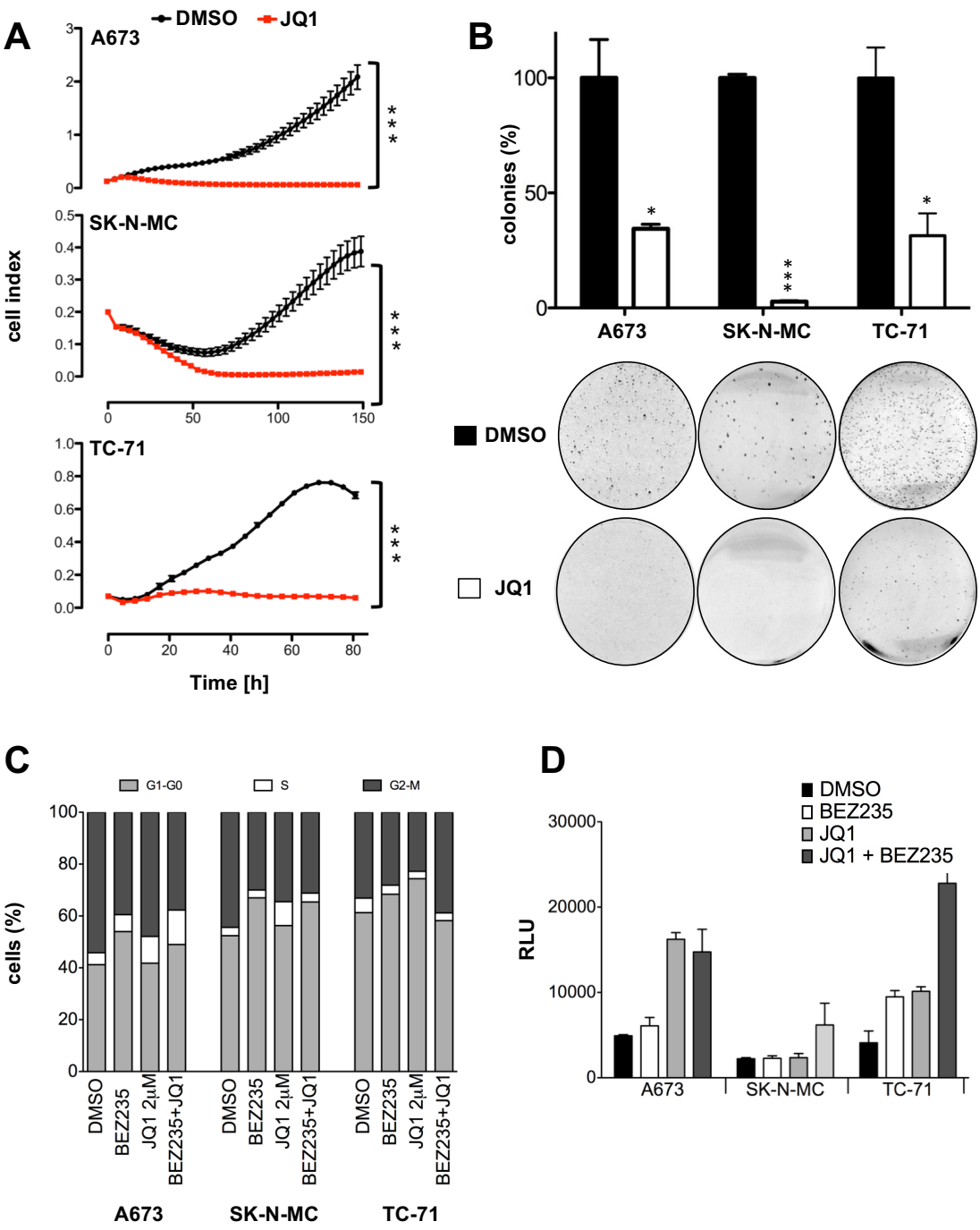

Figure 8: JQ1 blocks proliferation and induces apoptosis but does not influence cell cycle progression. A. Proliferation of JQ1 treated cell lines was analyzed using xCELLigence assay measuring cellular impedance every 4 h (relative cell index). Data are mean ± SEM (hexaplicates/group); t-test **B**. Anchorage-independent growth was measured by colony formation in methylcellulose-based media after JQ1 treatment. Top, data are mean ± SEM of 3 independent experiments (duplicates/group). Bottom, representative experiment with A673, SK-N-MC and TC-71. **C**. Cell cycle was analyzed upon JQ1 or BEZ235 treatment by FACS analysis and staining cells with Propidium iodide. **D**. Caspase 3/7 activity measured after 24 h treatment with 500 nM BEZ235, 2 µM JQ1, 500 nM BEZ235 in combination with 2 µM JQ1 in A673, SK-N- MC and TC-71. Bars represent mean values expressed as relative light unit (RLU) in percentage of DMSO treated control of 6 biological replicates analyzed in three technical replicates each (n=3; SE<0.01). ****P*-value < 0.0005.

3.1.7 JQ1 reduces tumor growth *in vivo* in a dose dependent manner

As already demonstrated by others [119, 155-157], JQ1 may provide certain therapeutic value. To test whether this is also true for ES, we evaluated JQ1 treatment in a xenograft mouse model of $Rag2^{-/-}$ $\gamma c^{-/-}$ mice by implanting 2 – 3 x 10^6 A673, SK-N-MC or TC-71 tumor cells subcutaneously (s.c.) into mice. As soon as tumors were palpable mice were randomized into two groups and treatment commenced. To do this, animals received a dosage of 50 mg/kg body weight JQ1 or vehicle every 48 h per intra peritoneal (i.p.) injection. Tumor size was measured daily until the tumor exceeded 1 cm^3 (see 2.2.17) in size whereupon mice were sacrificed.

Surprisingly, analysis by Kaplan-Meier plots demonstrated no prolonged survival on A673 or TC-71 cells (Figure 9A). Assuming that the initial dosage of JQ1 might be too low for a pharmaceutically effective supply, as supported by recent publications [158, 159], we also tested more frequent doses on TC-71 cells (Figure 9B, Top and D). Administration of 50 mg/kg body weight every 12 h over a period of 14 days significantly prolonged the survival of JQ1 administered mice. To confirm this observation, we chose SK-N-MC as a second cell line due to its strict dependency on EWS-FLI1 expression. Mice were likewise treated every 12 h for 23 days with 50 mg/kg body weight JQ1 per intra peritoneal injection and tumor size was measured daily. Consistent with high dose TC-71 treatment, also SK-N-MC bearing mice revealed a significant tumor growth reduction (Figure 9B, bottom) as well as a decreased tumor weight (Figure 9E).

Following sacrifice of mice, tumors were further analyzed by immunohistochemistry for caspase 3 expression. Corresponding to what we observed *in vitro* (Figure 5C and Figure 8D), induction of apoptosis mechanisms were also depicted to be activated *in vivo* (Figure 9C).

To further evaluate if an even more increased dosage might further potentiate the therapeutic outcome we also treated animals with 75 mg/kg body weight JQ1. However, this resulted in severe weight loss and death of mice (data not shown).

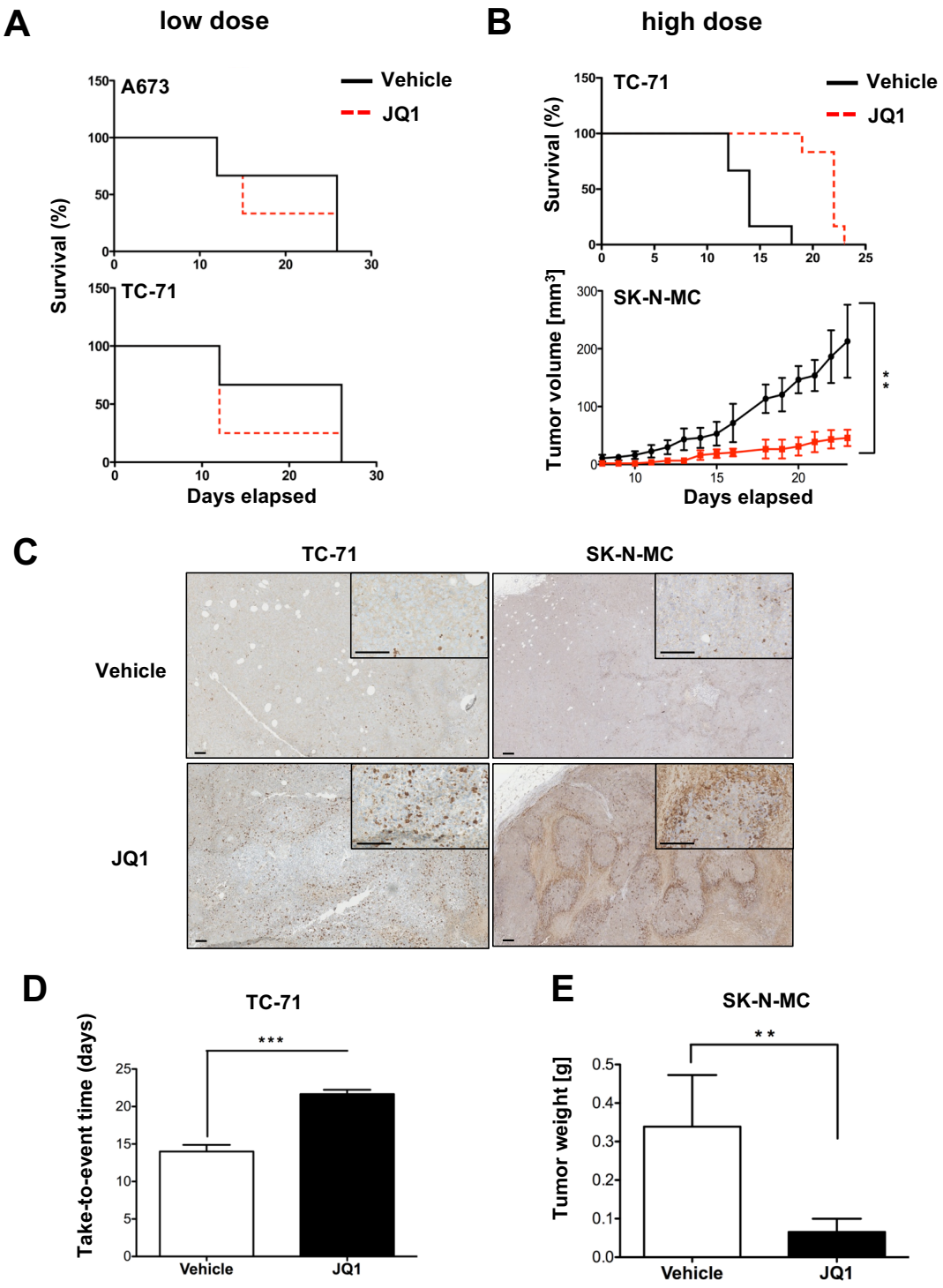

Figure 9: Treatment with JQ1 inhibits tumor growth dose dependently *in vivo.* Evaluation of the therapeutic potential of JQ1 application in immune deficient Rag2$^{-/-}$ $\gamma_c^{-/-}$ mice that were injected s.c. with 2x10^6 ES cells. As soon as the tumor was palpable mice received different doses of JQ1 or vehicle i.p.. Delay or inhibition of tumor growth was evaluated by Kaplan-Meier plots or tumor size. **A**. Mice were either injected with A673 or SK-N-MC cells and 7 days later received 50 mg/kg body weight JQ1 or vehicle every 48 h. Mice with an average tumor size >1 cm^3 were considered as positive and sacrificed. Kaplan–Meier plots of individual experiments with 5 mice per group are shown. **B.** Mice were injected with tumor cells s.c. and 5 days later received twice daily doses for 14 to 23 days for TC-71 and SK-N-MC, respectively. Top, survival of TC-71 inoculated mice. Bottom, tumor growth after inoculation with SK-N-MC cells. (6 mice/group). t-test.

3.1.8 BRD4 knock-down influences ES growth but does not activate apoptosis

To further investigate the mechanisms of the observed block in proliferation and the reasons behind the activation of apoptotic pathways, ES cell lines with constitutive knock-down of BRD2, BRD3 or BRD4 were established. Therefore, a doxycycline mediated shRNA system was used allowing for a selective activation of the knock-down (see 2.2.7). In a first analysis, knock-down efficiency after 72 h treatment with doxycycline was analyzed by western blot (Figure 10A). While protein levels for all three proteins were reduced after knock-down, it was further observed that after BRD3 knock-down, BRD4 presence was reduced as well. The same observation was made vice versa after BRD4 knock-down. A possible influence of BRD knock-down on proliferation ability as observed after JQ1 treatment was analyzed by xCELLigence assay (Figure 10B). However, only A673 and SK-N-MC showed a reduced growth after knock-down of BRD4, while knock-down of BRD2 and BRD3 in A673 as well as knock-down of BRD2, BRD3 and BRD4 in TC-71 cells (Supplemental Figure 22) did not indicate any significant growth impairment (Figure 10B, xCELLigence and western blotting was performed by Fiona Becker-Dettling, medical doctoral candidate). Also, apoptotic pathways, shown as activated after JQ1 treatment (see Figure 5C), did not display as activated after single knock-down of BRD2, BRD3 or BRD4 in all three cell lines analyzed (Figure 10C).

C. To analyze intratumoral changes after high dose JQ1 application tumors were collected upon tumor burden (TC-71) or after 23 days (SK-N-MC) and stained for caspase 3. The pictures show clear increased expression of cleaved caspase 3 in tumors treated with JQ1. Bar indicates 0.1 mm. **D**. Variation of tumor growth characteristics analyzed as a function of time until tumors reached >1 cm^3 size for TC-71 inoculated mice. **E**. Determined tumor weight of SK-N-MC inoculated mice at the end of the experiment. ***P*-value < 0.005, ****P*-value < 0.0005.

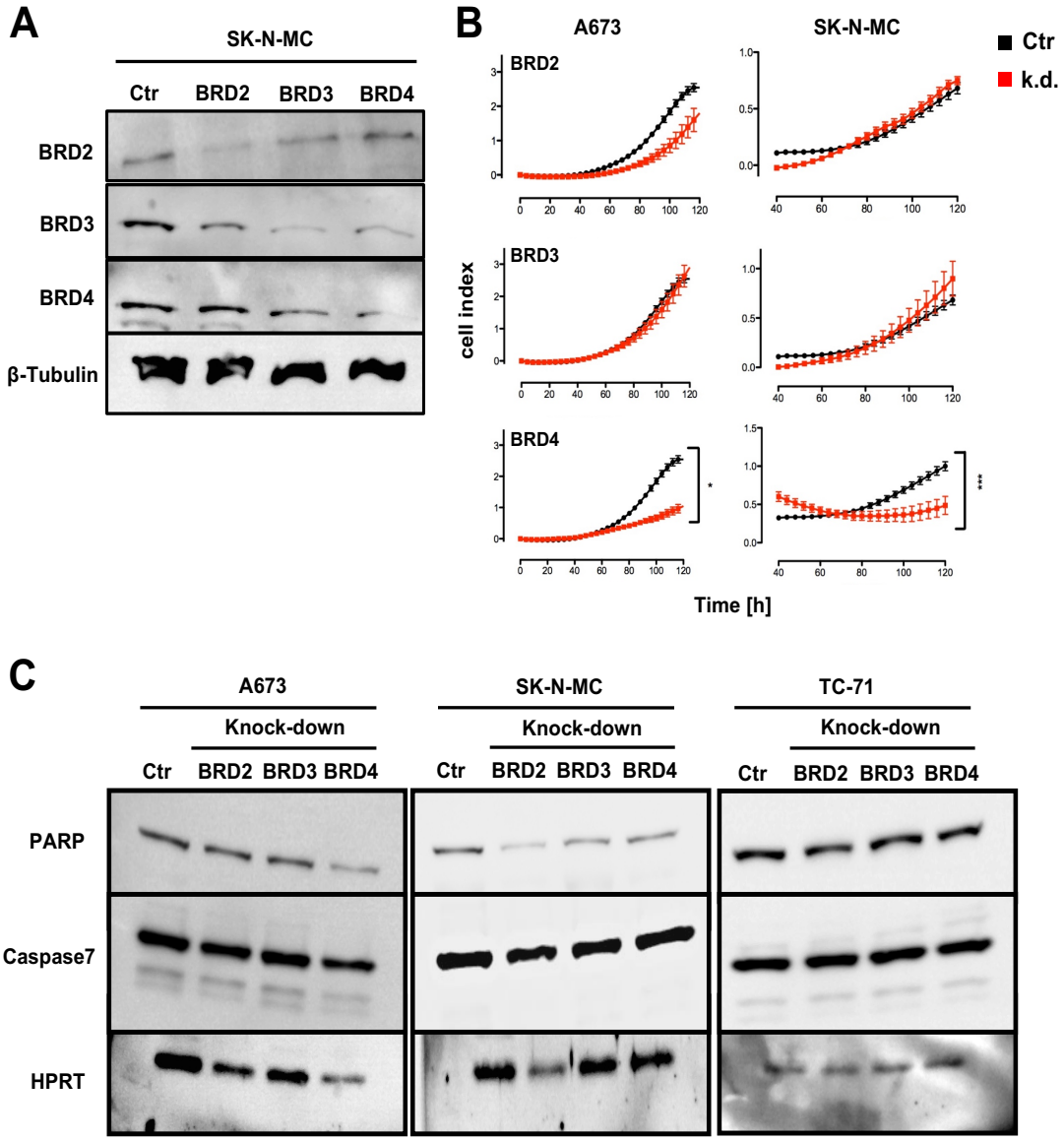

Figure 10: Induced knock-down of BRD2, BRD3 and BRD4 inhibits growth partially but does not activate apoptotic mechanisms. A. Knock-down efficiency for every BET protein was analyzed after 72 h doxycycline treatment by western blot. Shown is a representative experiment for SK-N-MC. β-Tubulin is used as loading control. **B.** Analysis of proliferation was done for A673 and SK-N-MC by xCELLigence assay measuring cellular impedance every 4 h (relative cell index). Data are mean ± SEM (hexaplicates/group); t-test. **C.** No activation of apoptotic pathways was indicated after knock-down by western blotting for PARP or caspase-7. Shown is a representative experiment. HPRT is used as loading control. **P*-value < 0.05, ****P*-value < 0.0005.

3.1.9 BRD4 interacts with P-CDK9, FLI1 and BRD3 on the protein level and binds to the EWS-FLI1 promotor

Previous publications indicated that BRD4 regulates polymerase II transcription by recruiting the positive transcription elongation factor p-TEFb and the concomitant stimulation of its kinase activity for phosphorylation of the C-terminal domain (CTD) of RNA polymerase II [160]. Subsequently, it was shown that anti-apoptotic genes are regulated through p-TEFb, especially through its subunit CDK9 [161, 162]. To evaluate whether this also applies for ES microarray data after JQ1 treatment were analyzed for the regulation of key anti-apoptotic genes (Supplemental Table 23). Herein, 26 genes were found as significantly down-regulated while only 7 were indicated as up-regulated. Interestingly, the x-linked inhibitor of apoptosis (XIAP) and the CASP8 and FADD like apoptosis regulator cFLAR (also known as cFLIP) which are described as regulated through CDK9 [163] were observed among the most significantly down-regulated genes. Mechanistically, XIAP inhibits the activation of caspase 3 by binding to the p19 – p12 of caspase 3 complex and thereby blocking apoptosis [164]. cFLIP on the other hand inhibits the CD95-mediated activation of caspase 8 as it blocks its processing at the death inducing signaling complex (DISC) [165]. To further study their possible involvement in the context of ES and the observed activation of apoptotic pathways after JQ1 treatment, co-immunoprecipitation (Co-IP) studies were carried out (see 2.2.13) to analyze whether EWS-FLI1 or BRD4 interact with each other and if the p-TEFb is part of this protein complex. Therefore, ES cell lines A673 and SK-N-MC expressing wild type EWS-FLI1 were used and analyzed after Co-IP for anti-FLI1 or anti-BRD4 antibodies (Figure 11A). Interestingly, both cell lines showed a co-immunoprecipitation of EWS-FLI1, BRD4 and BRD3 (Figure 11A lines 1 and 3). Further Co-IP of BRD4 revealed a co-elution of phosphorylated CDK9 (P-CDK9) as well as BRD3 as shown by western blot analysis (Figure 11A; lines 2 and 4).

While the observed co-immunoprecipitation of P-CDK9 and BRD4 was in agreement with previous observations [115, 166, 167], a proof of the interaction of BRD4 and EWS-FLI1 after FLI1-IP was only shown after FLI1

Co-IP but not after BRD4 Co-IP. To further investigate this interaction A673 and TC-71 cell lines carrying a flag-tagged FLI1 were used (flag-tagged FLI1 cell lines and corresponding Co-IP experiments were done by Chiara Giorgi, collaborating scientist). In addition, Benzonase treatment was used to verify whether the observed interactions did not rely on a protein-DNA-protein but on a direct protein-protein interaction. As shown in Figure 11B DNA fragmentation through treatment with Benzonase worked well but had no effect on the corresponding Co-IP`s as analyzed by western botting (Figure 11C). Both cell lines showed strong BRD4 bands after anti-Flag IP. Also, Co-IP and corresponding western blotting for BRD4 showed a significant signal for flag-tagged FLI1 in both cell lines, recapitulating initial observations after anti-Flag as well as after wild type EWS-FLI1 Co-IP.

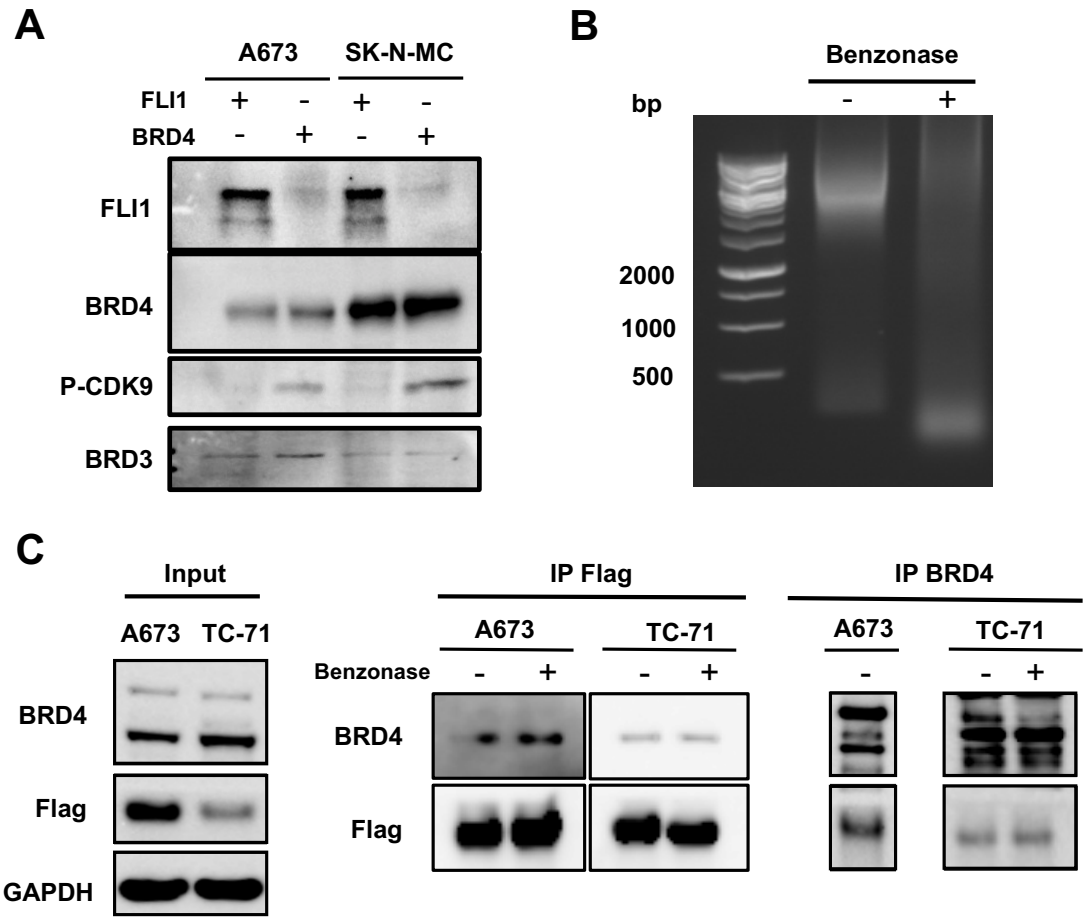

Figure 11: Interaction analysis by Co-IP for EWS-FLI1, BRD4 and P-CDK9. A. Co-IP for A673 and SK-N-MC cell lines using anti-FLI1 and anti-BRD4 antibodies. After Co-IP, proteins

Due to the observed decrease of EWS-FLI1 expression upon treatment with JQ1 we further asked if BRD4 might bind to the EWS-FLI1 promoter thereby regulating its expression. To investigate this hypothesis BRD4 ChIP was carried out for A673 and SK-N-MC cell lines (Figure 12). The DNA thereby obtained was subsequently analyzed by qRT-PCR for EWS-FLI1 specific genomic DNA content, genomic DNA not enriched for BRD4 binding served as a negative control. Interestingly, both cell lines demonstrated a significant enrichment of EWSR1 binding over negative control, assuming a selective binding of BRD4 to the EWS-FLI1 promoter and supervision of its expression.

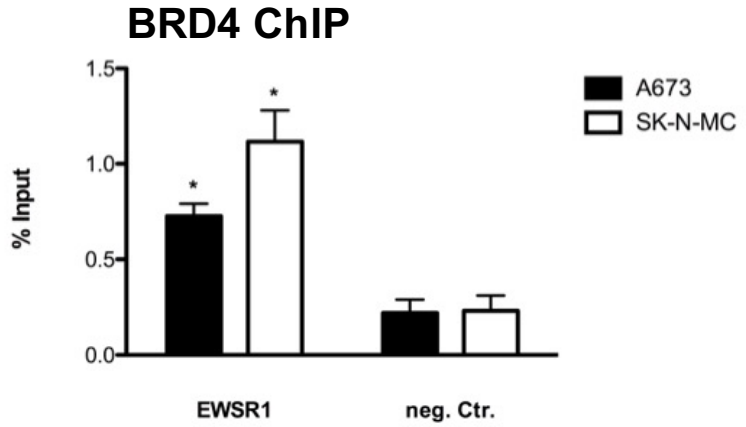

Figure 12: Interaction analysis of BRD4 and the EWS-FLI1 promoter by ChIP. ChIP for BRD4 in A673 and SK-N-MC cell lines was done as described in 2.2.12. Retained DNA was analyzed by qRT-PCR using primer specific for the EWS-FLI1 promoter (EWSR1) and compared to a region not enriched for BRD4 (neg. Ctr.) (Table 16). *P-value < 0.05.

were analyzed by western blotting for FLI1, BRD4, P-CDK9 and BRD3. **B.** Benzonase treatment was done for 1 h for DNA lysis. Co-IP using an anti-FLAG antibody was done subsequently for treated and untreated samples. **C.** Co-IP after Benzonase treatment using an anti-BRD4 and anti-Flag antibody for A673 and TC-71 cell lines. Samples were analyzed subsequently by western blotting. Input was used as a positive control.

3.1.10 CDK9 inhibition down-regulates EWS-FLI1, blocks growth and activates apoptosis

Having demonstrated that EWS-FLI1, BRD4 and P-CDK9 interact on the protein level, we further asked if inhibition of BRD4 by JQ1 and the resulting activation of apoptosis and growth inhibition could be caused due to an abrogation of P-CDK9 function. To analyze this hypothesis, we evaluated 5 different CDK9 inhibitors in A673, EW7 (both possessing a type 1 translocation) and MHH-ES1 (type 2 translocation) cell lines (Figure 13) (inhibitors were kindly provided by Shudong Wang, Adelaide, Australia). Interestingly, qRT-PCR for CDK9 but also for EWS-FLI1 and cyclin T1 (CCNT1) (a further subunit of the p-TEFb complex that activates CDK9) [168] revealed a significant decrease of expression especially after treatment for 24 h and 2 µM with ST2-58, LY3-29 or I-73 (Figure 13A). Furthermore, even though BRD4 expression was indicated as reduced especially after LY3-29 and I-73 treatment, BRD4 was much less influenced in relation to CDK9, CCNT1 or EWS-FLI1 expression reduction.

Based on the strong impact in all three cell lines, LY3-29, I-73 and ST2-58 were selected for subsequent experiments. Flow cytometry analysis was performed for EW7 and a second type 2 translocation cell line (RDES) after 2, 4 and 6 h of 2 µM treatment of selected CDK9 inhibitors to examine a possible correlation between CDK9 inhibition and cell cycle progression (Figure 13B) (cell cycle analysis was carried out by Chiara Giorgi). While only minimal changes were observed after 2 and 4 h of treatment of both cell lines, 6 h of treatment significantly reduced G1-G0 phase in both cell lines. Furthermore, results in EW7 indicated an elongated G2-M phase while RDES showed more cells to be in S phase. Even though changes were obvious for all three compounds tested after 6 h, most significant changes were observed for I-73 which was therefore selected for further testing.

To test whether the observed changes also influence growth properties, the xCELLigence assay was used for A673, EW7 and TC-71 cell lines. Cells were seeded and grown until they reached exponential growth phase. Subsequently, they were treated with 2 µM I-73 or DMSO as solvent control

and monitored until growth regressed in the control. Consistent among all cell lines tested, the addition of I-73 repressed growth most significant in EW7 and TC-71. A673 cells also revealed blocked growth with some delayed sensitivity.

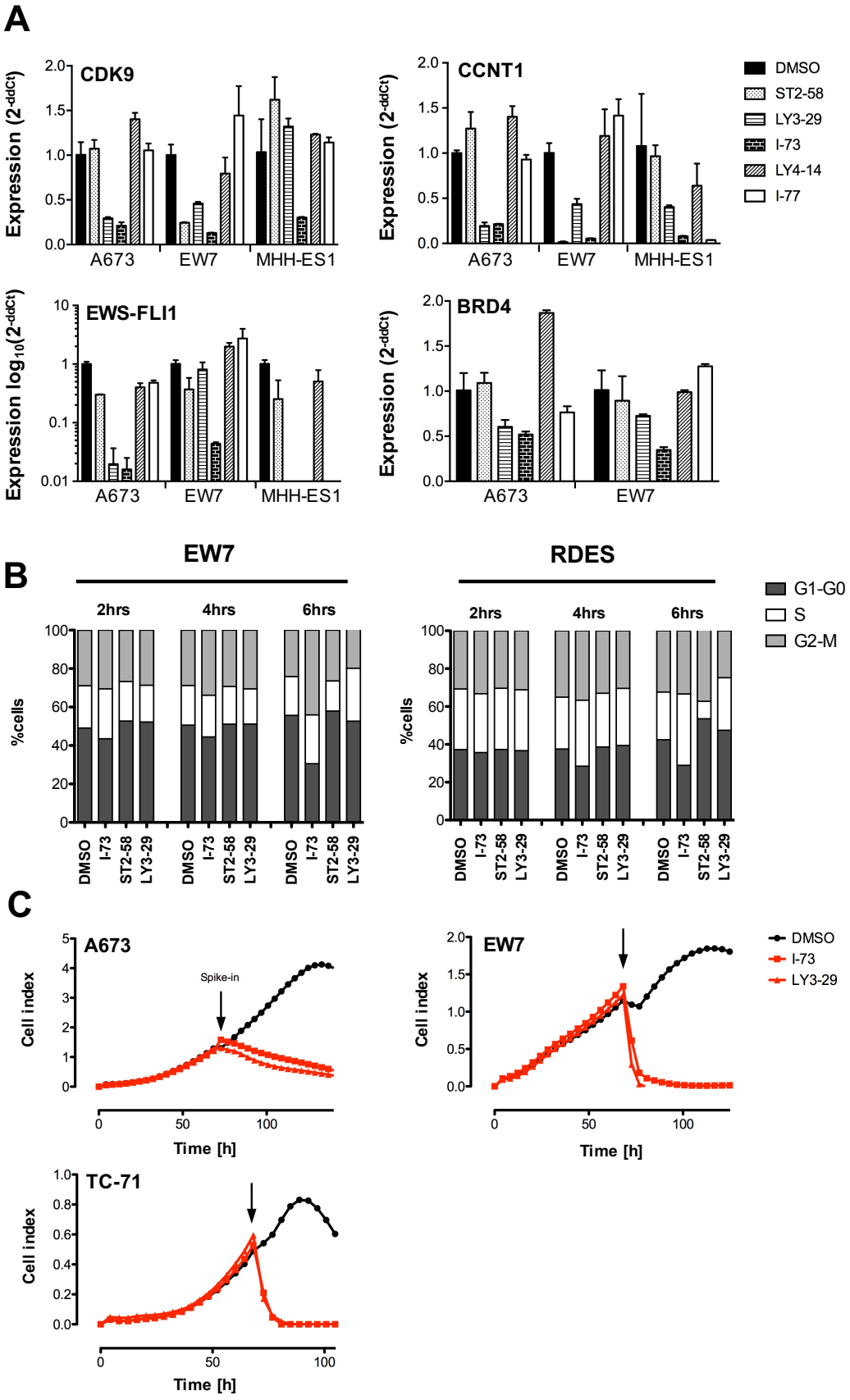
A
CDK9
CCNT1
EWS-FLI1
BRD4
Expression (2-ddCt)
Expression log10(2-ddCt)
A673
EW7
MHH-ES1
DMSO
ST2-58
LY3-29
I-73
LY4-14
I-77
B
EW7
RDES
2hrs
4hrs
6hrs
%cells
G1-G0
S
G2-M
C
A673
EW7
TC-71
Spike-in
Cell index
Time [h]
DMSO
I-73
LY3-29

In addition, we analyzed if apoptotic mechanisms became activated as previously observed after JQ1 treatment (Figure 5C). Therefore, SK-N-MC and A673 cell lines were treated with 2 µM LY3-29 or I-73 for 6 h and analyzed subsequently by western blot analysis (western blotting was carried out by Chiara Giorgi). As shown in Figure 14, both cell lines revealed an increased PARP and Caspase 7 cleavage as compared to vehicle or untreated control, similar to what we observed after JQ1 treatment.

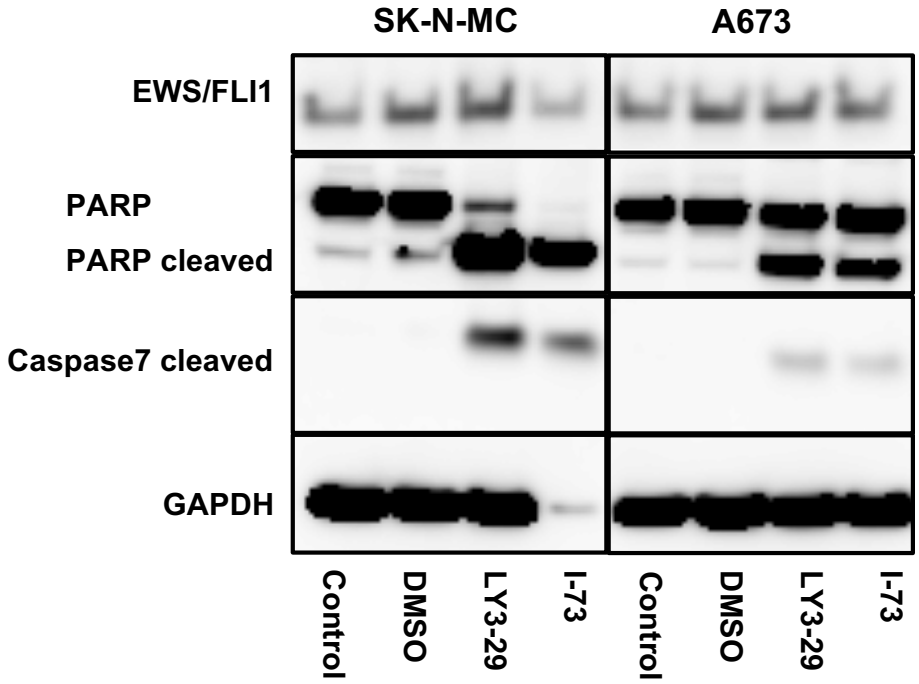

Figure 13: Analysis of activation of apoptotic mechanisms after CDK9 inhibition. SK-N-MC and A673 cell lines were treated with 2 µM LY3-29, I-73 or vehicle (DMSO) for 6 h and compared to an untreated and DMSO control by western-blotting.

Figure 13:Evaluation of different CDK9 inhibitors by qRT-PCR and cell cycle. A. Analysis of expression of CDK9, CCNT1 and EWS-FLI1 after 24 h treatment of 2 µM ST2-58, LY3-29, I-73, LY4-14 and I-77 CDK9 inhibitors in A673, EW7 and MHH-ES1 cell lines measured by qRT-PCR. Data are mean ± SEM; t-test. DMSO: solvent control. **B.** Cell cycle was analyzed 2, 4 and 6 h after treatment with I-73, ST2-58 and LY3-29 by flow cytometry for EW7 and RDES and cells were stained with propidium iodide. **C.** Proliferation of I-73 treated cell lines A673, EW7 and TC-71 was analyzed using xCELLigence assay measuring cellular impedance every 4 h (relative cell index). Data are mean ± SEM (hexaplicates/group); t-test.

3.1.11 Low dosage JQ1 and I-73 reduces tumor growth *in vivo*

To analyze whether I-73 might hold a therapeutic value *in vivo*, we tested a dual approach combining JQ1 and I-73 treatment at a low dosage and compared it to vehicle as well as single agent treatment of JQ1 and I-73. To do this, a xenograft mouse model of $Rag2^{-/-}$ $\gamma c^{-/-}$ mice was used and 3 – 4 x 10^6 A673 cells were injected subcutaneously (s.c.) into mice. As soon as tumors were palpable mice were randomly divided into four groups and treatment commenced. Animals received a dosage of 50 mg/kg body weight JQ1 or corresponding vehicle every 24 h per i.p. injection. I-73 or corresponding vehicle was administered via oral gavage at 50 mg/kg body weight every 48 h. Treatment was carried out for a maximum of 14 days. Tumor size was measured daily until the tumor exceeded 1 cm^3 (see 2.2.17) in size whereupon mice were sacrificed.

Analysis of tumor growth between different groups over time of treatment revealed the lowest tumor growth rate for low dosage treatment of JQ1 in combination with I-73 (Figure 15A). Interestingly, this combination treatment was similar in efficacy as observed after high dosage JQ1 treatment (Figure 9B). Single agent treatment of JQ1 or I-73 also delayed tumor growth, although they finally caught up to tumor size in the control group. Immunohistochemistry for all four groups showed an increased cleaved caspase 3 expression in treated tumors, with no significant differences within treatment groups (Figure 15B), indicating additional mechanisms influencing tumor growth.

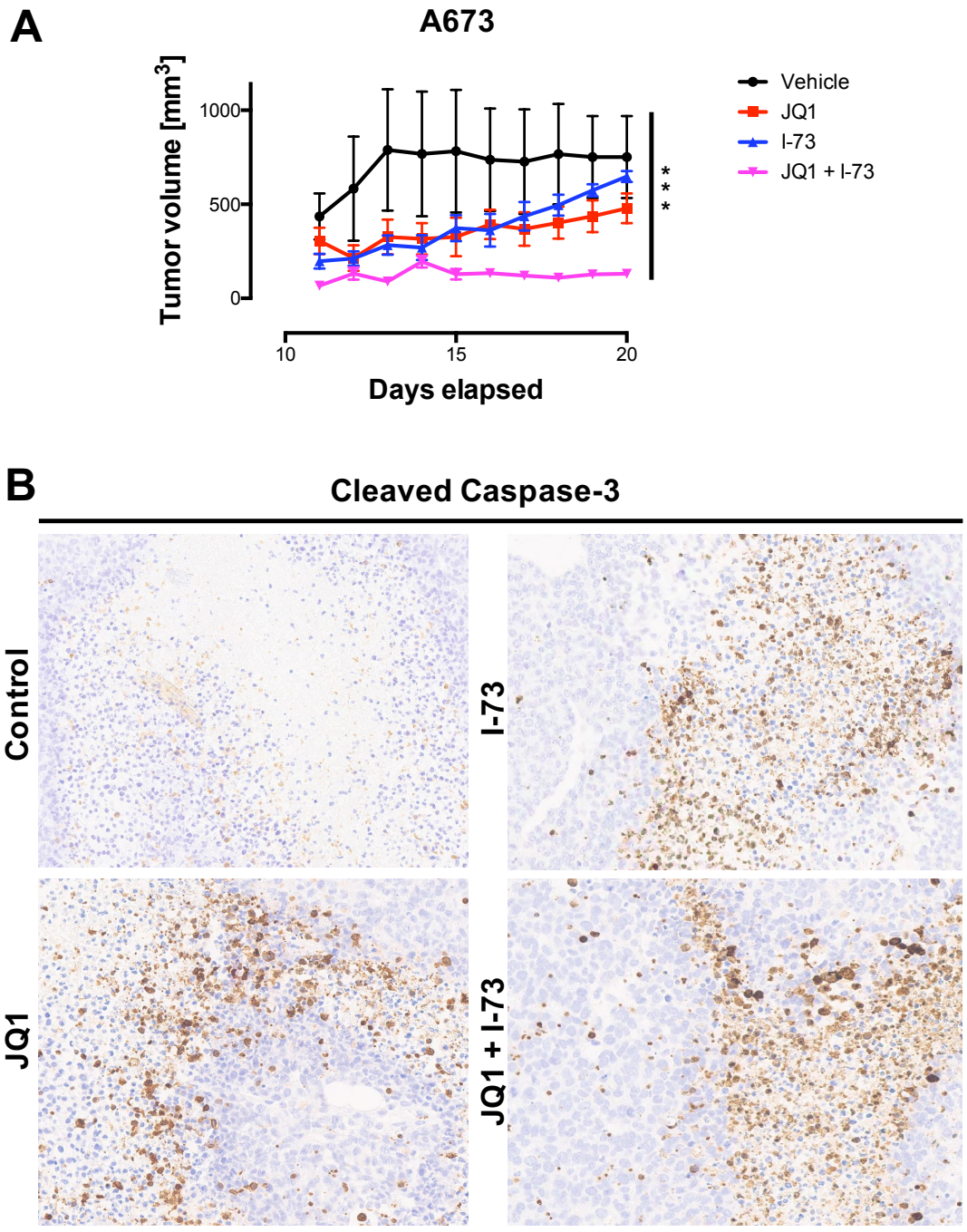

Figure 14: Combination treatment of JQ1 and I-73 in comparison to single agent treatment in a xenograft model. A. ES cell line A673 was injected s.c. into a xenograft mouse model. Once tumor was palpable mice were divided randomly into four groups and treated either with 50 mg/kg body weight JQ1, I-73 and JQ1 in combination with I-73. JQ1 was administered i.p. every 24 h while I-73 was administered by oral gavage every 48 h. (7 mice / group). t-test. ****P*-value < 0.0005 **B.** As soon as tumors reached 1 mm^3 (see 2.2.18) mice were sacrificed and tumors analyzed for Cleaved caspase 3 expression by immunohistochemistry.

3.1.12 JQ1 resistant cell lines are still sensitive to I-73 treatment

Previous reports suggested that cells treated with JQ1 can acquire resistance following sustained treatment with JQ1 [169]. To analyze if the same is true for ES cell lines, A673 and SK-N-MC were cultured continuously with 2 µM JQ1 over several month. To test whether growth capabilities have changed xCELLigence assay was used. Interestingly, cells that remained under continuous JQ1 treatment seemed to tolerate it and grew in the presence of JQ1 in contrast to wild type cells (Figure 16A). However, cell growth could be blocked for both, wild type and resistant cell lines upon addition of I-73 (Figure 16B).

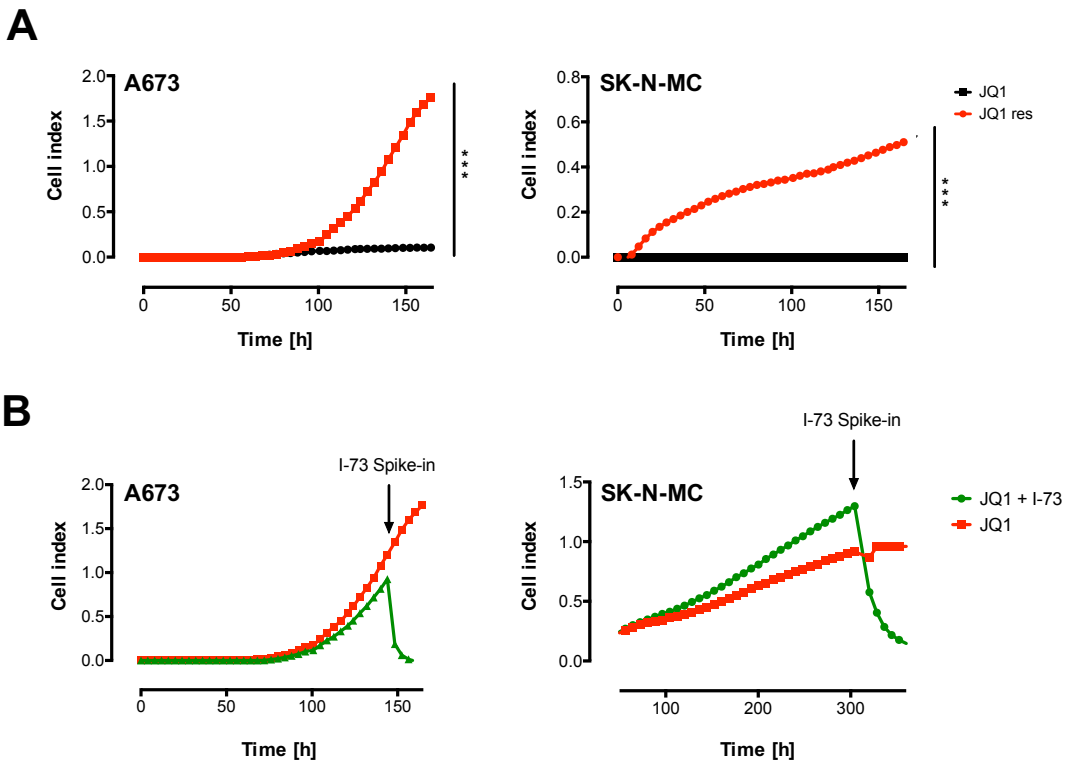

Figure 15: Treatment with I-73 blocks proliferation in JQ1 Resistant cell lines. A. ES cell lines A673 SK-N-MC were treated for several months with 2 µM JQ1 and analyzed subsequently by xCELLigence assay. Wild type A673 and SK-N-MC cell lines were used as controls. Cellular impedance was measured every 4 h (relative cell index). Data are mean ± SEM (hexaplicates/group); t-test. ****P*-value < 0.0005 **B.** Proliferation of JQ1 resistant A673 and SK-N-MC cell lines was analyzed by xCELLigence assay. Upon reaching exponential growth rate cells were treated with 2 µM I-73 or DMSO as negative control. Cellular impedance was measured every 4 h (relative cell index). Data are mean ± SEM (hexaplicates/group).

3.2 Function of EZH2 in ES

3.2.1 Inhibition of EZH2 reduces H3K27me3 and increases H3K27ac

In a previous study [18] it was shown that the PRC2 complex and EZH2 in particular play an important role influencing the metastatic spread, local tumor growth and differentiation of ES cell lines *in vitro* and *in vivo*. To further analyze the mechanism behind this regulation and to assess potential clinical applications, small molecule inhibitors were used and evaluated.

In a study published in 2012 [170], Verma and colleagues reported the development of GSK343, a novel, highly potent, selective, S-(S`-adenosyl)-1-methionine (SAM) competitive and cell-active inhibitor of EZH2. Even though EZH1, a homolog of EZH2 that associates with somewhat different PRC2 complexes, shares an overall 76 % sequence identity and a 96 % sequence identity within the SET-domain [170] this inhibitor was described to be selective, especially for EZH2, with albeit lower activity for other methyltransferases.

To test the effectivity of this small molecule, ES cell lines A673, SK-N-MC and TC-71 were treated with 3 µM GSK343 or solvent control (DMSO) for 72 h. Subsequently, proteins were isolated and samples analyzed by western blotting or qRT-PCR. Consistent with previous observations, GSK343 significantly reduced overall H3K27me3 levels in all cell lines analyzed (Figure 17A), although a faint band for H3K27me3 was still detectable after treatment. Furthermore, qRT-PCR showed a decreased expression of EZH2, which, however, was not statistically significant ($p > 0.05$) (Figure 17B). In addition, on the protein level western blot analysis indicated no decrease of EZH2 after treatment and thereby confirmed qRT-PCR findings (Figure 17C).

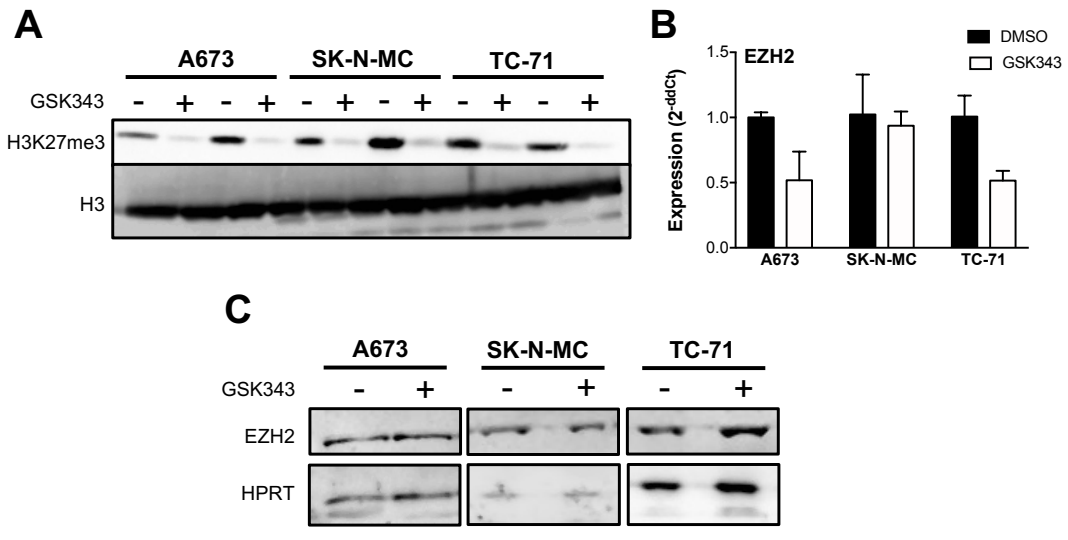

Figure 16: Evaluation of GSK343 effectivity on protein and RNA level. A. ES cell lines A673, SK-N-MC and TC-71 were treated with 3 µM GSK343 or DSMO for 72 h. Treatment effectivity was analyzed by western blot analysis for H3K27me3. H3 was used as loading

To further test the specificity of this small molecule and whether it may influence the expression of core components of the PRC2 complex (e.g. SUZ12) or other histone marks as activating (H3K27ac, H3K4me2) or inactivating (H3K9me2) histone marks, additional western blots were carried out after treatment of cells for 72 h with 3 µM GSK343 or solvent control (DMSO). Interestingly, only H3K27ac revealed a consistent increase after treatment while the other marks showed no replicable changes (Figure 18).

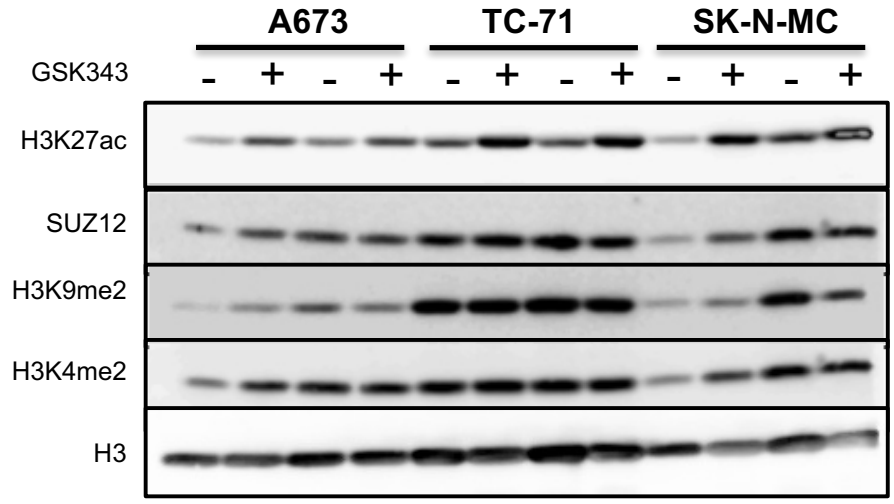

Figure 17: Immunoblot of different histone marks and SUZ12 as a PRC2 core component. Treatment with 3 µM GSK343 or DMSO for 72hrs markedly decreased H3K27ac while no other changes were observed. H3 was used as loading control.

control. Experiments were performed in duplicates. **B.** qRT-PCR and **C.** western blot analysis for A673, SK-N-MC and TC-71 after 72 h and 3 µM GSK343 or DMSO treatment revealed no statistical significant changes in EZH2 expression after treatment.

3.2.2 Inhibition of EZH2 does not affect contact independent tumor growth and endothelial differentiation

Since it was shown in previous studies that knock-down of EZH2 exerted substantial changes to cells by means of proliferation and differentiation [18], we also tested if inhibition of EZH2 by GSK343 results in concordant changes. To do this we analyzed the capability of ES cell lines A673 and TC-71 to grow contact independently in a colony forming assay in the presence of this drug (Figure 19A). However, no differences were observed between control or GSK343 treated cells, which contrasted with previous observations made after knock-down of EZH2 by RNA interference [18]. Endothelial differentiation assays were performed to investigate, whether drug-mediated EZH2 inhibition similarly induces a more differentiated ES phenotype. However, no increased differentiation capabilities were observed contrasting previous observations (Figure 19B).

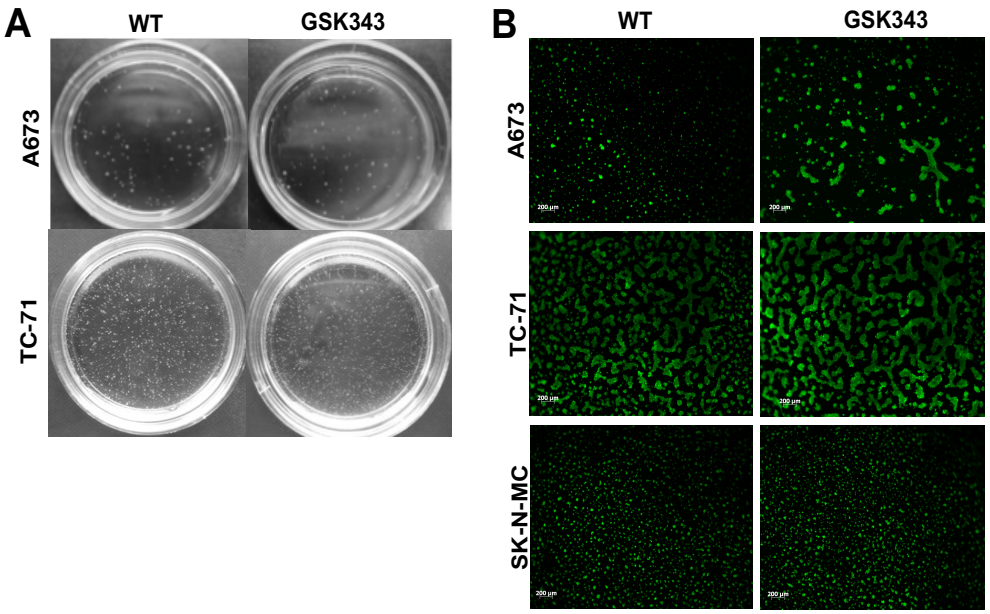

Figure 18: Colony formation and endothelial differentiation assay of after enzymatic inhibition of EZH2. A. A673 and SK-N-MC cells were seeded in duplicates into GSK343 containing methylcellulose based media to analyze *in vitro* contact independent growth. **B.** Endothelial differentiation of GSK343 treated A673, SK-N-MC and TC-71 ES cell lines. 72 h after GSK343 treatment, 5 x 10^4 cells per well were seeded onto matrigel and incubated for 24 h at 37 °C in a humidified atmosphere. Representative pictures of Calcein AM staining are shown. WT cells only received solvent control.

3.2.3 Tumor growth is not influenced by EZH2 inhibition *in vitro* and *in vivo*

While working on the influence of EZH2 inhibition and the evaluation of GSK343, we recognized a publication by McCabe et. al [170] describing a new small molecule. GSK126 a highly potent, selective, S-adenosyl-methionine-competitve, inhibitor that selectively targets the SET domain of EZH2 was described to decrease global H3K27me3 levels and reactivate PRC2 target genes. Therefore, this new inhibitor was tested for different treatment concentrations and exposure times by western blot analysis (Figure 20A and B).

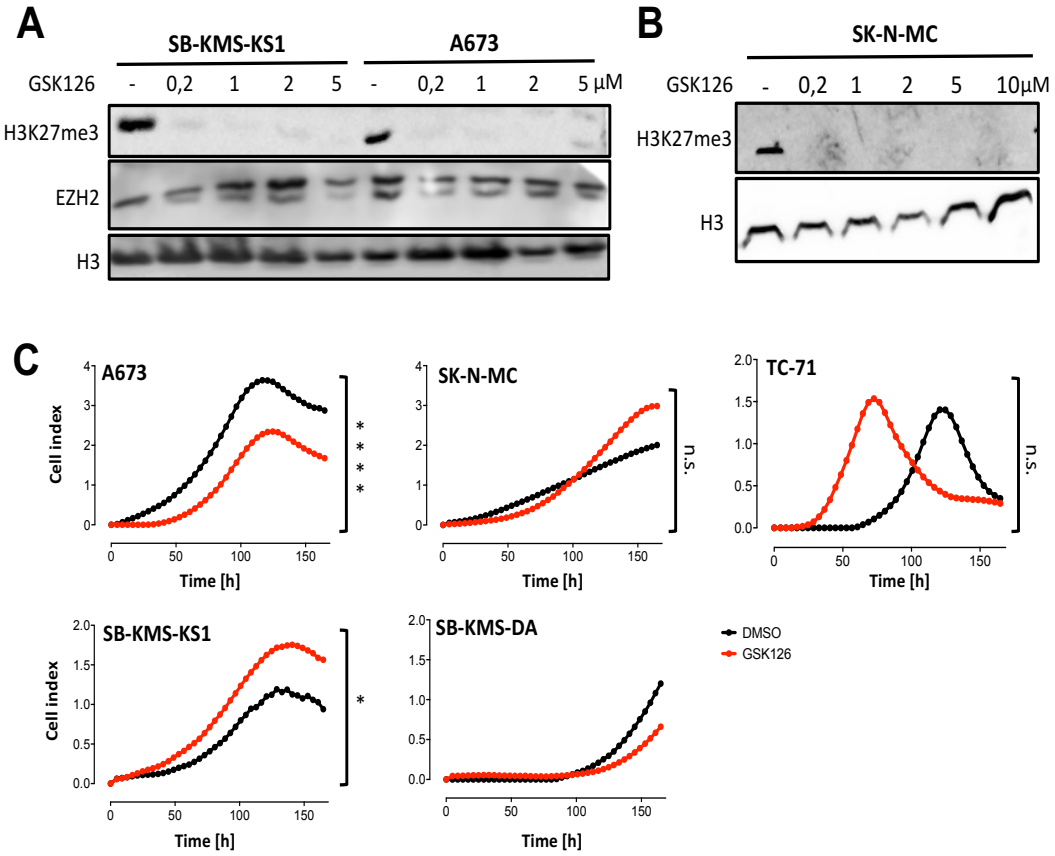

Figure 19: GSK126 decreases H3K27me3 levels globally but has inconsistent effects on cell growth. A. Analysis of SB-KMS-KS1 and A673 ES cell lines with concentrations varying from 0.2 up to 5 µM for 7 days on protein level by western blotting. H3K27me3 showed a broad and sustained decrease while EZH2 levels were indicated as increased upon treatment. H3 was used as loading control. **B**. SK-N-MC was treated with 0.2 - 10 µM GSK126 for 72 h, proteins isolated and analyzed by western blotting. H3K27me3 levels were indicated as decreased for all concentrations used. H3 loading control. **C**. xCELLigence proliferation assay over a period of 7 days and 2 µM GSK126 or DMSO treatment in different cell lines. **P*-value < 0.05, *****P*-value < 0.0001, n.s. not significant**.**

In addition to the commonly used cell line A673 another primary cell line SB-KMS-KS1, established in our lab from an extra osseous inguinal metastasis of a ES patient, was evaluated for treatment. Both cell lines demonstrated a broad and sustained decrease in H3K27me3 levels after 7 days of treatment starting at concentrations of 0.2 µM GSK126 (Figure 20A). Furthermore, EZH2 showed an increased expression especially after 1 or 2 µM GSK126 treatment in SB-KMS-KS1 and 1, 2 or 5 µM treatment in A673 cells after 7 days (Figure 20A). Also, treatment for only 72 h and different concentrations showed a marked decrease of H3K27me3 levels in SK-N-MC (Figure 20B). Because of the broad effect for all concentrations tested and based on the

observations made by McCabe et. al, the 2 µM treatment option was chosen for subsequent analysis.

Comparisons between GSK343 and GSK126 by means of anchorage independent colony formation and endothelial differentiation were done with no observable differences (data not shown). However, since GSK126 was described to have a 150-fold selectivity for EZH2 over EZH1, GSK126 was used for further studies like the anchorage dependent xCELLigence assay. SK-N-MC, TC-71 and SB-KMS-DA cells treated with 2 µM GSK126 or DMSO and tested in this assay with no statistical significant differences. A673 and SB-KMS-KS1 in contrast showed a significant differential growth which was inhibited after treatment in A673 and enhanced in SB-KMS-KS1 even though this was less significant (Figure 20C).

To test if the observed differences *in vitro* for A673 cells might also influence tumor growth *in vivo*, 2 x 10^6 cells were injected s.c. into Rag2$^{-/-}$ $\gamma_c^{-/-}$ mice. Once the tumor was palpable mice were randomized into two groups (4 mice /group) and treated daily with 150 mg per kg body weight GSK126 per intraperitoneal injection. Unfortunately, no significant differences in survival could be observed between control and GSK126 treated animals (Figure 21).

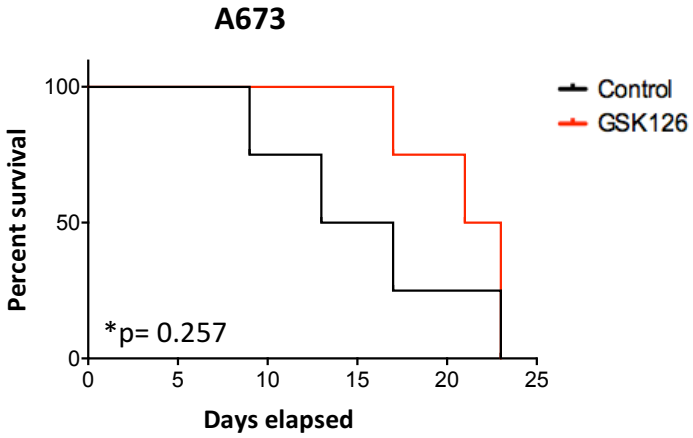

Figure 20: Treatment with GSK126 does not prolong survival *in vivo*. 2x10^6 A673 cells were injected s.c. into Rag2$^{-/-}$ $\gamma_c^{-/-}$ mice. Once tumor was palpable mice were randomized into 2 groups and treated with 150 mg/kg body weight GSK126 or DMSO as solvent control via daily i.p. injection.

4 Discussion

The present study was realized to clarify the relevance of specific epigenetic reader and writer proteins for the occurrence and maintenance of ES and the evaluation of their therapeutic potential.

ES are bone and soft tissue tumors predominantly affecting children and young adolescents in the second decade of life. ES are characterized by early metastasis into the lungs or other bones often associated with poor prognosis. Despite the knowledge of the molecular and pathognomonic foundation of this disease, therapeutic options for patients with metastatic or recurrent disease are scarce and novel approaches are needed. Over the last couple of years targeted therapies tried to fill this gap by addressing the oncogenic driver protein EWS-FLI1 as well as other previously identified downstream targets [171-176]. However, owing to the poor pharmacokinetic properties of this oncogenic driver and poorly understood mechanisms contributing to possible escape mechanisms further analysis is needed to tackle this disease at its roots.

The deregulation of components of the epigenetic machinery was previously demonstrated as an important step for ES tumor formation [18, 105]. Furthermore, it was recently shown that EWS-FLI1 employs divergent chromatin remodeling mechanisms to activate or repress transcription [20, 177]. Thereby altered epigenetic marks were identified that generated specific acetyl-lysine moieties on histones. Bromodomains (BRDs) as readers of acetyl marks have been thoroughly investigated throughout the last couple of years. Especially the BET family has been an ongoing field of research owing to its ubiquitous expression (except for BRDT) and their important role in transcriptional activation. Interestingly, all three BET proteins were found as well expressed in ES. Targeting by specific inhibitors of BET proteins such as I-BET151 [152] or JQ1 [119] resulted in dislodgment of BRDs from chromatin in other tumors and inhibition of transcription at key genes involved in apoptosis, cell cycle regulation and oncogenesis [156, 157, 178, 179]. It was further demonstrated that JQ1 could block tumor

growth and a recurring feature of the consequences of JQ1 / I-BET151 treatment was inhibition of MYC, N-MYC or FOSL expression, respectively in these tumors.

MYC over-expression is a salient feature in ES and could be demonstrated as constitutively up-regulated in comparison to normal body tissue. Its level of expression seems to be directly regulated via EWS-FLI1 [180]. By use of JQ1 and BEZ235 in different ES cell lines we aimed to disrupt this potentially EWS-FLI1-mediated modulation. In doing so we observed a significantly blocked proliferation and a strong downregulation of the pathognomonic EWS-FLI1 protein. However, no inhibition of MYC expression in ES lines was observed. Interestingly, MSC as the presumed progenitor cells showed an up to 50% downregulation of MYC.

Further analysis of the impact of JQ1 treatment showed a number of suppressed genes typical for ES specific expression profiles [11, 105, 154]. For example, GPR64, a new excellent marker of ES [34], was down-regulated after JQ1 treatment. Similarly, the expression of DKK2, a key player of ES invasiveness and osteolytic tumor growth [6], was greatly reduced by JQ1. Also other genes consistently up-regulated and/or shown to be involved in ES pathogenesis such as *EZH2*, *PAPPA*, *STEAP1*, and *STK32B* [18, 33, 105] were uniformly inhibited by JQ1. Consistently, whole transcriptome analysis showed fewer genes to be up-regulated after JQ1 treatment and included genes involved mainly in pathways for cell maturation, differentiation, etc. (GSE72673), confirming that EWS-FLI1 itself is abrogating differentiation programs and is the driver of the immature phenotype of this disease [18, 181].

Interestingly, the treatment effect of JQ1 on the expression program of ES cell lines could be mimicked by specific siRNA-mediated knock-down of BRD3 or BRD4 but not BRD2, indicating not only BRD4 to be an important epigenetic reader protein in ES. Displacement of BRD3/4 by specific inhibitors has already been shown in MLL-fusion positive leukemia [152]. While BRD3 seems to preferentially associate with hyper-acetylated chromatin along the entire lengths of transcribed genes [116], BRD4-binding

has also been observed in enhancer regions [182]. Furthermore, JQ1 treatment not only suppressed an ES specific expression profile but also blocked contact dependent and independent proliferation of different ES lines. A partial G1 arrest and S phase elongation of the cell cycle was demonstrated previously [119] and could be observed for ES as well. In addition, induction of apoptosis as demonstrated by PARP1-, CASP7-cleavage and increased CASP3 activity seems to significantly contribute to the reduction of the proliferative ability of ES lines. Single or combination treatment with the PI3K/mTOR inhibitor BEZ235 [150] did increase apoptosis of ES cell lines although single treatment with BEZ235 was less effective than JQ1 application. Testing of JQ1 in an *in vivo* setting demonstrated that tumor development was dose dependently suppressed by intra-peritoneal JQ1 application in a xeno-transplant model of ES–bearing immune deficient $Rag2^{-/-}\gamma c^{-/-}$ mice. Therapeutic efficacious doses, although high, were within the range published previously [119, 157, 178]. Consistent to results *in vitro*, treatment of mice with JQ1 also caused a significant intratumoral induction of cleaved caspase 3. Overall, these results demonstrated that MYC or EWS-FLI1 mediated pathognomonic expression programs may be similarly targeted by BET bromodomain inhibition, casting BET protein inhibition appropriate as a potential platform for future combination therapy of this disease.

Further investigation, generating constitutive BRD knock-down cell lines to recapitulate JQ1 treatment effects and analyze the underlying mechanisms revealed that reduced growth was observed only after knock-down of BRD4 in A673, whereas none of the analyzed knock-down cell lines demonstrated an activation of apoptotic markers. Although BRD4 is presumed to bind to different lysine residues on histone 3 and 4, BRD2 and BRD3 were reported to bind to overlapping subsets [183, 184], explaining for a presumably compensation upon loss of only one BET protein. However, the lack of intra-BET selectivity limits the scope of current inhibitors for target validation. New opportunities to elucidate the cellular phenotypes and therapeutic implications associated with selective targeting have been described recently with new tools such as PROTACs (Proteolysis Targeting Chimera) [185] and

other BET protein degrader [186]. Recent findings in MLL leukemia underline the notion of compensation by individual BRDs or others by the observation that the disruptor of telomeric silencing complex (DOT1L) can functionally compensate for inhibition of BRD4 [187]. In ES a number of substances initially also demonstrated efficacy in preclinical models such as single treatment with ARA-C [188] or anti-IGFR [140] but in phase I clinical trials delivered transient [181] or disappointing results [189]. Therefore, combination treatment of JQ1 with substances like YK-4-279 that directly binds to EWS-FLI1 and inhibits its oncogenic activity [190, 191] via blockade of specific protein interaction with factors important for mRNA splicing [192] and transcription [190] may result in synergistic effects inhibiting tumor growth. For example, treatment with BEZ235 clearly inhibited EWS-FLI1 expression and in combination with JQ1 further increased apoptosis induction indicating that combination treatment of JQ1 with PI3K/mTOR inhibition should be a promising strategy for future therapy of ES.

Irrespective of the therapeutic virtue of JQ1 proven in numerous cancers, mechanisms determining the response to BET inhibition remain poorly understood. To identify factors helping to provide predictive information we further analyzed the interactome of BRD4 by co-immunoprecipitation as well as ChIP experiments. A very salient feature of BRD4 is its interaction with the positive transcription elongation factor b (P-TEFb) triggering the transition of RNA polymerase II (RNAPII) into productive elongation. Therefore, BRD4 binds to the core complex of p-TEFb, CDK9/cyclinT, through its C-terminal extra terminal domain region [115]. Here we showed via Co-IP experiments a consistent interaction of BRD4 with p-CDK9 in ES. Moreover, we observed that EWS-FLI1 directly interacts with BRD4 as well. While the molecular consequences of this interaction need to be validated, previous studies already identified a significant association of EWS-FLI1 and chromatin states of promoters, enhancers and super-enhancers [177]. However, whether this binding occurred directly through EWS-FLI1 or in conjunction with other proteins is unknown so far. Interestingly, promoters of highly expressed genes and those bound by EWS-FLI1 had high levels of the open-chromatin associated marks H3K4me3, H3K27ac and H3K56ac. We therefore queried

previously established ChIP-seq data for enrichment of acetylation marks in the vicinity of EWSR1 [20, 177]. H3K27ac was indicated as strongly enriched close to the promoter. To test if BRD4 might bind to H3K27ac and thereby possibly regulate the expression of EWS-FLI1, ChIP experiments for BRD4 were carried out. Subsequent qPCR for primer covering the H3K27ac enriched genomic region of the EWSR1 promoter was performed and demonstrated an enrichment of BRD4 at this promoter, concluding that the observed downregulation of EWS-FLI1 after JQ1 treatment was due to a blocked binding of BRD4 to the promoter region of EWS-FLI1.

In addition to these site-specific effects we further pursued to analyze if CDK9 might be a useful therapeutic target in ES. Deregulation of cyclin-dependent kinases (CDKs) has been associated with many cancer types and has evoked an interest in chemical inhibitors. In recent years, several CDK9 inhibitors have been designed and demonstrated good antitumoral activity. Unfortunately, clinical studies of the drugs flavopiridol, dinaciclib, seliciclib, SNS-032 and RGB-286638 remained unsuccessful and involved many advert effects [193]. However, as the tools to design new drugs improved over time, new and more selective inhibitors became available. Here we tested 6 new CDK9 inhibitors and demonstrated their effectivity by means of cell cycle analysis, growth inhibition and regulation of EWS-FLI1 as well as CCNT1 and CDK9. Interestingly, I-73 an inhibitor shown to be very specific in ovarian cancer cells [194] was also most effective among all ES cell lines tested. Similar to results obtained after JQ1 treatment, I-73 treatment also down regulated EWS-FLI1 expression, facilitated induction of apoptotic pathways and abrogated cell growth *in vitro*.

While several reports showed that JQ1 can influence a plethora of different pathways, e.g. the WNT or the hedgehog pathway [195, 196] one of the main conclusions from our results in ES could therefore be that JQ1 abrogates activation of Pol II through P-TEFb followed by the shutdown of different transcriptional programs, an observation further supported by recent publications [197, 198]. An ubiquitous challenge of modern therapies is the emergence of tumor cells resistant to the therapeutic agent [199]. While

emerging evidence suggests that transcriptional inhibitors combined with other therapeutic agents can suppress the development of drug resistant cells, further work is needed to establish a system of concept for a tumor cell specific combination therapy [200]. Recently, Fong et al. [201] as well as Kurimchak et al. [169] showed that cancer cells can acquire resistance to BET inhibition, demonstrating a major concern in successful cancer treatment. Here we analyzed this concern and showed that ES cell lines can likewise become resistant to JQ1 after long term treatment. However, treatment of resistant cells with I-73 still abrogated growth *in vitro,* highlighting the opportunity of a combined therapy using BRD and CDK9 inhibitors. Therefore, we tested a combination therapy in a xenograft mouse model and showed that tumor growth could be blocked at low dosages for A673 cell line. Further experiments, conducted while preparing this thesis, confirm this blockade of tumor growth for a second cell line in the same xeno-transplant model (data not shown). This emphasizes the importance of both inhibitors as candidates for a refined targeted therapy of ES patients.

Another interesting combination might arise from EZH2 inhibitors [170, 202] which have the potential to further increase the therapeutic efficacy and due to potential synergistic effects decrease JQ1 dose levels required for successful treatment. Previously published results from our group [18, 105] clearly indicated a dependency of ES cell lines on the repressive effects mediated by EZH2 and the PRC2 complex. Further, it was shown that overexpression of EZH2 in ES is most likely due to the binding of EWS/FLI1 in close proximity to the EZH2 promoter. This was further strengthened by the observed broad downregulation of EZH2 after EWS/FLI1 knock-down. Therefore, we tested two novel and highly potent EZH2 inhibitors GSK343A and GSK126 as possible candidates for future targeted therapy.

Blockade of the enzymatic pocket of EZH2 by SAM-competitive compounds has been shown to be very effective in a broad range of cancers and has been reviewed recently [203]. GSK126 as the most currently developed inhibitor tested here also binds to this pocket and shows up to 1000-fold selectivity for EZH2 compared to other methyltransferases and 150-fold

compared to EZH1 [170, 204]. Subsequent *in vivo* experiments of GSK126 markedly impeded the growth of lymphomas carrying an activating EZH2 mutation [170]. While the exact function of EZH2 can be versatile, its canonical role is to mediate gene silencing through H3K27me3. However, accumulating evidence suggests that EZH2 can also have non-canonical functions, as for example the methylation catalyst of other substrates than histones or even in a methylase-independent fashion [205-207]. To analyze this behavior also in the context of ES we first analyzed H3K27me3 levels by western blotting after treatment with both inhibitors. Interestingly, both inhibitors showed a strong reduction of H3K27me3 levels which was accompanied by an increase in H3K27ac. Blockade of the enzymatic pocket however did not lead to a reduction of EZH2 or other components of the PRC2 complex on the protein level, thus reduction of H3K27me3 is not due to degradation of H3 or PRC2 as observed previously for inhibitors as DZNep [208]. Because of the described superior potency of GSK126 over GSK343A [209] we further pursued using only GSK126. We evaluated the effect of GSK126 on cell proliferation in a panel of different ES cell lines. However, none of the tested showed an impaired growth in the anchorage dependent or independent assays used. Similarly, experiments analyzing endothelial differentiation after EZH2 inhibition showed no differences. To analyze if tumor growth might be influenced *in vivo* we used a xenotransplantation model and injected ES cell lines s.c. into the inguinal region. However, no significant differences between animals treated with GSK126 or vehicle were observed. On the contrary, these results were in contradiction to experiments reported previously, showing a clearly prolonged survival as well as reduced metastatic spread using EZH2 knock-down cell lines *in vivo* [18]. Even though there are no published reports on these diverse effects of EZH2 knock-down or inhibition, different options arise from this observation that need to be validated. Previous reports by Lee et al. [103] reported the interaction of the RelA/p65 and RelB subunits of NF-κB and EZH2 independent of its HMT activity in triple negative breast cancer (TNBC). Further was it shown by Holm et al. [210] that TNBC were having elevated levels of EZH2 but surprisingly low levels of H3K27me3, supporting the idea of an HMT independent role of EZH2. Several studies have also

identified a PRC2-independent function in transcriptional repression rather than activation.

While the actual role of EZH2 in ES needs to be further elucidated our results clearly indicated that other functions than its pure HMT activity on H3K27me3 are the real reason for the observed decrease in metastatic spread and prolonged survival reported previously.

5 Summary

Epigenetics and approaches for targeted therapies provide unique opportunities for targeted treatment using specific inhibitors. In this thesis, we analyzed the epigenetic landscape of ES in order to find new and more improved ways to treat ES patients. Thereby BET bromodomain proteins, CDK9 and EZH2 got into the specific focus of our research. BET proteins, have attracted much interest as candidate therapeutic target due to their putative involvement in the pathogenesis of various diseases, including cancer and inflammatory diseases [211]. Here we showed that inhibition of BRD2, BRD3 and BRD4 through the small molecule JQ1 effectively abrogated a ES specific expression profile, blocked cell growth and activated apoptotoic mechanisms as shown by cleavage of caspase 3, 7 and PARP. Interestingly, continuous administration of JQ1 via i.p. injection blocked tumor growth *in vivo* significantly and activated apoptotic mechanisms intratumoral. Knock-down of single BET proteins showed a specific dependence on BRD3 and BRD4 for the expression of ES associated gene sets. Efforts trying to analyze the underlying mechanistics further revealed that EWS-FLI1 interacts with BRD4, which in turn could be shown to interact with CDK9 on the protein level.

CDK9, which together with Cyclin T builds the p-TEFb, is a protein critical for transcriptional elongation promoting the activation of RNA polymerase II. Further, CDK9, due to its key role in transcriptional activation, is an attractive target in modern cancer therapy. Here we showed that inhibition of CDK9 by the small molecule I-73 effectively inhibited growth and activated apoptotic mechanism. Further these results supported the notion of CDK9 as a downstream actor of EWS-FLI1. Interestingly, cells that had become resistant after longterm treatment with JQ1 could still be effectively treated with I-73. A combination therapy of JQ1 and I-73 at low dosages compared to single treatment proved as effective blocking growth of tumor cells.

EZH2 the core component of the PRC2 complex, being the catalyst in generating H3K27me3 marks. EZH2 has important roles during development and its deregulation was shown in a plethora of different cancers and ES.

Here we analyzed if the inhibition of the catalytic center of EZH2 through small molecules could be a suitable treatment option for future targeted therapies of ES patients. Strikingly, even though inhibition of EZH2 showed a significant decrease in H3K27me3 levels and an increase in H3K27ac, no influence on growth or differentiation was observed *in vitro* and *in vivo*. While the main task of EZH2 might be to mediate trimethylation on H3K27, other factors might be implicated in ES and must be analyzed in the future.

6 Zusammenfassung

Epigenetische Mechanismen stellen einen vielversprechenden Ansatz der modernen Therapie dar und ermöglichen eine zielgenaue Behandlung einer Vielzahl verschiedener Erkrankungen. Ziel dieser Arbeit war es, das epigenetische Profil des Ewing Sarkoms zu untersuchen und mit den gewonnenen Erkenntnissen neue und effektivere Wege für eine zielgerichtete Therapie von ES Patienten zu ermöglichen. Hierbei standen BET Bromodomänen Proteine, CDK9 sowie EZH2 im Fokus der Arbeit. Untersuchungen von BET Proteinen konnten in der jüngsten Vergangenheit eine vielfache Beteiligung bei der Pathogenese verschiedener Erkrankungen wie Krebs oder von Entzündungsreaktionen aufzeigen und gelten als vielversprechender Kandidat für mögliche neuartige Therapien. Mit dieser Doktorarbeit konnte gezeigt werden, dass die Inhibition der Bromodomänen von BRD2, BRD3 und BRD4 durch den Inhibitor JQ1 ein ES spezifisches Expressionsprofil beeinflusst, welches das Zellwachstum blockiert und apoptotische Mechanismen wie Caspase-3, -7 und PARP aktiviert.

Interessanterweise konnte in *in vivo* Experimenten mit einer kontinuierlichen intraperitonealen Gabe von JQ1 das Tumorwachstum blockiert und apoptotische, intratumorale Mechanismen aktiviert werden. Die Suppression einzelner BET Proteine mittels siRNA zeigte, dass speziell BRD3 und BRD4 für eine Aufrechterhaltung eines ES spezifischen Epressionsprofils von Bedeutung waren. Weitere Untersuchungen der mechanistischen Hintergründe dieser Regulierung zeigten, dass EWS-FLI1 mit BRD4 sowie BRD4 mit CDK9 auf der Proteinebene direkt miteinander interagieren.

CDK9 ist ein Protein, das zusammen mit Cyclin T den p-TEFb Komplex bildet und von entscheidender Bedeutung bei der Aktivierung der RNA Polymerase II ist. Außerdem ist CDK9 durch seine entscheidende Rolle bei der transkriptionellen Aktivierung ein sehr interessantes Ziel der modernen Krebstherapie. In dieser Arbeit konnte gezeigt werden, dass die Inhibition von CDK9 mit der Substanz I-73 das Wachstum verhindert und apoptotische Mechanismen aktiviert. Des Weiteren deuteten diese Ergebnisse darauf hin, dass CDK9 nach EWS-FLI1 agiert. Auch konnten Zellen, die eine Resistenz

nach JQ1 Langzeitbehandlung erworben hatten, weiterhin effektiv mit I-73 behandelt werden und stellen eine attraktive Therapieoption dar. Eine Kombination von JQ1 und I-73 zeigte darüber hinaus schon bei niedrigen Dosierungen eine effektive Blockade des Tumorwachstums *in vivo*.

EZH2 als Hauptbestandteil des PRC2 Komplexes ist ein katalytisch aktives Protein dessen Aktivität zur Trimethylierung von Lysin 27 auf Histon H3 (H3K27me3) führt. Histone mit diesen Modifikationen sind dichter verpackt und reprimieren die Transkription. Aufgrund dieser repressiven Wirkung spielt EZH2 eine sehr bedeutende Rolle während verschiedener entwicklungsphysiologischer Prozesse und eine Deregulation konnte in einer Vielzahl verschiedener Krebsarten, sowie beim ES gezeigt werden. In dieser Arbeit wurde die Inhibition des katalytischen Zentrums von EZH2 mittels spezifischer Inhibitoren als eine weitere zukünftige Behandlungsoption untersucht. Besonders auffallend dabei war, dass trotz der effektiven Inhibition von EZH2, der damit verbundenen Reduzierung von H3K27me3 Markierungen und verstärkten H3K27-Acetylierung, keine Veränderungen im Wachstum oder der Differenzierung der Zellen *in vitro* und *in vivo* beobachtet werden konnten. Obwohl die wesentliche, enzymatische Funktion von EZH2 die Vermittlung der Methylierung von H3K27 ist, gibt es weitere biologische Prozesse in die EZH2-haltige PRC2 Komplexe im ES involviert sein können und in weiteren Analysen untersucht werden müssen.

7 References

1. Ewing J: **Classics in oncology. Diffuse endothelioma of bone. James Ewing. Proceedings of the New York Pathological Society, 1921.** *CA Cancer J Clin* 1972, **22:**95-98.
2. von Levetzow C, Jiang X, Gwye Y, von Levetzow G, Hung L, Cooper A, Hsu JH, Lawlor ER: **Modeling initiation of Ewing sarcoma in human neural crest cells.** *PLoS One* 2011, **6:**e19305.
3. Jedlicka P: **Ewing Sarcoma, an enigmatic malignancy of likely progenitor cell origin, driven by transcription factor oncogenic fusions.** *Int J Clin Exp Pathol* 2010, **3:**338-347.
4. Burchill SA: **Ewing's sarcoma: diagnostic, prognostic, and therapeutic implications of molecular abnormalities.** *J Clin Pathol* 2003, **56:**96-102.
5. Delattre O, Zucman J, Melot T, Garau XS, Zucker JM, Lenoir GM, Ambros PF, Sheer D, Turc-Carel C, Triche TJ, et al.: **The Ewing family of tumors--a subgroup of small-round-cell tumors defined by specific chimeric transcripts.** *N Engl J Med* 1994, **331:**294-299.
6. Glass AG, Fraumeni JF, Jr.: **Epidemiology of bone cancer in children.** *J Natl Cancer Inst* 1970, **44:**187-199.
7. Bernstein M, Kovar H, Paulussen M, Randall RL, Schuck A, Teot LA, Juergens H: **Ewing's sarcoma family of tumors: current management.** *Oncologist* 2006, **11:**503-519.
8. Riggi N, Suva ML, Stamenkovic I: **Ewing's sarcoma origin: from duel to duality.** *Expert Rev Anticancer Ther* 2009, **9:**1025-1030.
9. Ushigome S, Machinami R, Sorensen P: **WHO Classification of Tumours. Pathology and Genetics. Tumours of Soft Tissue and Bone.** 2002.
10. Riggi N, Stamenkovic I: **The Biology of Ewing sarcoma.** *Cancer Lett* 2007, **254:**1-10.
11. Staege MS, Hutter C, Neumann I, Foja S, Hattenhorst UE, Hansen G, Afar D, Burdach SE: **DNA microarrays reveal relationship of Ewing**

family tumors to both endothelial and fetal neural crest-derived cells and define novel targets. *Cancer Res* 2004, **64:**8213-8221.

12. Schmidt D, Harms D, Burdach S: **Malignant peripheral neuroectodermal tumours of childhood and adolescence.** *Virchows Arch A Pathol Anat Histopathol* 1985, **406:**351-365.
13. Turc-Carel C, Philip I, Berger MP, Philip T, Lenoir GM: **Chromosome study of Ewing's sarcoma (ES) cell lines. Consistency of a reciprocal translocation t(11;22)(q24;q12).** *Cancer Genet Cytogenet* 1984, **12:**1-19.
14. Aurias A, Rimbaut C, Buffe D, Zucker JM, Mazabraud A: **Translocation involving chromosome 22 in Ewing's sarcoma. A cytogenetic study of four fresh tumors.** *Cancer Genet Cytogenet* 1984, **12:**21-25.
15. Delattre O, Zucman J, Plougastel B, Desmaze C, Melot T, Peter M, Kovar H, Joubert I, de Jong P, Rouleau G, et al.: **Gene fusion with an ETS DNA-binding domain caused by chromosome translocation in human tumours.** *Nature* 1992, **359:**162-165.
16. Dockhorn-Dworniczak B, Schafer KL, Dantcheva R, Blasius S, van Valen F, Burdach S, Winkelmann W, Jurgens H, Bocker W: **[Molecular genetic detection of t(11;22)(q24;12) translocation in Ewing sarcoma and malignant peripheral neuroectodermal tumors].** *Pathologe* 1994, **15:**103-112.
17. Turc-Carel C, Aurias A, Mugneret F, Lizard S, Sidaner I, Volk C, Thiery JP, Olschwang S, Philip I, Berger MP, et al.: **Chromosomes in Ewing's sarcoma. I. An evaluation of 85 cases of remarkable consistency of t(11;22)(q24;q12).** *Cancer Genet Cytogenet* 1988, **32:**229-238.
18. Richter GH, Plehm S, Fasan A, Rossler S, Unland R, Bennani-Baiti IM, Hotfilder M, Lowel D, von Luettichau I, Mossbrugger I, et al: **EZH2 is a mediator of EWS/FLI1 driven tumor growth and metastasis blocking endothelial and neuro-ectodermal differentiation.** *Proc Natl Acad Sci U S A* 2009, **106:**5324-5329.

19. Uren A, Toretsky JA: **Ewing's sarcoma oncoprotein EWS-FLI1: the perfect target without a therapeutic agent.** *Future Oncol* 2005, **1:**521-528.

20. Riggi N, Knoechel B, Gillespie SM, Rheinbay E, Boulay G, Suva ML, Rossetti NE, Boonseng WE, Oksuz O, Cook EB, et al: **EWS-FLI1 utilizes divergent chromatin remodeling mechanisms to directly activate or repress enhancer elements in Ewing sarcoma.** *Cancer Cell* 2014, **26:**668-681.

21. Sorensen PH, Triche TJ: **Gene fusions encoding chimaeric transcription factors in solid tumours.** *Semin Cancer Biol* 1996, **7:**3-14.

22. Widhe B, Widhe T: **Initial symptoms and clinical features in osteosarcoma and Ewing sarcoma.** *J Bone Joint Surg Am* 2000, **82:**667-674.

23. Cotterill SJ, Ahrens S, Paulussen M, Jurgens HF, Voute PA, Gadner H, Craft AW: **Prognostic factors in Ewing's tumor of bone: analysis of 975 patients from the European Intergroup Cooperative Ewing's Sarcoma Study Group.** *J Clin Oncol* 2000, **18:**3108-3114.

24. Burdach S, Jurgens H: **High-dose chemoradiotherapy (HDC) in the Ewing family of tumors (EFT).** *Crit Rev Oncol Hematol* 2002, **41:**169-189.

25. Miser JS, Krailo MD, Tarbell NJ, Link MP, Fryer CJ, Pritchard DJ, Gebhardt MC, Dickman PS, Perlman EJ, Meyers PA, et al: **Treatment of metastatic Ewing's sarcoma or primitive neuroectodermal tumor of bone: evaluation of combination ifosfamide and etoposide--a Children's Cancer Group and Pediatric Oncology Group study.** *J Clin Oncol* 2004, **22:**2873-2876.

26. Bacci G, Ferrari S, Longhi A, Donati D, De Paolis M, Forni C, Versari M, Setola E, Briccoli A, Barbieri E: **Therapy and survival after recurrence of Ewing's tumors: the Rizzoli experience in 195 patients treated with adjuvant and neoadjuvant chemotherapy from 1979 to 1997.** *Ann Oncol* 2003, **14:**1654-1659.

27. Gaspar N, Hawkins DS, Dirksen U, Lewis IJ, Ferrari S, Le Deley MC, Kovar H, Grimer R, Whelan J, Claude L, et al: **Ewing Sarcoma: Current Management and Future Approaches Through Collaboration.** *J Clin Oncol* 2015, **33:**3036-3046.
28. Burdach S, Thiel U, Schoniger M, Haase R, Wawer A, Nathrath M, Kabisch H, Urban C, Laws HJ, Dirksen U, et al: **Total body MRI-governed involved compartment irradiation combined with high-dose chemotherapy and stem cell rescue improves long-term survival in Ewing tumor patients with multiple primary bone metastases.** *Bone Marrow Transplant* 2010, **45:**483-489.
29. Thiel U, Wawer A, Wolf P, Badoglio M, Santucci A, Klingebiel T, Basu O, Borkhardt A, Laws HJ, Kodera Y, et al: **No improvement of survival with reduced- versus high-intensity conditioning for allogeneic stem cell transplants in Ewing tumor patients.** *Ann Oncol* 2011, **22:**1614-1621.
30. Brohl AS, Solomon DA, Chang W, Wang J, Song Y, Sindiri S, Patidar R, Hurd L, Chen L, Shern JF, et al: **The genomic landscape of the Ewing Sarcoma family of tumors reveals recurrent STAG2 mutation.** *PLoS Genet* 2014, **10:**e1004475.
31. Crompton BD, Stewart C, Taylor-Weiner A, Alexe G, Kurek KC, Calicchio ML, Kiezun A, Carter SL, Shukla SA, Mehta SS, et al: **The genomic landscape of pediatric Ewing sarcoma.** *Cancer Discov* 2014, **4:**1326-1341.
32. Agelopoulos K, Richter GH, Schmidt E, Dirksen U, von Heyking K, Moser B, Klein HU, Kontny U, Dugas M, Poos K, et al: **Deep Sequencing in Conjunction with Expression and Functional Analyses Reveals Activation of FGFR1 in Ewing Sarcoma.** *Clin Cancer Res* 2015, **21:**4935-4946.
33. Grunewald TG, Diebold I, Esposito I, Plehm S, Hauer K, Thiel U, da Silva-Buttkus P, Neff F, Unland R, Muller-Tidow C, et al: **STEAP1 is associated with the invasive and oxidative stress phenotype of Ewing tumors.** *Mol Cancer Res* 2012, **10:**52-65.
34. Richter GH, Fasan A, Hauer K, Grunewald TG, Berns C, Rossler S, Naumann I, Staege MS, Fulda S, Esposito I, Burdach S: **G-Protein**

coupled receptor 64 promotes invasiveness and metastasis in Ewing sarcomas through PGF and MMP1. *J Pathol* 2013, **230:**70-81.

35. Hauer K, Calzada-Wack J, Steiger K, Grunewald TG, Baumhoer D, Plehm S, Buch T, Prazeres da Costa O, Esposito I, Burdach S, Richter GH: **DKK2 mediates osteolysis, invasiveness, and metastatic spread in Ewing sarcoma.** *Cancer Res* 2013, **73:**967-977.
36. Berger SL, Kouzarides T, Shiekhattar R, Shilatifard A: **An operational definition of epigenetics.** *Genes Dev* 2009, **23:**781-783.
37. Kouzarides T: **Chromatin modifications and their function.** *Cell* 2007, **128:**693-705.
38. Campos EI, Reinberg D: **Histones: annotating chromatin.** *Annu Rev Genet* 2009, **43:**559-599.
39. Falls JG, Pulford DJ, Wylie AA, Jirtle RL: **Genomic imprinting: implications for human disease.** *Am J Pathol* 1999, **154:**635-647.
40. Gardiner-Garden M, Frommer M: **CpG islands in vertebrate genomes.** *J Mol Biol* 1987, **196:**261-282.
41. Saxonov S, Berg P, Brutlag DL: **A genome-wide analysis of CpG dinucleotides in the human genome distinguishes two distinct classes of promoters.** *Proc Natl Acad Sci U S A* 2006, **103:**1412-1417.
42. Kaur S, Lotsari-Salomaa JE, Seppanen-Kaijansinkko R, Peltomaki P: **MicroRNA Methylation in Colorectal Cancer.** *Adv Exp Med Biol* 2016, **937:**109-122.
43. Deaton AM, Bird A: **CpG islands and the regulation of transcription.** *Genes Dev* 2011, **25:**1010-1022.
44. Subramaniam D, Thombre R, Dhar A, Anant S: **DNA methyltransferases: a novel target for prevention and therapy.** *Front Oncol* 2014, **4:**80.
45. Feinberg AP, Vogelstein B: **Hypomethylation distinguishes genes of some human cancers from their normal counterparts.** *Nature* 1983, **301:**89-92.

46. Feinberg AP, Tycko B: **The history of cancer epigenetics.** *Nat Rev Cancer* 2004, **4:**143-153.
47. Esteller M: **Cancer epigenomics: DNA methylomes and histone-modification maps.** *Nat Rev Genet* 2007, **8:**286-298.
48. Herman JG, Baylin SB: **Gene silencing in cancer in association with promoter hypermethylation.** *N Engl J Med* 2003, **349:**2042-2054.
49. Esteller M, Almouzni G: **How epigenetics integrates nuclear functions.** *EMBO Rep* 2005, **6:**624-628.
50. Fuks F: **DNA methylation and histone modifications: teaming up to silence genes.** *Curr Opin Genet Dev* 2005, **15:**490-495.
51. Gieni RS, Hendzel MJ: **Polycomb group protein gene silencing, non-coding RNA, stem cells, and cancer.** *Biochem Cell Biol* 2009, **87:**711-746.
52. Peterson CL, Laniel MA: **Histones and histone modifications.** *Curr Biol* 2004, **14:**R546-551.
53. Murr R: **Interplay between different epigenetic modifications and mechanisms.** *Adv Genet* 2010, **70:**101-141.
54. Cosgrove MS, Boeke JD, Wolberger C: **Regulated nucleosome mobility and the histone code.** *Nat Struct Mol Biol* 2004, **11:**1037-1043.
55. Grant PA: **A tale of histone modifications.** *Genome Biol* 2001, **2:**REVIEWS0003.
56. Shahbazian MD, Grunstein M: **Functions of site-specific histone acetylation and deacetylation.** *Annu Rev Biochem* 2007, **76:**75-100.
57. Brownell JE, Allis CD: **An activity gel assay detects a single, catalytically active histone acetyltransferase subunit in Tetrahymena macronuclei.** *Proc Natl Acad Sci U S A* 1995, **92:**6364-6368.
58. Kleff S, Andrulis ED, Anderson CW, Sternglanz R: **Identification of a gene encoding a yeast histone H4 acetyltransferase.** *J Biol Chem* 1995, **270:**24674-24677.
59. Bannister AJ, Kouzarides T: **The CBP co-activator is a histone acetyltransferase.** *Nature* 1996, **384:**641-643.

60. Brownell JE, Zhou J, Ranalli T, Kobayashi R, Edmondson DG, Roth SY, Allis CD: **Tetrahymena histone acetyltransferase A: a homolog to yeast Gcn5p linking histone acetylation to gene activation.** *Cell* 1996, **84:**843-851.
61. Struhl K: **Histone acetylation and transcriptional regulatory mechanisms.** *Genes Dev* 1998, **12:**599-606.
62. Zeng L, Zhou MM: **Bromodomain: an acetyl-lysine binding domain.** *FEBS Lett* 2002, **513:**124-128.
63. Suzuki J, Chen YY, Scott GK, Devries S, Chin K, Benz CC, Waldman FM, Hwang ES: **Protein acetylation and histone deacetylase expression associated with malignant breast cancer progression.** *Clin Cancer Res* 2009, **15:**3163-3171.
64. Glozak MA, Seto E: **Histone deacetylases and cancer.** *Oncogene* 2007, **26:**5420-5432.
65. Sun XJ, Man N, Tan Y, Nimer SD, Wang L: **The Role of Histone Acetyltransferases in Normal and Malignant Hematopoiesis.** *Front Oncol* 2015, **5:**108.
66. Zhang Y, Reinberg D: **Transcription regulation by histone methylation: interplay between different covalent modifications of the core histone tails.** *Genes Dev* 2001, **15:**2343-2360.
67. Rice JC, Briggs SD, Ueberheide B, Barber CM, Shabanowitz J, Hunt DF, Shinkai Y, Allis CD: **Histone methyltransferases direct different degrees of methylation to define distinct chromatin domains.** *Mol Cell* 2003, **12:**1591-1598.
68. Wang Z, Zang C, Rosenfeld JA, Schones DE, Barski A, Cuddapah S, Cui K, Roh TY, Peng W, Zhang MQ, Zhao K: **Combinatorial patterns of histone acetylations and methylations in the human genome.** *Nat Genet* 2008, **40:**897-903.
69. Barski A, Cuddapah S, Cui K, Roh TY, Schones DE, Wang Z, Wei G, Chepelev I, Zhao K: **High-resolution profiling of histone methylations in the human genome.** *Cell* 2007, **129:**823-837.
70. Bernstein BE, Mikkelsen TS, Xie X, Kamal M, Huebert DJ, Cuff J, Fry B, Meissner A, Wernig M, Plath K, et al: **A bivalent chromatin**

structure marks key developmental genes in embryonic stem cells. *Cell* 2006, **125:**315-326.

71. Martin C, Zhang Y: **The diverse functions of histone lysine methylation.** *Nat Rev Mol Cell Biol* 2005, **6:**838-849.
72. Allis CD, Berger SL, Cote J, Dent S, Jenuwien T, Kouzarides T, Pillus L, Reinberg D, Shi Y, Shiekhattar R, et al: **New nomenclature for chromatin-modifying enzymes.** *Cell* 2007, **131:**633-636.
73. Keppler BR, Archer TK: **Chromatin-modifying enzymes as therapeutic targets--Part 1.** *Expert Opin Ther Targets* 2008, **12:**1301-1312.
74. Byvoet P, Shepherd GR, Hardin JM, Noland BJ: **The distribution and turnover of labeled methyl groups in histone fractions of cultured mammalian cells.** *Arch Biochem Biophys* 1972, **148:**558-567.
75. Thomas G, Lange HW, Hempel K: **[Relative stability of lysine-bound methyl groups in arginie-rich histones and their subfrations in Ehrlich ascites tumor cells in vitro].** *Hoppe Seylers Z Physiol Chem* 1972, **353:**1423-1428.
76. Mosammaparast N, Shi Y: **Reversal of histone methylation: biochemical and molecular mechanisms of histone demethylases.** *Annu Rev Biochem* 2010, **79:**155-179.
77. Albert M, Helin K: **Histone methyltransferases in cancer.** *Semin Cell Dev Biol* 2010, **21:**209-220.
78. Varier RA, Timmers HT: **Histone lysine methylation and demethylation pathways in cancer.** *Biochim Biophys Acta* 2011, **1815:**75-89.
79. Chase A, Cross NC: **Aberrations of EZH2 in cancer.** *Clin Cancer Res* 2011, **17:**2613-2618.
80. Valk-Lingbeek ME, Bruggeman SW, van Lohuizen M: **Stem cells and cancer; the polycomb connection.** *Cell* 2004, **118:**409-418.
81. Wang H, Wang L, Erdjument-Bromage H, Vidal M, Tempst P, Jones RS, Zhang Y: **Role of histone H2A ubiquitination in Polycomb silencing.** *Nature* 2004, **431:**873-878.
82. Margueron R, Reinberg D: **The Polycomb complex PRC2 and its mark in life.** *Nature* 2011, **469:**343-349.

83. Margueron R, Li G, Sarma K, Blais A, Zavadil J, Woodcock CL, Dynlacht BD, Reinberg D: **Ezh1 and Ezh2 maintain repressive chromatin through different mechanisms.** *Mol Cell* 2008, **32:**503-518.
84. Schmitges FW, Prusty AB, Faty M, Stutzer A, Lingaraju GM, Aiwazian J, Sack R, Hess D, Li L, Zhou S, et al: **Histone methylation by PRC2 is inhibited by active chromatin marks.** *Mol Cell* 2011, **42:**330-341.
85. Kim H, Kang K, Kim J: **AEBP2 as a potential targeting protein for Polycomb Repression Complex PRC2.** *Nucleic Acids Res* 2009, **37:**2940-2950.
86. Nekrasov M, Klymenko T, Fraterman S, Papp B, Oktaba K, Kocher T, Cohen A, Stunnenberg HG, Wilm M, Muller J: **Pcl-PRC2 is needed to generate high levels of H3-K27 trimethylation at Polycomb target genes.** *EMBO J* 2007, **26:**4078-4088.
87. Li G, Margueron R, Ku M, Chambon P, Bernstein BE, Reinberg D: **Jarid2 and PRC2, partners in regulating gene expression.** *Genes Dev* 2010, **24:**368-380.
88. Ku M, Koche RP, Rheinbay E, Mendenhall EM, Endoh M, Mikkelsen TS, Presser A, Nusbaum C, Xie X, Chi AS, et al: **Genomewide analysis of PRC1 and PRC2 occupancy identifies two classes of bivalent domains.** *PLoS Genet* 2008, **4:**e1000242.
89. Schuettengruber B, Cavalli G: **Recruitment of polycomb group complexes and their role in the dynamic regulation of cell fate choice.** *Development* 2009, **136:**3531-3542.
90. Wilkinson FH, Park K, Atchison ML: **Polycomb recruitment to DNA in vivo by the YY1 REPO domain.** *Proc Natl Acad Sci U S A* 2006, **103:**19296-19301.
91. Xi H, Yu Y, Fu Y, Foley J, Halees A, Weng Z: **Analysis of overrepresented motifs in human core promoters reveals dual regulatory roles of YY1.** *Genome Res* 2007, **17:**798-806.
92. Plath K, Fang J, Mlynarczyk-Evans SK, Cao R, Worringer KA, Wang H, de la Cruz CC, Otte AP, Panning B, Zhang Y: **Role of histone H3 lysine 27 methylation in X inactivation.** *Science* 2003, **300:**131-135.

93. Tsai MC, Manor O, Wan Y, Mosammaparast N, Wang JK, Lan F, Shi Y, Segal E, Chang HY: **Long noncoding RNA as modular scaffold of histone modification complexes.** *Science* 2010, **329:**689-693.

94. Bracken AP, Pasini D, Capra M, Prosperini E, Colli E, Helin K: **EZH2 is downstream of the pRB-E2F pathway, essential for proliferation and amplified in cancer.** *EMBO J* 2003, **22:**5323-5335.

95. Yap DB, Chu J, Berg T, Schapira M, Cheng SW, Moradian A, Morin RD, Mungall AJ, Meissner B, Boyle M, et al: **Somatic mutations at EZH2 Y641 act dominantly through a mechanism of selectively altered PRC2 catalytic activity, to increase H3K27 trimethylation.** *Blood* 2011, **117:**2451-2459.

96. Gui Y, Guo G, Huang Y, Hu X, Tang A, Gao S, Wu R, Chen C, Li X, Zhou L, et al: **Frequent mutations of chromatin remodeling genes in transitional cell carcinoma of the bladder.** *Nat Genet* 2011, **43:**875-878.

97. Pugh TJ, Weeraratne SD, Archer TC, Pomeranz Krummel DA, Auclair D, Bochicchio J, Carneiro MO, Carter SL, Cibulskis K, Erlich RL, et al: **Medulloblastoma exome sequencing uncovers subtype-specific somatic mutations.** *Nature* 2012, **488:**106-110.

98. Waddell N, Pajic M, Patch AM, Chang DK, Kassahn KS, Bailey P, Johns AL, Miller D, Nones K, Quek K, et al: **Whole genomes redefine the mutational landscape of pancreatic cancer.** *Nature* 2015, **518:**495-501.

99. Bruggeman SW, Valk-Lingbeek ME, van der Stoop PP, Jacobs JJ, Kieboom K, Tanger E, Hulsman D, Leung C, Arsenijevic Y, Marino S, van Lohuizen M: **Ink4a and Arf differentially affect cell proliferation and neural stem cell self-renewal in Bmi1-deficient mice.** *Genes Dev* 2005, **19:**1438-1443.

100. Cao Q, Yu J, Dhanasekaran SM, Kim JH, Mani RS, Tomlins SA, Mehra R, Laxman B, Cao X, Yu J, et al: **Repression of E-cadherin by the polycomb group protein EZH2 in cancer.** *Oncogene* 2008, **27:**7274-7284.

101. Du J, Li L, Ou Z, Kong C, Zhang Y, Dong Z, Zhu S, Jiang H, Shao Z, Huang B, Lu J: **FOXC1, a target of polycomb, inhibits metastasis of breast cancer cells.** *Breast Cancer Res Treat* 2012, **131:**65-73.
102. Xu K, Wu ZJ, Groner AC, He HH, Cai C, Lis RT, Wu X, Stack EC, Loda M, Liu T, et al: **EZH2 oncogenic activity in castration-resistant prostate cancer cells is Polycomb-independent.** *Science* 2012, **338:**1465-1469.
103. Lee ST, Li Z, Wu Z, Aau M, Guan P, Karuturi RK, Liou YC, Yu Q: **Context-specific regulation of NF-kappaB target gene expression by EZH2 in breast cancers.** *Mol Cell* 2011, **43:**798-810.
104. Kim E, Kim M, Woo DH, Shin Y, Shin J, Chang N, Oh YT, Kim H, Rheey J, Nakano I, et al: **Phosphorylation of EZH2 activates STAT3 signaling via STAT3 methylation and promotes tumorigenicity of glioblastoma stem-like cells.** *Cancer Cell* 2013, **23:**839-852.
105. Burdach S, Plehm S, Unland R, Dirksen U, Borkhardt A, Staege MS, Muller-Tidow C, Richter GH: **Epigenetic maintenance of stemness and malignancy in peripheral neuroectodermal tumors by EZH2.** *Cell Cycle* 2009, **8:**1991-1996.
106. Taverna SD, Li H, Ruthenburg AJ, Allis CD, Patel DJ: **How chromatin-binding modules interpret histone modifications: lessons from professional pocket pickers.** *Nat Struct Mol Biol* 2007, **14:**1025-1040.
107. Bannister AJ, Kouzarides T: **Regulation of chromatin by histone modifications.** *Cell Res* 2011, **21:**381-395.
108. Marchand JR, Caflisch A: **Binding Mode of Acetylated Histones to Bromodomains: Variations on a Common Motif.** *ChemMedChem* 2015, **10:**1327-1333.
109. Florence B, Faller DV: **You bet-cha: a novel family of transcriptional regulators.** *Front Biosci* 2001, **6:**D1008-1018.
110. Wu SY, Chiang CM: **The double bromodomain-containing chromatin adaptor Brd4 and transcriptional regulation.** *J Biol Chem* 2007, **282:**13141-13145.

111. Kanno T, Kanno Y, Siegel RM, Jang MK, Lenardo MJ, Ozato K: **Selective recognition of acetylated histones by bromodomain proteins visualized in living cells.** *Mol Cell* 2004, **13:**33-43.
112. You J, Croyle JL, Nishimura A, Ozato K, Howley PM: **Interaction of the bovine papillomavirus E2 protein with Brd4 tethers the viral DNA to host mitotic chromosomes.** *Cell* 2004, **117:**349-360.
113. Abbate EA, Voitenleitner C, Botchan MR: **Structure of the papillomavirus DNA-tethering complex E2:Brd4 and a peptide that ablates HPV chromosomal association.** *Mol Cell* 2006, **24:**877-889.
114. Malik S, Roeder RG: **The metazoan Mediator co-activator complex as an integrative hub for transcriptional regulation.** *Nat Rev Genet* 2010, **11:**761-772.
115. Jang MK, Mochizuki K, Zhou M, Jeong HS, Brady JN, Ozato K: **The bromodomain protein Brd4 is a positive regulatory component of P-TEFb and stimulates RNA polymerase II-dependent transcription.** *Mol Cell* 2005, **19:**523-534.
116. LeRoy G, Rickards B, Flint SJ: **The double bromodomain proteins Brd2 and Brd3 couple histone acetylation to transcription.** *Mol Cell* 2008, **30:**51-60.
117. French CA, Miyoshi I, Kubonishi I, Grier HE, Perez-Atayde AR, Fletcher JA: **BRD4-NUT fusion oncogene: a novel mechanism in aggressive carcinoma.** *Cancer Res* 2003, **63:**304-307.
118. French CA, Ramirez CL, Kolmakova J, Hickman TT, Cameron MJ, Thyne ME, Kutok JL, Toretsky JA, Tadavarthy AK, Kees UR, et al: **BRD-NUT oncoproteins: a family of closely related nuclear proteins that block epithelial differentiation and maintain the growth of carcinoma cells.** *Oncogene* 2008, **27:**2237-2242.
119. Filippakopoulos P, Qi J, Picaud S, Shen Y, Smith WB, Fedorov O, Morse EM, Keates T, Hickman TT, Felletar I, et al: **Selective inhibition of BET bromodomains.** *Nature* 2010, **468:**1067-1073.
120. Dang Chi V: **MYC on the Path to Cancer.** *Cell* 2012, **149:**22-35.
121. Duesberg PH, Vogt PK: **Avian acute leukemia viruses MC29 and MH2 share specific RNA sequences: evidence for a second class**

of transforming genes. *Proc Natl Acad Sci U S A* 1979, **76:**1633-1637.

122. Hu SS, Lai MM, Vogt PK: **Genome of avian myelocytomatosis virus MC29: analysis by heteroduplex mapping.** *Proc Natl Acad Sci U S A* 1979, **76:**1265-1268.
123. Sheiness D, Bishop JM: **DNA and RNA from uninfected vertebrate cells contain nucleotide sequences related to the putative transforming gene of avian myelocytomatosis virus.** *J Virol* 1979, **31:**514-521.
124. Vennstrom B, Sheiness D, Zabielski J, Bishop JM: **Isolation and characterization of c-myc, a cellular homolog of the oncogene (v-myc) of avian myelocytomatosis virus strain 29.** *J Virol* 1982, **42:**773-779.
125. Huang X, Dixit VM: **Drugging the undruggables: exploring the ubiquitin system for drug development.** *Cell Res* 2016, **26:**484-498.
126. Albihn A, Johnsen JI, Henriksson MA: **MYC in oncogenesis and as a target for cancer therapies.** *Adv Cancer Res* 2010, **107:**163-224.
127. Henriksson M, Luscher B: **Proteins of the Myc network: essential regulators of cell growth and differentiation.** *Adv Cancer Res* 1996, **68:**109-182.
128. Oster SK, Ho CS, Soucie EL, Penn LZ: **The myc oncogene: MarvelousIY Complex.** *Adv Cancer Res* 2002, **84:**81-154.
129. Ponzielli R, Katz S, Barsyte-Lovejoy D, Penn LZ: **Cancer therapeutics: targeting the dark side of Myc.** *Eur J Cancer* 2005, **41:**2485-2501.
130. Goldman JP, Blundell MP, Lopes L, Kinnon C, Di Santo JP, Thrasher AJ: **Enhanced human cell engraftment in mice deficient in RAG2 and the common cytokine receptor gamma chain.** *Br J Haematol* 1998, **103:**335-342.
131. Benelli R, Albini A: **In vitro models of angiogenesis: the use of Matrigel.** *Int J Biol Markers* 1999, **14:**243-246.
132. Helson L, Das SK, Hajdu SI: **Human neuroblastoma in nude mice.** *Cancer Res* 1975, **35:**2594-2599.

133. Hensel T, Giorgi C, Schmidt O, Calzada-Wack J, Neff F, Buch T, Niggli FK, Schafer BW, Burdach S, Richter GH: **Targeting the EWS-ETS transcriptional program by BET bromodomain inhibition in Ewing sarcoma.** *Oncotarget* 2016, **7:**1451-1463.
134. Tusher VG, Tibshirani R, Chu G: **Significance analysis of microarrays applied to the ionizing radiation response.** *Proc Natl Acad Sci U S A* 2001, **98:**5116-5121.
135. Subramanian A, Tamayo P, Mootha VK, Mukherjee S, Ebert BL, Gillette MA, Paulovich A, Pomeroy SL, Golub TR, Lander ES, Mesirov JP: **Gene set enrichment analysis: a knowledge-based approach for interpreting genome-wide expression profiles.** *Proc Natl Acad Sci U S A* 2005, **102:**15545-15550.
136. Vita M, Henriksson M: **The Myc oncoprotein as a therapeutic target for human cancer.** *Seminars in Cancer Biology* 2006, **16:**318-330.
137. Miller DM, Thomas SD, Islam A, Muench D, Sedoris K: **c-Myc and Cancer Metabolism.** *Clinical Cancer Research* 2012, **18:**5546-5553.
138. Soucek L, Evan GI: **THE UPS AND DOWNS OF MYC BIOLOGY.** *Curr Opin Genet Dev* 2010, **20:**91.
139. Giorgi C, Boro A, Rechfeld F, Lopez-Garcia LA, Gierisch ME, Schafer BW, Niggli FK: **PI3K/AKT signaling modulates transcriptional expression of EWS/FLI1 through specificity protein 1.** *Oncotarget* 2015, **6:**28895-28910.
140. Scotlandi K, Benini S, Nanni P, Lollini PL, Nicoletti G, Landuzzi L, Serra M, Manara MC, Picci P, Baldini N: **Blockage of insulin-like growth factor-I receptor inhibits the growth of Ewing's sarcoma in athymic mice.** *Cancer Res* 1998, **58:**4127-4131.
141. Scotlandi K, Benini S, Sarti M, Serra M, Lollini PL, Maurici D, Picci P, Manara MC, Baldini N: **Insulin-like growth factor I receptor-mediated circuit in Ewing's sarcoma/peripheral neuroectodermal tumor: a possible therapeutic target.** *Cancer Res* 1996, **56:**4570-4574.
142. Scotlandi K, Picci P: **Targeting insulin-like growth factor 1 receptor in sarcomas.** *Curr Opin Oncol* 2008, **20:**419-427.

143. van Valen F, Winkelmann W, Jurgens H: **Type I and type II insulin-like growth factor receptors and their function in human Ewing's sarcoma cells.** *J Cancer Res Clin Oncol* 1992, **118:**269-275.

144. Rikhof B, de Jong S, Suurmeijer AJ, Meijer C, van der Graaf WT: **The insulin-like growth factor system and sarcomas.** *J Pathol* 2009, **217:**469-482.

145. Toretsky JA, Steinberg SM, Thakar M, Counts D, Pironis B, Parente C, Eskenazi A, Helman L, Wexler LH: **Insulin-like growth factor type 1 (IGF-1) and IGF binding protein-3 in patients with Ewing sarcoma family of tumors.** *Cancer* 2001, **92:**2941-2947.

146. Zhu J, Blenis J, Yuan J: **Activation of PI3K/Akt and MAPK pathways regulates Myc-mediated transcription by phosphorylating and promoting the degradation of Mad1.** *Proc Natl Acad Sci U S A* 2008, **105:**6584-6589.

147. Schild C, Wirth M, Reichert M, Schmid RM, Saur D, Schneider G: **PI3K signaling maintains c-myc expression to regulate transcription of E2F1 in pancreatic cancer cells.** *Mol Carcinog* 2009, **48:**1149-1158.

148. Wilker E, Lu J, Rho O, Carbajal S, Beltran L, DiGiovanni J: **Role of PI3K/Akt signaling in insulin-like growth factor-1 (IGF-1) skin tumor promotion.** *Mol Carcinog* 2005, **44:**137-145.

149. Han G, Wang Y, Bi W: **C-Myc overexpression promotes osteosarcoma cell invasion via activation of MEK-ERK pathway.** *Oncol Res* 2012, **20:**149-156.

150. Maira SM, Stauffer F, Brueggen J, Furet P, Schnell C, Fritsch C, Brachmann S, Chene P, De Pover A, Schoemaker K, et al: **Identification and characterization of NVP-BEZ235, a new orally available dual phosphatidylinositol 3-kinase/mammalian target of rapamycin inhibitor with potent in vivo antitumor activity.** *Mol Cancer Ther* 2008, **7:**1851-1863.

151. Rahl PB, Lin CY, Seila AC, Flynn RA, McCuine S, Burge CB, Sharp PA, Young RA: **c-Myc regulates transcriptional pause release.** *Cell* 2010, **141:**432-445.

152. Dawson MA, Prinjha RK, Dittmann A, Giotopoulos G, Bantscheff M, Chan WI, Robson SC, Chung CW, Hopf C, Savitski MM, et al: **Inhibition of BET recruitment to chromatin as an effective treatment for MLL-fusion leukaemia.** *Nature* 2011, **478:**529-533.

153. Hu-Lieskovan S, Zhang J, Wu L, Shimada H, Schofield DE, Triche TJ: **EWS-FLI1 fusion protein up-regulates critical genes in neural crest development and is responsible for the observed phenotype of Ewing's family of tumors.** *Cancer Res* 2005, **65:**4633-4644.

154. Riggi N, Suva ML, Suva D, Cironi L, Provero P, Tercier S, Joseph JM, Stehle JC, Baumer K, Kindler V, Stamenkovic I: **EWS-FLI-1 expression triggers a Ewing's sarcoma initiation program in primary human mesenchymal stem cells.** *Cancer Res* 2008, **68:**2176-2185.

155. Delmore JE, Issa GC, Lemieux ME, Rahl PB, Shi J, Jacobs HM, Kastritis E, Gilpatrick T, Paranal RM, Qi J, et al: **BET bromodomain inhibition as a therapeutic strategy to target c-Myc.** *Cell* 2011, **146:**904-917.

156. Zuber J, Shi J, Wang E, Rappaport AR, Herrmann H, Sison EA, Magoon D, Qi J, Blatt K, Wunderlich M, et al: **RNAi screen identifies Brd4 as a therapeutic target in acute myeloid leukaemia.** *Nature* 2011, **478:**524-528.

157. Puissant A, Frumm SM, Alexe G, Bassil CF, Qi J, Chanthery YH, Nekritz EA, Zeid R, Gustafson WC, Greninger P, et al: **Targeting MYCN in neuroblastoma by BET bromodomain inhibition.** *Cancer Discov* 2013, **3:**308-323.

158. Matzuk MM, McKeown MR, Filippakopoulos P, Li Q, Ma L, Agno JE, Lemieux ME, Picaud S, Yu RN, Qi J, et al: **Small-molecule inhibition of BRDT for male contraception.** *Cell* 2012, **150:**673-684.

159. Bolden JE, Tasdemir N, Dow LE, van Es JH, Wilkinson JE, Zhao Z, Clevers H, Lowe SW: **Inducible in vivo silencing of Brd4 identifies potential toxicities of sustained BET protein inhibition.** *Cell Rep* 2014, **8:**1919-1929.

160. Itzen F, Greifenberg AK, Bosken CA, Geyer M: **Brd4 activates P-TEFb for RNA polymerase II CTD phosphorylation.** *Nucleic Acids Res* 2014, **42:**7577-7590.

161. Walsby E, Pratt G, Shao H, Abbas AY, Fischer PM, Bradshaw TD, Brennan P, Fegan C, Wang S, Pepper C: **A novel Cdk9 inhibitor preferentially targets tumor cells and synergizes with fludarabine.** *Oncotarget* 2014, **5:**375-385.

162. Sonawane YA, Taylor MA, Napoleon JV, Rana S, Contreras JI, Natarajan A: **Cyclin Dependent Kinase 9 Inhibitors for Cancer Therapy.** *J Med Chem* 2016, **59:**8667-8684.

163. Klingbeil O, Lesche R, Gelato KA, Haendler B, Lejeune P: **Inhibition of BET bromodomain-dependent XIAP and FLIP expression sensitizes KRAS-mutated NSCLC to pro-apoptotic agents.** *Cell Death Dis* 2016, **7:**e2365.

164. Bratton SB, Cohen GM: **Death receptors leave a caspase footprint that Smacs of XIAP.** *Cell Death Differ* 2003, **10:**4-6.

165. Scaffidi C, Schmitz I, Krammer PH, Peter ME: **The role of c-FLIP in modulation of CD95-induced apoptosis.** *J Biol Chem* 1999, **274:**1541-1548.

166. Bisgrove DA, Mahmoudi T, Henklein P, Verdin E: **Conserved P-TEFb-interacting domain of BRD4 inhibits HIV transcription.** *Proc Natl Acad Sci U S A* 2007, **104:**13690-13695.

167. Yang Z, Yik JH, Chen R, He N, Jang MK, Ozato K, Zhou Q: **Recruitment of P-TEFb for stimulation of transcriptional elongation by the bromodomain protein Brd4.** *Mol Cell* 2005, **19:**535-545.

168. Peterlin BM, Price DH: **Controlling the elongation phase of transcription with P-TEFb.** *Mol Cell* 2006, **23:**297-305.

169. Kurimchak AM, Shelton C, Duncan KE, Johnson KJ, Brown J, O'Brien S, Gabbasov R, Fink LS, Li Y, Lounsbury N, et al: **Resistance to BET Bromodomain Inhibitors Is Mediated by Kinome Reprogramming in Ovarian Cancer.** *Cell Rep* 2016, **16:**1273-1286.

170. McCabe MT, Ott HM, Ganji G, Korenchuk S, Thompson C, Van Aller GS, Liu Y, Graves AP, Della Pietra A, 3rd, Diaz E, et al: **EZH2**

inhibition as a therapeutic strategy for lymphoma with EZH2-activating mutations. *Nature* 2012, **492:**108-112.

171. Pappo AS, Patel SR, Crowley J, Reinke DK, Kuenkele K-P, Chawla SP, Toner GC, Maki RG, Meyers PA, Chugh R, et al: **R1507, a Monoclonal Antibody to the Insulin-Like Growth Factor 1 Receptor, in Patients With Recurrent or Refractory Ewing Sarcoma Family of Tumors: Results of a Phase II Sarcoma Alliance for Research Through Collaboration Study.** *Journal of Clinical Oncology* 2011, **29:**4541-4547.
172. Mita MM, Mita AC, Chu QS, Rowinsky EK, Fetterly GJ, Goldston M, Patnaik A, Mathews L, Ricart AD, Mays T, et al: **Phase I Trial of the Novel Mammalian Target of Rapamycin Inhibitor Deforolimus (AP23573; MK-8669) Administered Intravenously Daily for 5 Days Every 2 Weeks to Patients With Advanced Malignancies.** *Journal of Clinical Oncology* 2008, **26:**361-367.
173. Bond M, Bernstein ML, Pappo A, Schultz KR, Krailo M, Blaney SM, Adamson PC: **A phase II study of imatinib mesylate in children with refractory or relapsed solid tumors: a Children's Oncology Group study.** *Pediatr Blood Cancer* 2008, **50:**254-258.
174. Jimeno A, Daw NC, Amador ML, Cusatis G, Kulesza P, Krailo M, Ingle AM, Blaney SM, Adamson P, Hidalgo M, Children's Oncology G: **Analysis of biologic surrogate markers from a Children's Oncology Group Phase I trial of gefitinib in pediatric patients with solid tumors.** *Pediatr Blood Cancer* 2007, **49:**352-357.
175. Fox E, Aplenc R, Bagatell R, Chuk MK, Dombi E, Goodspeed W, Goodwin A, Kromplewski M, Jayaprakash N, Marotti M, et al: **A Phase 1 Trial and Pharmacokinetic Study of Cediranib, an Orally Bioavailable Pan–Vascular Endothelial Growth Factor Receptor Inhibitor, in Children and Adolescents With Refractory Solid Tumors.** *Journal of Clinical Oncology* 2010, **28:**5174-5181.
176. Choy E, Butrynski JE, Harmon DC, Morgan JA, George S, Wagner AJ, D'Adamo D, Cote GM, Flamand Y, Benes CH, et al: **Phase II study of olaparib in patients with refractory Ewing sarcoma**

following failure of standard chemotherapy. *BMC Cancer* 2014, **14**.

177. Tomazou EM, Sheffield NC, Schmidl C, Schuster M, Schonegger A, Datlinger P, Kubicek S, Bock C, Kovar H: **Epigenome mapping reveals distinct modes of gene regulation and widespread enhancer reprogramming by the oncogenic fusion protein EWS-FLI1.** *Cell Rep* 2015, **10:**1082-1095.
178. Cheng Z: **Inhibition of BET Bromodomain Targets Genetically Diverse Glioblastoma.** 2013, **19:**1748-1759.
179. Henssen A, Thor T, Odersky A, Heukamp L, El-Hindy N, Beckers A, Speleman F, Althoff K, Schäfers S, Schramm A, et al: **BET bromodomain protein inhibition is a therapeutic option for medulloblastoma.** *Oncotarget* 2013, **4:**2080-2095.
180. Dauphinot L, De Oliveira C, Melot T, Sevenet N, Thomas V, Weissman BE, Delattre O: **Analysis of the expression of cell cycle regulators in Ewing cell lines: EWS-FLI-1 modulates p57KIP2and c-Myc expression.** *Oncogene* 2001, **20:**3258-3265.
181. Kovar H: **Blocking the road, stopping the engine or killing the driver? Advances in targeting EWS/FLI-1 fusion in Ewing sarcoma as novel therapy.** *Expert Opin Ther Targets* 2014, **18:**1315-1328.
182. Kanno T, Kanno Y, LeRoy G, Campos E, Sun H-W, Brooks SR, Vahedi G, Heightman TD, Garcia BA, Reinberg D, et al: **BRD4 assists elongation of both coding and enhancer RNAs by interacting with acetylated histones.** *Nat Struct Mol Biol* 2014, **21:**1047-1057.
183. LeRoy G, Rickards B, Flint S: **The double bromodomain proteins Brd2 and Brd3 couple histone acetylation to transcription.** *Mol Cell* 2008, **30:**51-60.
184. Dey A: **The double bromodomain protein Brd4 binds to acetylated chromatin during.** 2003, **100:**8758-8763.
185. Zengerle M, Chan KH, Ciulli A: **Selective Small Molecule Induced Degradation of the BET Bromodomain Protein BRD4.** *ACS Chem Biol* 2015, **10:**1770-1777.

186. Bai L, Zhou B, Yang CY, Ji J, McEachern D, Przybranowski S, Jiang H, Hu J, Xu F, Zhao Y, et al: **Targeted Degradation of BET Proteins in Triple-Negative Breast Cancer.** *Cancer Res* 2017.

187. Gilan O, Lam EY, Becher I, Lugo D, Cannizzaro E, Joberty G, Ward A, Wiese M, Fong CY, Ftouni S, et al: **Functional interdependence of BRD4 and DOT1L in MLL leukemia.** *Nat Struct Mol Biol* 2016, **23:**673-681.

188. Stegmaier K, Wong JS, Ross KN, Chow KT, Peck D, Wright RD, Lessnick SL, Kung AL, Golub TR: **Signature-based small molecule screening identifies cytosine arabinoside as an EWS/FLI modulator in Ewing sarcoma.** *PLoS Med* 2007, **4:**e122.

189. DuBois SG, Krailo MD, Lessnick SL, Smith R, Chen Z, Marina N, Grier HE, Stegmaier K, Children's Oncology G: **Phase II study of intermediate-dose cytarabine in patients with relapsed or refractory Ewing sarcoma: a report from the Children's Oncology Group.** *Pediatr Blood Cancer* 2009, **52:**324-327.

190. Erkizan HV, Kong Y, Merchant M, Schlottmann S, Barber-Rotenberg JS, Yuan L, Abaan OD, Chou TH, Dakshanamurthy S, Brown ML, et al: **A small molecule blocking oncogenic protein EWS-FLI1 interaction with RNA helicase A inhibits growth of Ewing's sarcoma.** *Nat Med* 2009, **15:**750-756.

191. Hong SH, Youbi SE, Hong SP, Kallakury B, Monroe P, Erkizan HV, Barber-Rotenberg JS, Houghton P, Uren A, Toretsky JA: **Pharmacokinetic modeling optimizes inhibition of the 'undruggable' EWS-FLI1 transcription factor in Ewing Sarcoma.** *Oncotarget* 2014, **5:**338-350.

192. Selvanathan SP, Graham GT, Erkizan HV, Dirksen U, Natarajan TG, Dakic A, Yu S, Liu X, Paulsen MT, Ljungman ME, et al: **Oncogenic fusion protein EWS-FLI1 is a network hub that regulates alternative splicing.** *Proc Natl Acad Sci U S A* 2015, **112:**E1307-1316.

193. Morales F, Giordano A: **Overview of CDK9 as a target in cancer research.** *Cell Cycle* 2016, **15:**519-527.

194. Lam F, Abbas AY, Shao H, Teo T, Adams J, Li P, Bradshaw TD, Fischer PM, Walsby E, Pepper C, et al: **Targeting RNA transcription and translation in ovarian cancer cells with pharmacological inhibitor CDKI-73.** *Oncotarget* 2014, **5:**7691-7704.
195. Alghamdi S, Khan I, Beeravolu N, McKee C, Thibodeau B, Wilson G, Chaudhry GR: **BET protein inhibitor JQ1 inhibits growth and modulates WNT signaling in mesenchymal stem cells.** *Stem Cell Res Ther* 2016, **7**.
196. Tang Y, Gholamin S, Schubert S, Willardson MI, Lee A, Bandopadhayay P, Bergthold G, Masoud S, Nguyen B, Vue N, et al: **Epigenetic targeting of Hedgehog pathway transcriptional output through BET bromodomain inhibition.** *Nat Med* 2014, **20:**732-740.
197. Anand P, Brown JD, Lin CY, Qi J, Zhang R, Artero PC, Alaiti MA, Bullard J, Alazem K, Margulies KB, et al: **BET bromodomains mediate transcriptional pause release in heart failure.** *Cell* 2013, **154:**569-582.
198. Patel MC, Debrosse M, Smith M, Dey A, Huynh W, Sarai N, Heightman TD, Tamura T, Ozato K: **BRD4 coordinates recruitment of pause release factor P-TEFb and the pausing complex NELF/DSIF to regulate transcription elongation of interferon-stimulated genes.** *Mol Cell Biol* 2013, **33:**2497-2507.
199. Bradner JE, Hnisz D, Young RA: **Transcriptional Addiction in Cancer.** *Cell* 2017, **168:**629-643.
200. Sharma SV, Lee DY, Li B, Quinlan MP, Takahashi F, Maheswaran S, McDermott U, Azizian N, Zou L, Fischbach MA, et al: **A Chromatin-Mediated Reversible Drug-Tolerant State in Cancer Cell Subpopulations.** *Cell* 2010, **141:**69-80.
201. Fong CY, Gilan O, Lam EYN, Rubin AF, Ftouni S, Tyler D, Stanley K, Sinha D, Yeh P, Morison J, et al: **BET inhibitor resistance emerges from leukaemia stem cells.** *Nature* 2015, **525:**538-542.
202. Bitler BG, Aird KM, Garipov A, Li H, Amatangelo M, Kossenkov AV, Schultz DC, Liu Q, Shih Ie M, Conejo-Garcia JR, et al: **Synthetic lethality by targeting EZH2 methyltransferase activity in ARID1A-mutated cancers.** *Nat Med* 2015, **21:**231-238.

203. Kim KH, Roberts CW: **Targeting EZH2 in cancer.** *Nat Med* 2016, **22:**128-134.

204. Verma SK, Tian X, LaFrance LV, Duquenne C, Suarez DP, Newlander KA, Romeril SP, Burgess JL, Grant SW, Brackley JA, et al: **Identification of Potent, Selective, Cell-Active Inhibitors of the Histone Lysine Methyltransferase EZH2.** *ACS Med Chem Lett* 2012, **3:**1091-1096.

205. Shi B, Liang J, Yang X, Wang Y, Zhao Y, Wu H, Sun L, Zhang Y, Chen Y, Li R, et al: **Integration of estrogen and Wnt signaling circuits by the polycomb group protein EZH2 in breast cancer cells.** *Mol Cell Biol* 2007, **27:**5105-5119.

206. Li X, Gonzalez ME, Toy K, Filzen T, Merajver SD, Kleer CG: **Targeted overexpression of EZH2 in the mammary gland disrupts ductal morphogenesis and causes epithelial hyperplasia.** *Am J Pathol* 2009, **175:**1246-1254.

207. Jung HY, Jun S, Lee M, Kim HC, Wang X, Ji H, McCrea PD, Park JI: **PAF and EZH2 induce Wnt/beta-catenin signaling hyperactivation.** *Mol Cell* 2013, **52:**193-205.

208. Miranda TB, Cortez CC, Yoo CB, Liang G, Abe M, Kelly TK, Marquez VE, Jones PA: **DZNep is a global histone methylation inhibitor that reactivates developmental genes not silenced by DNA methylation.** *Mol Cancer Ther* 2009, **8:**1579-1588.

209. Morera L, Lubbert M, Jung M: **Targeting histone methyltransferases and demethylases in clinical trials for cancer therapy.** *Clin Epigenetics* 2016, **8:**57.

210. Holm K, Grabau D, Lovgren K, Aradottir S, Gruvberger-Saal S, Howlin J, Saal LH, Ethier SP, Bendahl PO, Stal O, et al: **Global H3K27 trimethylation and EZH2 abundance in breast tumor subtypes.** *Mol Oncol* 2012, **6:**494-506.

211. Noguchi-Yachide T: **BET Bromodomain as a Target of Epigenetic Therapy.** *Chem Pharm Bull (Tokyo)* 2016, **64:**540-547.

8 Appendix

8.1 Supplemental figures

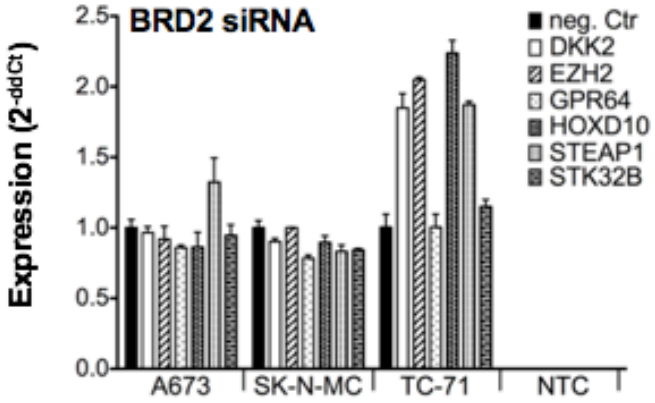

Figure 21: Knock-down of BRD2 by RNAi did not influence gene expression as observed after JQ1 treatment. RNA interference (RNAi) by specific siRNA for BRD2 in A673, SK-N-MC and TC-71 compared to neg. control (non-silencing RNA). Results of qRT-PCR 48 h after transfection are shown. Genes found as down regulated after JQ1 treatment were not influenced after knock-down of BRD2. Data are mean ± SEM; t-test. NTC: non-template control.

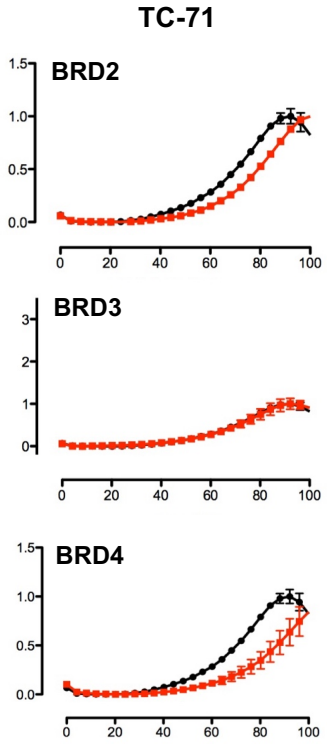

Figure 22: Analysis of proliferation after induced knock-down of BRD2, BRD3 and BRD4. Analysis of proliferation was done for TC-71 by xCELLigence assay measuring cellular impedance every 4 h (relative cell index). No significant growth differences were observed for either knock-down. Data are mean ± SEM (hexaplicates/group); t-test.

8.2 Supplemental tables

Table 21: Selected genes down-regulated after 48 h 2 µM JQ1 treatment in TC-71 cells

Gene symbol	Gene Description	Q-JQ1
GPR64	G protein-coupled receptor 64	0.243
JMJD1C	jumonji domain containing 1C SWI/SNF-related, matrix-associated actin-dependent	0.249
SMARCAD1	regulator of chromatin, subfamily a, containing DEAD/H box 1	0.275
STAG2	stromal antigen 2	0.283
LYN	v-yes-1 Yamaguchi sarcoma viral related oncogene homolog	0.288
PAPPA	pregnancy-associated plasma proteinA, pappalysin 1	0.313

PCDHB5	protocadherin beta 5	0.325
IDH1	isocitrate dehydrogenase 1 (NADP+), soluble	0.334
STEAP1	six transmembrane epithelial antigen of the prostate 1	0.367
HDAC9	histone deacetylase 9	0.371
RGS4	regulator of G-protein signaling 4	0.380
CCNA1	cyclin A1	0.382
STEAP2	six transmembrane epithelial antigen of the prostate 2	0.388
HOXB2	homeobox B2	0.393
TET2	tet oncogene family member 2	0.405
IGF2BP1	insulin-like growth factor 2 mRNA binding protein 1	0.425
HIST1H2AB	histone cluster 1, H2ab	0.427
LIPI	lipase, member I	0.436
HIST1H1T	histone cluster 1, H1t	0.442
HOXD10	homeobox D10	0.445
HIST1H2BB	histone cluster 1, H2bb	0.448
CCNB2	cyclin B2	0.451
JARID2	jumonji, At rich interactive domain 2	0.458
HDAC8	histone deacetylase 8	0.470
TET1	tet oncogene 1	0.473
STK32B	serine/threonine kinase 32B	0.480
DKK2	dickkopf homolog 2 (Xenopus laevis) SWI/SNF related, matrix associated, actin dependent	0.480
SMARCAL1	regulator of chromatin, subfamily a-like 1	0.482
CCNA2	cyclin A2	0.483
JHDM1D	jumonji C domain containing histone demethylase 1 homolog D (S. cerevisae)	0.492
EZH2	enhancer of zeste homolog 2 (Drosophila)	0.495
PAX7	paired box 7	0.499

Table 22: Genes found as significantly deregulated in A673 and TC-71 microarrays after 48 h JQ1 treatment. Fold change was compared to DMSO control.

Gene Accession	Gene Name	Description	Fold change	
			A673	TC-71
NM_003879	**CFLAR**	CASP8 and FADD-like apoptosis regulator	0,51	0,33
NM_006333	**C1D**	C1D nuclear receptor co-repressor	0,49	0,38
NM_015087	**SPG20**	spastic paraplegia 20 (Troyer syndrome)	0,40	0,47
NM_006333	**C1D**	C1D nuclear receptor co-repressor	0,49	0,40
NM_005445	**SMC3**	structural maintenance of chromosomes 3	0,64	0,36
NM_013979	**BNIP1**	BCL2/adenovirus E1B 19kDa interacting protein 1	0,59	0,38
NM_006333	**C1D**	C1D nuclear receptor co-repressor	0,41	0,61
NM_001211	**BUB1B**	budding uninhibited by benzimidazoles 1 homolog beta (yeast)	0,49	0,53
NM_001033568	**RHOT1**	ras homolog gene family, member T1	0,65	0,42
NM_152266	**C19orf40**	chromosome 19 open reading frame 40	0,43	0,66
NM_006333	**C1D**	C1D nuclear receptor co-repressor	0,45	0,60
NM_173685	**NSMCE2**	non-SMC element 2, MMS21 homolog (S. cerevisiae)	0,73	0,37
NM_139178	**ALKBH3**	alkB, alkylation repair homolog 3 (E. coli)	0,58	0,42
NM_001136194	**FASTKD2**	FAST kinase domains 2	0,52	0,56
NM_021821	**MRPS35**	mitochondrial ribosomal protein S35	0,66	0,44
NM_000165	**GJA1**	gap junction protein, alpha 1, 43kDa	0,55	0,63
NM_001167	**XIAP**	X-linked inhibitor of apoptosis	0,68	0,50

NM_007027	**TOPBP1**	topoisomerase (DNA) II binding protein 1	0,61	0,55
NM_199320	**PHF17**	PHD finger protein 17	0,56	0,61
NM_197956	**NAIF1**	nuclear apoptosis inducing factor 1	0,53	0,62
NM_152463	**EME1**	essential meiotic endonuclease 1 homolog 1 (S. pombe)	0,63	0,54
NM_001033030	**FAIM**	Fas apoptotic inhibitory molecule	0,62	0,56
NM_022740	**HIPK2**	homeodomain interacting protein kinase 2	0,66	0,46
NM_024622	**FASTKD1**	FAST kinase domains 1	0,58	0,65
NM_002875	**RAD51**	RAD51 homolog (RecA homolog, E. coli) (S. cerevisiae)	0,66	0,56
NM_004938	**DAPK1**	death-associated protein kinase 1	0,57	0,66
NM_001831	**CLU**	clusterin	1,54	1,52
NM_030809	**CSRNP2**	cysteine-serine-rich nuclear protein 2	1,89	1,56
NM_015068	**PEG10**	paternally expressed 10	1,67	1,90
NM_002105	**H2AFX**	H2A histone family, member X	1,79	2,37
NM_003897	**IER3**	immediate early response 3	2,24	1,62
NM_003811	**TNFSF9**	tumor necrosis factor (ligand) superfamily, member 9	3,04	1,61
NM_006875	**PIM2**	pim-2 oncogene	3,21	3,53

8.3 List of figures

8.4 List of tables

8.5 List of Abbreviations

BCA	bichinonic assay
BCP	1-bromo-3-chloropropane
bp	base pairs
BS3	bis(sulfosuccinimidyl)suberate
cDNA	complementary DNA
CpG	5`-C-phosphate-G-3`
ChIP	Chromatin immunoprecipitation
DSMO	Dimethylsulfoxid
DNA	Desoxyribonucleic acid
DNMT	DNA methyltransferase
dNTP	Deoxyribonucleotide triphosphate
ds	double stranded
DKK2	dickkopf 2
DZNep	3-deazaneplanocin A
EDTA	Ethylenediaminetetraacetic acid
EED	Embryonic ectoderm development
ES	Ewing Sarcoma
ESFT	Ewing sarcoma family of tumors
ET	Ewing tumors
EWS	Ewing`s Sarcoma oncogene
EZH1	Enhancer of Zeste (Drosophila), homolog 1
EZH2	Enhancer of Zeste (Drosophila), homolog 2
FAM	6-carboxy-fluorescin
FBS	Fetal bovine serum
FLI1	Friend leukemia integration
For (primer)	forward
GAPDH	Glyceraldehyde-2-phosphate dehydrogenase
GPR64	G protein-coupled receptor 64
H3	Histone 3
H3K27ac	Histone 3 lysine 27 acetylation

H3K27me3	Histone 3 lysine 27 trimethylation
H&E	Hematoxylin & Eosin
HPRT	Hypoxanthine-guanine phosphoribosyltransferase
HRP	Horseradish peroxidase
IFITM1	Interferon induced transmembrane protein 1
IFN	Interferon
IgG	Immunoglobulin G
IHC	Immunohistochemistry
i.p.	intra peritoneal
kDa	Kilo Dalton
LTR	Long terminal repeats
mRNA	messenger RNA
MSC	Mesenchymal stem cell
NTC	non-template control
PBS	Phospahte buffered saline
PCR	Polymerase chain reaction
PI	Propidium iodide
PNET	primitive neurectodermal tumor
PRC2	Polycomb repressive complex 2
PVDF	Polyvinylidene Fluoride
qRT-PCR	quantitative real time PCR
rev (primer)	reverse
RT	Reverse transcriptase or room temperature
SAM	Significance analysis of microarrays
s.c.	sub-cuntaneous
SDS	Sodium dodecyl sulfate
SDS-PAGE	SDS polyacrylamide gel electrophoresis
shRNA	small hairpin RNA
siRNA	small interfering RNA
ss	single stranded
STEAP1	Six transmembrane epithelial antigen of prostate 1
SUZ12	Suppressor ofzeste homolog 12 (Drosophila)
TBST	Tris-buffered saline Tween-20
TEMED	N,N,N`,N`-Tetramethylethan-1,2-diamin

TSA	Trichostatin A
TSS	Transcriptional start site
VC	Vector control

8.6 Publications

Original articles (peer-reviewed)

Hensel T, Giorgi C, Schmidt O, Calzada-Wack J, Neff F, Buch T, Niggli FK, Schäfer BW, Burdach S, Richter GH
"Targeting the EWS-ETS transcriptional program by BET bromodomain inhibition in Ewing sarcoma"
Oncotarget, 2016 7(2):1451-63

von Heyking K, Calzada-Wack J, Göllner S, Neff F, Schmidt O, **Hensel T**, Schirmer D, Fasan A, Esposito I, Müller-Tidow C, Sorensen PH, Burdach S, Richter GH
"The endochondral bon protein CHM1 sustains an undifferentiated, invasive phenotype, promoting lung metastasis in Ewing sarcoma"
Molecular Oncology, 2017

Contributions to congresses

Tim Hensel, Chiara Giorgi, Fiona Becker-Dettling, Julia Calzada-Wack, Frauke Neff, Thorsten Buch, Oxana Schmidt, Beat W. Schäfer, Stefan Burdach, Günther HS Richter

Talk: “Targeting the EWS/ETS transcriptional program by BET bromodomain inhibition in Ewing sarcoma”
Deutscher Krebskongress, Berlin, 02/2016

Tim Hensel, Chiara Giorgi, Fiona Becker-Dettling, Julia Calzada-Wack, Frauke Neff, Thorsten Buch, Oxana Schmidt, Beat W. Schäfer, Stefan Burdach, Günther HS Richter
Poster: “Combined targeting of the EWS/ETS transcriptional program and PI3Kpathway inhibition blocks tumorigenicity and increases apoptosis in Ewing sarcoma”
Annual Meeting of the American Association for Cancer Research, New Orleans, 04/2016

Tim Hensel, Chiara Giorgi, Fiona Becker-Dettling, Julia Calzada-Wack, Frauke Neff, Thorsten Buch, Oxana Schmidt, Shudong Wang Beat W. Schäfer, Stefan Burdach, Günther HS Richter
Poster: “BET bromodomain proteins in Ewing sarcoma regulate a specific transcriptional program, tumorigenicity and apoptosis by interacting with EWS-FLI1 and the positive transcription elongation factor”
New Frontiers in Cancer Research, Cape Town, 01/2017

Tim Hensel, Chiara Giorgi, Fiona Becker-Dettling, Julia Calzada-Wack, Frauke Neff, Thorsten Buch, Oxana Schmidt, Shudong Wang Beat W. Schäfer, Stefan Burdach, Günther HS Richter
Poster: “Combined targeting of the EWS/ETS transcriptional program by blocking epigenetic readers and transcription initiation in Ewing sarcoma”
Annual Meeting of the American Association for Cancer Research, Washington D.C., 04/2017